Frequency control coordination among non-synchronous AC areas connected by a multi-terminal HVDC grid.

Jing Dai

N° d'ordre : 2011-12-TH

THÈSE DE DOCTORAT

SPÉCIALITÉ: PHYSIQUE

École doctorale Sciences et Technologies de l'Information, des Télécommunications et des Systèmes

Présentée par:

Jing DAI

Sujet:

Coordination du réglage de la fréquence entre plusieurs systèmes électriques non-synchrones reliés par un réseau à courant continu haute tension

(Frequency control coordination among non-synchronous AC areas connected by a multi-terminal HVDC grid)

Soutenue le 3 octobre 2011 devant les membres du jury:

Mme. Anne-Marie DENIS,	Réseau de Transport d'Electricité, La Défense,	Examinateur
M. Stefano DI GENNARO,	Laboratoire des Signaux et Systèmes, Gif-sur-Yvette,	Examinateur et Président
M. Damien ERNST,	Université de Liège,	Encadrant de Thèse
M. Chen-Ching LIU,	University College Dublin,	Rapporteur
M. Yannick PHULPIN,	Département Energie-E3S, Supélec, Gif-sur-Yvette,	Encadrant de Thèse
M. Bayram TOUNSI,	Electricité de France, Clamart,	Examinateur
M. Jean-Claude VANNIER,	Département Energie-E3S, Supélec, Gif-sur-Yvette,	Directeur de Thèse
M. Constantine VOURNAS,	National Technical University of Athens,	Rapporteur

Acknowledgments

My deepest gratitude goes to Dr. Damien ERNST, my supervisor from the University of Liège (ULg), Belgium. By warmly hosting me during my four trimestral scientific visits to the ULg, he selflessly and unremittingly gave me invaluable guidance and comprehensive assistance that are crucial to a Ph.D. candidate at his initializing phase of a scientific career. From the concretization of the research orientation to the final submission of papers, he closely followed my research activities, despite sometimes the inconvenience brought about by the geographical distance when I am in France. In addition, he also introduced me to the domain of artificial intelligence, which not only diversified my research, but also proves to be a powerful and promising tool to solve problems in power engineering. Thanks to these visits to the ULg, I have the opportunity to meet professors, researchers, and Ph.D. candidates in the Department of Electrical Engineering and Computer Science of the ULg, and attend the weekly seminars to enlarge my horizon.

My deepest gratitude also goes to Dr. Yannick PHULPIN, my supervisor from Supélec, France. From my final year as an engineering student to my three years of Ph.D. candidacy, in passing the sandwich year as a research-oriented master student at the University of Paris XI, he kept to be the very person who is always ready to help me and to whom I would always seek resort whenever I encountered difficulties, be they scientific or personal. By helping me through all the administrative red tape, he made it possible for me to pursue a doctor's degree at Supélec; and by giving me constant advice in research and career orientation, he helped me to mature in research and scientific writing, and to build an equilibrium between work and life that makes my Ph.D. years a pleasant life journey.

I am indebted to Professor Jean-Claude VANNIER, my doctoral advisor and the head of the Department of Power and Energy Systems of Supélec. He admitted me as a Ph.D. candidate in the department and granted me the access to all the facilities and resources in the laboratory. He also gave me the agreement to conduct research at the ULg. In addition, he also permitted me to monitor the experiments of undergraduate students from Supélec, which allowed me to obtain a first-hand teaching experience, to maintain contact with young people, and to touch a decent complementary salary.

Among all my age peers, I am most thankful to Dr. Alain SARLETTE from the ULg, who is physically younger than me but academically much more experienced, and with whom I had the honor to collaborate. Once a paper is put under his scrutiny, a high writing standard is incarnated in his constant feedbacks, which not only point out problems and weaknesses, but also propose solutions. This makes the interaction with him a pleasant and enriching learning experience. Thanks to his perspicacity, the ideas are elucidated, the structure is streamlined, and the mathematical proofs shine with strictness, concision and elegance.

Many thanks to the former and the current faculty, personnel, Ph.D. students from the Department of Power and Energy Systems of Supélec, who constantly helped me in research and contributed to building a convivial ambiance for work, including but not limited to: Amir ARZANDE, Romain COUILLET, Philippe DESSANTE, Martin HENNEBEL, Robert KACZMAREK, Charif KARIMI, Mike KIRKPATRICK, Pierre LEFRANC, Yanfu LI, Bruno LORCET, Philippe MOLINIÉ, Emmanuel ODIC, Marc PETIT, François PROTAT, Vincent RIOUS, Daniel SADARNAC, Micheline VIDAL, Pierre VIDAL, Christiane LEBOUQUIN, Stéphanie DOUESNARD, Si-Mohamed BENHAMED, Damien HUCHET, José DE FREITAS, Jean-Pierre METENIER, Gilbert BERGNADIAZ, Maialen BOYRA, José Luis CALVO DE MIGUEL, Mathieu CAUJOLLE, Benjamin DAGUSÉ, Mazhar EZZEDDINE, Wilfried FRÉLIN, Christophe GUTFRIND, Ali JAAFAR, Xavier JANNOT, Tanguy JANSSEN, Trung Dũng LÊ, Christophe LEDOUX, Soukayna LIMAM, Nicolas MÉRICAM-BOURDET, Hoàng Nam NGUYEN, Haitham RAMADAN, and Nathalie SAKER. I would like to thank Professors Rodolphe SEPULCHRE and Louis WEHENKEL from the ULg, which warmly received me at the ULg with great common touch and approachability despite their academic reputation and seniority. My gratitude also goes to the researchers, personnel, and Ph.D. students that I encountered at but not necessarily affiliated to the Systems and Modeling research unit of the Department of Electrical Engineering and Computer Science of the ULg, who made my stays in Liège pleasant and enjoyable and with whom I had inspiring talks, including but not limited to: Julien BECKER, Florence BELMUDES, Vincent BOTTA, Florin CAPITANESCU, Boris DEFOURNY, Marc FRÉDÉRIC, Raphaël FONTENAU, Samuel HIARD, Alexandre MAUROY, Tan MIN, François SCHNITZLER, Oliver STERN, and Da WANG.

I am also thankful to those researchers who gave me comments and suggestions on my work during conferences and seminars, such as: Prof. Thierry Van Cutsem from the ULg, Mr. Patrick PANCIATICI from Réseau de Transport d'Életricité (French TSO), Prof. Peter Crossley from the University of Manchester, and Prof. Bikash Pal from Imperial College London.

I am indebted to French Ministry for Education and Research for its financial support in the form of a monthly research allowance.

At a national level, I am grateful to the People's Republic of China where I gained solid foundation in natural sciences in the primary, the secondary and the undergraduate education. I am thankful to the French Republic, which provided me with a picturesque natural environment and an exemplary social system, both for work and for life, and which instilled in me through immersion the values of Liberty, Equality, and Fraternity. I am also grateful to the Kingdom of Belgium, which offered me a serene environment and top-level research ambiance.

My pious gratefulness is to the Almighty, who created this fascinating world to explore and also me who explore the former. His divine providence bestowed on me health, sanity, intelligence, financial viability, and the opportunity in my lifetime to carry out scientific research in developed countries, and dotted my life trajectory with a lot of intersecting points and line segments with researchers from all over the world, who prove to be among the most brilliant and the most dedicated people of a given population.

Last but not least, I would like to extend my gratitude to my parents and my family in China, who reared me up and taught me the value of knowledge and cultivated me the eagerness to seek truth. Despite my constant absence, they kept encouraging me throughout all the vicissitudes of life. They remain my spiritual haven wherever I am around the globe.

Résumé

Cette thèse se focalise sur le problème du contrôle des flux de puissance entre plusieurs systèmes électriques AC non-synchrones reliés par un réseau à courant continu (DC). Elle propose trois schémas de commande afin de permettre aux sous-systèmes de partager leurs efforts de réglage de la fréquence et réduire ainsi le besoin de réserves propres et les coûts associés. Deux schémas s'appliquent au réglage primaire de la fréquence et le troisième au réglage secondaire.

Le premier schéma de commande, appelé « schéma de commande basé sur la puissance injectée », est distribué par nature. A partir des mesures des fréquences de toutes les zones, il modifie les puissances injectées par chaque zone AC vers le réseau DC, de manière à faire réagir le système collectivement à des déséquilibres de charge. La mise au point du schéma de commande s'appuie sur des algorithmes introduits pour résoudre le problème du consensus qui lui-même est extensivement étudié à ce titre par la communauté d'automatique. Puisque des mesures distantes sont utilisées, les effets de délais sur l'efficacité du schéma de commande sont étudiés. Une analyse de stabilité sur le système en boucle fermée montre que sous certaines hypothèses, pour autant que les délais ne dépassent pas une limite acceptable, le système converge vers un point d'équilibre où les déviations de fréquence des zones AC sont égales entre elles. Les résultats de simulation sur un réseau électrique de référence avec cinq zones AC démontrent l'efficacité du schéma de commande.

Le deuxième schéma de commande a le même objectif que le premier, mais il agit sur les tensions continues des convertisseurs HVDC, et est ainsi appelé « le schéma de commande basé sur la tension DC ». En particulier, il modifie la tension continue de chaque convertisseur en fonction de la déviation de fréquence de la zone AC à laquelle il est connecté. Ce caractère décentralisé le libère des problèmes liés à la dépendance d'informations distantes. Une étude théorique montre que, en n'utilisant que des informations locales, le schéma de commande permet de réduire considérablement l'impact d'un déséquilibre de puissance en distribuant la déviation de fréquence parmi toutes les zones. Les résultats de simulation sur le même système de référence illustrent la bonne performance du schéma de commande.

Le dernier schéma de commande vise à rétablir les fréquences et les échanges de puissance à leurs valeurs nominales et prévues, respectivement, à la suite d'un déséquilibre. Il peut être combiné avec les deux autres schémas de commande. Pour étudier ses propriétés de stabilité, une décomposition temporelle est effectuée sur le système lorsque ce schéma de commande est combiné avec le schéma de commande basé sur la tension DC. Les deux sous-systèmes d'ordres réduits ainsi obtenus, qui décrivent la dynamique lente et la dynamique rapide du système original, sont stables, ce qui implique la stabilité de l'ensemble du système. Les résultats de simulation sur le même système de référence confirment la bonne performance du schéma de commande.

Abstract

This thesis addresses the problem of frequency control in a power system composed of several non-synchronous AC areas connected by a multi-terminal HVDC grid. For this system, we propose three control schemes, two for primary frequency control and one for secondary frequency control.

The first control scheme, called power-injection-based control scheme, is distributed by nature. Based on remote measurements of the other areas' frequencies, this control scheme modifies the power injections from the different AC areas into the DC grid so as to make the system collectively react to load imbalances. This collective reaction allows each individual AC area to downscale its primary reserves. The scheme is inspired by algorithms for the consensus problem extensively studied by the control theory community. As remote measurements are used, the effects of time-delays on the control scheme's effectiveness are investigated. A stability analysis of the closed-loop system shows that with some assumptions, as long as the time-delays are within an acceptable limit, the system converges to an equilibrium point at which the AC areas' frequency deviations are equal to each other. Simulation results on a benchmark power system with five AC areas show the effectiveness of the control scheme.

The second control scheme has the same objective with the first one, but acts on the DC voltages of the HVDC converters, and thus is called DC-voltage-based control scheme. In particular, it modifies the DC voltage of each converter based on the frequency deviation of the AC area it is connected to. This decentralized nature frees it from the problems related to the dependence on remote information. A theoretical study shows that, by using local information only, the control scheme allows to significantly reduce the impact of a power imbalance by distributing the associated frequency deviation over all areas. Simulation results on the same benchmark system illustrate the good performance of the control scheme.

The last control scheme aims at restoring the frequencies and the power exchanges to their nominal or scheduled values in the aftermath of a power imbalance. It can be combined with the other two control schemes. To study its stability properties, a timescale decomposition is carried out on the closed-loop system under this control scheme combined with the DC-voltage-based control scheme. The two reduced-order subsystems thus obtained describing the slow and the fast dynamics respectively are both shown to be stable, which implies the stability of the entire system. Simulation results on the benchmark system confirm the good performance of the control scheme.

Contents

List of Figures

List of Tables

List of Acronyms

AC	Alternating Current
AGC	Automatic Generation Control
CC	Constant Current
CEA	Constant Extinction Angle
CLF	Control Lyapunov Function
CSC	Current Source Converters
DC	Direct Current
DFT	Discrete Fourier Transform
HVDC	High Voltage Direct Current
IGBT	Insulated-Gate Bipolar Transistors
LFC	Load-Frequency Control
NPFC	Network Power Frequency Characteristic
MIMO	Multi Input Multi Output
MT-HVDC	Multi-Terminal High Voltage Direct Current
PID	Proportional Integral Derivative
PMU	Phasor Measurement Units
PWM	Pulse Width Modulation
SCADA	Supervisory Control And Data Acquisition
TSO	Transmission System Operator
UAV	Unmanned Aerial Vehicles
UCTE	Union for the Co-ordination of Transmission of Electricity
VSC	Voltage Source Converters
WAMS	Wide Area Measurement System

Coordination du réglage de la fréquence entre plusieurs systèmes électriques non-synchrones reliés par un réseau à courant continu haute tension

1 Introduction

1.1 Contexte

Pour présenter le contexte de cette thèse sur l'utilisation de systèmes HVDC pour le réglage de la fréquence, ce chapitre est divisé en trois parties. Tout d'abord, nous décrivons brièvement différents types de stabilité de systèmes électriques, dont la stabilité de fréquence. Deuxièmement, nous présentons la technologie HVDC, qui offre de nouvelles possibilités de renforcer la stabilité de systèmes électriques. Troisièmement, nous discutons de l'utilisation des systèmes HVDC pour le réglage de la fréquence en particulier.

Stabilité de systèmes électriques et le réglage de la fréquence

La stabilité de systèmes électriques est définie comme la capacité d'un système électrique à retrouver un état d'équilibre après avoir subi une perturbation [1]. Il y a trois catégories de stabilité : la stabilité de l'angle de rotor, la stabilité en fréquence, et la stabilité en tension.

- La stabilité de l'angle de rotor porte sur la capacité des génératrices synchrones à couplage direct au réseau à rester en synchronisme. La stabilité transitoire, comme l'on l'appelle communément, concerne la stabilité de l'angle de rotor lorsque la perturbation est tellement grande que la linéarisation des équations du système n'est plus valable pour l'analyse.
- La stabilité en fréquence correspond à la capacité d'un système électrique à maintenir la fréquence après un déséquilibre important entre la production et la demande.
- La stabilité en tension porte sur la capacité d'un système à maintenir la tension à tous les jeux de barres du système après avoir été soumis à une perturbation.

Des mesures de sécurité sont prises pour renforcer la stabilité de systèmes électriques. Les actions pour renforcer de la stabilité transitoire visent à réduire l'influence de perturbations,

à augmenter le couple synchronisant et à réduire le couple d'accélération [2]. Pour la stabilité en fréquence, des schémas de commande pour ajuster la production des générateurs ont été développés pour maintenir l'équilibre de la puissance et de réguler la fréquence [3]. Les moyens les plus courants pour améliorer la stabilité en tension est de générer / consommer de la puissance réactive à différents jeux de barres et d'ajuster la prise de transformateur [4]. En pratique, le maintien de la stabilité en fréquence et de la stabilité en tension fait appel aux services système, qui comprennent plusieurs types de services visant à soutenir le fonctionnement de base de la production, l'approvisionnement d'énergie, et la fourniture de courant [5].

Les schémas de commande que les gestionnaires de réseau de transport ont développés pour réguler la fréquence sont habituellement classés selon l'échelle de temps de leurs actions [6]. Les actions les plus rapides sont généralement désignés sous le nom de « réglage primaire de la fréquence ». Il s'agit d'un ajustement automatique, en quelques secondes, de la puissance injectée par des générateurs en fonction de variations de fréquence mesurées localement. Pour y participer (contre rémunération dans la plupart des pays), les générateurs doivent disposer de « réserves primaires », c'est à dire de marges pour augmenter ou diminuer rapidement l'injection de puissance.

La fréquence moyenne en quelques secondes peut être considérée comme identique dans l'ensemble d'une zone synchrone. Avec une fréquence commune, tous les générateurs participant au réglage primaire de la fréquence ajustent leur production en réponse aux variations de la fréquence, indépendamment de l'emplacement du déséquilibre correspondant. Puisque les efforts de ces générateurs s'ajoutent les uns aux autres dans la zone synchrone, les systèmes plus grands éprouvent habituellement des déviations de fréquence plus faibles. En outre, la fourniture de réserves primaires représente des coûts non-négligeables. Par exemple, en 2007, le prix moyen de la réserve primaire est d'environ 1,4 c€/kW/h en Allemagne [7]. Par conséquent, un des avantages de l'élargissement des zones synchrones par interconnexion de systèmes régionaux est de partager leurs réserves primaires, de sorte que chaque zone déploie moins de sa réserve primaire en réponse à un déséquilibre de puissance donnée, et que l'ensemble du système interconnecté fasse l'objet d'une déviation de fréquence plus faible. Comme les réserves sont partagées dans toute la zone synchrone, l'exigence sur les réserves de chaque zone est réduite [8, 9], ce qui apporte des avantages économiques [10].

Technologie HVDC et ses apports à la stabilité

HVDC est l'acronyme anglais pour « High Voltage Direct Current », c'est à dire « courant continu haute tension ». Il s'agit d'une technologie permettant de transporter de fortes puissances [11]. En utilisant des composants de l'électroniques de puissance, de la puissance en courant alternatif est convertie en puissance en courant continu pour la transporter à grande distance, ce qui donne lieu à un coût moins cher et de pertes électriques moins importantes. En outre, la technologie HVDC est également avantageuse pour les interconnexions asynchrones et les câbles sous-marins de longue distance [12]. Alors que des convertisseurs classiques à source de courant ont besoins d'injection locale de la puissance réactive, des convertisseurs modernes à source de tension sont capables de commander la puissance active et la puissance réactive de manière indépendante [13].

Les systèmes HVDC les plus courants ont deux convertisseurs, l'un fonctionnant comme un redresseur tandis que l'autre comme un onduleur. Lorsqu'il faut connecter plus de deux zones

géographiques, un système HVDC à plusieurs terminaux (ou MT-HVDC pour « multi-terminal HVDC » en anglais) [14] peut être utilisé. Un tel système avec plusieurs convertisseurs donne lieu à de nombreux défis technologiques (notamment en termes de protections et de commande), mais promet une plus grande flexibilité en termes de connexion au réseau et plus de fiabilité. En tant qu'un dispositif hautement contrôlable, les systèmes HVDC ouvrent de nouvelles opportunités pour améliorer la fiabilité de systèmes électriques. En effet, un certain nombre d'études ont montré les avantages d'un système HVDC pour améliorer la stabilité, en termes de la stabilité transitoire [15, 16, 17, 18, 19, 20, 21], la stabilité en tension [16, 17, 22, 18, 20], la stabilité en fréquence [23, 21], et des oscillations inter-zones à basses fréquences [16, 17, 23, 20].

Utilisation de la technologie HVDC pour le réglage de la fréquence

Le développement de la technologie HVDC ouvre de nouvelles perspectives pour interconnecter des zones non-synchrones. Dans ce contexte, il est généralement prévu que les flux d'énergie sur un système HVDC sont fixés à des valeurs programmées, tandis que les fréquences des zones AC restent indépendantes. Ce type de commande peut éviter un cascade des pannes en limitant les effets d'une perturbation grave dans une zone [12]. Il est également judicieux lorsque les gestionnaires des réseaux de transport interconnectés ne peuvent s'entendre sur une pratique commune en termes du réglage de la fréquence. Toutefois, ce type de commande empêche les réserves primaires d'être partagées entre les zones non-synchrones, parce que les générateurs dans une zone sont insensibles à des excursions de fréquence dans d'autres zones. Puisque l'approvisionnement en réserves primaires représente une part importante des coûts opérationnels des gestionnaires de réseau de transport d´électricité [24], il serait économiquement avantageux de partager les réserves primaires parmi les zones non-synchrones en faisant usage de la capacité de suivi rapide de puissance de convertisseurs HVDC.

1.2 Objectif

Les potentiels de la technologie HVDC pour la stabilité en fréquence n'ont pas été étudiés d'une manière aussi approfondie que pour la stabilité transitoire et la stabilité en tension. Ceci est partiellement dû à la loi de commande apparemment simple, qui consiste à ajouter au flux de puissance programmé du convertisseur HVDC un terme qui est proportionnelle à la différence de fréquence entre les deux zones reliées par le lien HVDC. Cependant, nous croyons que plus de résultats restent encore à découvrir dans cet aspect, en particulier pour le cas de systèmes HVDC à plusieurs-terminaux.

Ainsi, cette thèse a pour objectif d'étudier l'utilisation d'un système MT-HVDC pour coordonner le réglage de la fréquence entre les zones non-synchrones connectées. Ses contributions principales sont

- Nous proposons trois schémas de commande, deux pour le réglage primaire de la fréquence et un pour le réglage secondaire de la fréquence.
- Nous démontrons la stabilité des trois schémas de commande, où nous utilisons des résultats théoriques de la communauté d'automatique sur le problème du consensus.
- Nous validons ces résultats à l´aide de simulations sur un système de référence.

1.3 Organisation de la thèse

Le reste de cette thèse est organisé comme suit :

Chapitre 2.1 modélise un système électrique HVDC à plusieurs-terminaux qui servira de référence pour les chapitres suivants où des schémas de commande pour le réglage de la fréquence seront introduits.

Chapitre 3 introduit le premier schéma de commande pour le réglage primaire de la fréquence d'un système HVDC à plusieurs terminaux. Ce schéma de commande modifie les injections de puissance des différentes zones AC vers le réseau DC en fonction des mesures à distance des fréquences d'autres zones, de manière à faire réagir collectivement le système à des déséquilibres de puissance. Une analyse théorique prouve sa stabilité pour un cas particulier où toutes les zones AC ont des paramètres identiques. Les résultats des simulations sur un système de référence avec cinq zones AC démontrent l'efficacité du schéma de commande. En outre, comme le retard est inévitable dans la communication des mesures à distance, l'efficacité du schéma de commande en présence du retard est étudié à la fois théoriquement et empiriquement.

Chapitre 4 propose le deuxième schéma de commande pour le réglage primaire de la fréquence. Contrairement au premier, le deuxième schéma de commande utilise les tensions continues des convertisseurs HVDC comme les variables de commande. En particulier, il modifie la tension continue de chaque convertisseur en fonction de la déviation de fréquence de la zone AC à laquelle il est connecté. Ce caractère décentralisé lui permet de se dégager des problèmes liés à la dépendance vis-à-vis des informations à distance. En utilisant une approche novatrice dans le domaine fréquentiel, une analyse théorique prouve sa stabilité pour le cas général de zones AC aux paramètres hétérogènes. Les résultats de simulations sur le même système de référence montrent son efficacité.

Chapitre 5 décrit le dernier schéma de commande, conçu pour le réglage secondaire de la fréquence. Ce schéma de commande est largement inspiré par la pratique de l'UCTE pour le réglage secondaire de la fréquence dans une zone synchrone, et il doit être utilisé en combinaison avec l'un des deux schémas de commande introduits dans les Chapitres 3 et 4. Les résultats de simulations sur le même système de référence montrent son effcacité.

Chapitre 6 conclut la thèse et propose des orientations de recherche future.

2 Modèle d'un système HVDC à plusieurs terminaux et système de référence

Ce chapitre modélise un système électrique avec un lien HVDC à plusieurs terminaux qui servira de référence pour les chapitres suivants, où des schémas de commande pour le réglage de la fréquence seront introduits.

Section 2.1 présente un modèle de système MT-HVDC, à l'égard duquel le schéma de commande est donné. Section 2.2 définit le point d'équilibre auquel le système est supposé être exploité avant la perturbation et qui sera appelé le *point de fonctionnement de référence*. Section 2.3 présente un système de référence qui sera utilisé pour tester les schémas de commande.

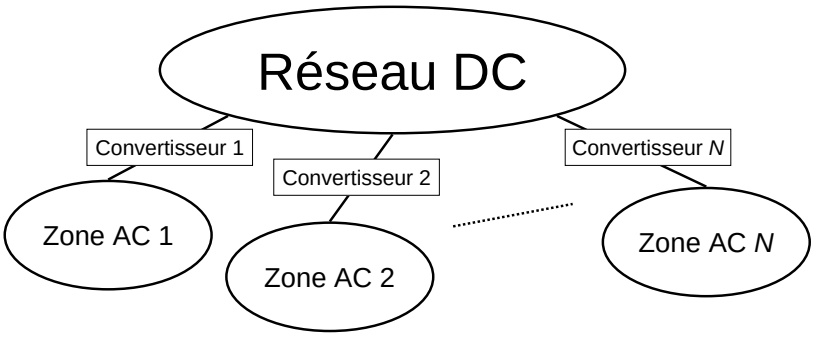

FIG. 1 – Un système HVDC à plusieurs terminaux reliant N zones AC via N convertisseurs.

2.1 Modèle d'un système HVDC à plusieurs terminaux

Nous considérons un système avec trois types de composants : un réseau DC, N zones non-synchrones, et N convertisseurs qui interfacent les zones AC avec le réseau DC, comme illustré sur la Figure 1. Ces éléments sont détaillés dans cette section.

Réseau DC

Puisque la constante de temps électrique d'un réseau DC est de l'ordre de quelques dizaines de millisecondes [4], la dynamique transitoire du réseau DC n'est pas prise en compte.

Nous supposons que chaque noeud du réseau DC est relié à un convertisseur. Chaque noeud hérite donc le numéro d'indice de la zone AC à laquelle il est connecté. Ensuite, la puissance injectée de la zone i vers le réseau DC, notée P_i^{dc}, satisfait

$$P_i^{dc} = \sum_{k=1}^{N} \frac{V_i^{dc}(V_i^{dc} - V_k^{dc})}{R_{ik}} \ , \tag{1}$$

où V_i^{dc} et V_k^{dc} sont les tensions au niveau des noeuds i et k, respectivement, et R_{ik} est la résistance entre ces deux noeuds. V_i^{dc} est appelée la tension DC du convertisseur i dans la suite. Notez que $R_{ik} = R_{ki}$. Si les noeuds i et j ne sont pas directement liés, R_{ik} est considérée comme égale à l'infini. Nous considérons un réseau DC dans lequel il existe un lien soit direct, soit indirect, entre tous les deux noeuds, de sorte que le réseau DC ne soit pas composé de plusieurs parties isolées.

Dans des conditions de fonctionnement normales, une très petite différence de tension entre deux noeuds correspond à un flux de puissance considérable. Par conséquent, $V_1^{dc}, V_2^{dc}, \ldots, V_N^{dc}$ sont proches de la tension nominale du système HVDC, notée V_{ref}^{dc}.

Convertisseurs

Nous négligeons les caractéristiques à hautes fréquences des convertisseurs, pour la même raison que le réseau DC. Nous supposons qu'un convertisseur est capable de suivre instantanément

un signal de consigne pour la puissance injectée vers le réseau DC par le convertisseur P_i^{dc} ou pour la tension DC du convertisseur V_i^{dc}.

Zones AC

Sur l'échelle de temps du réglage primaire de la fréquence, la fréquence peut être considérée comme identique dans n'importe quelle partie d'une zone AC. Nous utilisons donc un modèle agrégé pour représenter les charges et les générateurs au sein de chaque zone.

La somme des charges dans la zone i, notée P_{li}, est représentée par un modèle de charge statique [25]

$$P_{li} = P_{li}^o \cdot (1 + D_{li}(f_i - f_{nom,i})) \ , \tag{2}$$

où f_i est la fréquence de la zone i, $f_{nom,i}$ est sa valeur nominale, P_{li}^o est la puissance absorbée par la charge lorsque $f_i = f_{nom,i}$ et D_{li} est le facteur de sensibilité de la consommation à la fréquence.

La dynamique mécanique du générateur agrégé pour la zone i est décrite par l'équation du mouvement

$$2\pi J_i \frac{df_i}{dt} = \frac{P_{mi} - P_{li} - P_i^{dc}}{2\pi f_i} - 2\pi D_{gi}(f_i - f_{nom,i}) \ , \tag{3}$$

où P_{mi}, J_i, et D_{gi} sont respectivement la puissance mécanique, le moment d'inertie, et le facteur d'amortissement du générateur agrégé pour la zone i. Ces paramètres peuvent être obtenus par des méthodes d'agrégation comme dans [26].

Nous supposons que toutes les zones AC ont le même type de réglage primaire de la fréquence, où le générateur agrégé est équipé d'un régulateur de vitesse qui observe la vitesse de rotation de l'arbre et ajuste en conséquence P_{mi}, suivant

$$T_{smi} \frac{dP_{mi}}{dt} = P_{mi}^o - P_{mi} - \frac{P_{nom,i}}{\sigma_i} \frac{f_i - f_{nom,i}}{f_{nom,i}} \ , \tag{4}$$

où σ_i est le statisme du générateur, T_{smi} la constante de temps du servomoteur du régulateur de vitesse, $P_{nom,i}$ la puissance nominale du générateur, et P_{mi}^o la valeur de consigne pour P_{mi}.

Les variations de P_{mi} sont délimitées par des contraintes techniques et économiques. Formellement, nous supposons que pour le générateur de la zone i, les contraintes peuvent être exprimées par

$$P_{mi}^{\min} \leq P_{mi} \leq P_{mi}^{\max} \ , \tag{5}$$

où $P_{mi}^{\max}$ et $P_{mi}^{\min}$ sont la puissance maximale et minimale qui peut être produite par le générateur i. La différence entre $P_{mi}^{\max}$ et P_{mi} est appelée la « réserve primaire ».

2.2 Point de fonctionnement de référence

Le point de fonctionnement de référence du système est un état d'équilibre défini par des valeurs spécifiques des paramètres d'entrée (P_{li}^o, P_{mi}^o) et des variables (f_i, P_{mi}, P_{li}, P_i^{dc}, V_i^{dc}). Dans la suite, nous notons par $\bar{P}_{li}^o$ et $\bar{P}_{mi}^o$ les valeurs de P_{li}^o et P_{mi}^o au point de fonctionnement

de référence, respectivement. Nous notons aussi les valeurs des variables à ce point-là par leurs symboles correspondants surmontés d'une barre.

Nous prenons les fréquences au point de fonctionnement de référence égale à leurs valeurs nominales, soit

$$\bar{f}_i = f_{nom,i} \ , \quad \forall i \in \{1, 2, \ldots, N\} \ . \tag{6}$$

Puis, (2) donne directement

$$\bar{P}_{li} = \bar{P}^o_{li} \ , \quad \forall i \in \{1, 2, \ldots, N\} \ . \tag{7}$$

Puisque ce point de fonctionnement de référence est un point d'équilibre pour chaque zone, nous obtenons de (3) et (4)

$$\bar{P}_{mi} = \bar{P}^o_{mi} \ , \qquad \forall i \in \{1, 2, \ldots, N\} \ , \tag{8}$$

$$\bar{P}^{dc}_i = \bar{P}^o_{mi} - \bar{P}^o_{li} \ , \quad \forall i \in \{1, 2, \ldots, N\} \ . \tag{9}$$

L'équation de flux de charge DC (1) fournit un ensemble final d'équations qui lient les valeurs de tension avec les autres variables

$$\bar{P}^{dc}_i = \sum_{k=1}^{N} \frac{\bar{V}^{dc}_i(\bar{V}^{dc}_i - \bar{V}^{dc}_k)}{R_{ik}} \ , \quad \forall i \in \{1, 2, \ldots, N\} \ . \tag{10}$$

En pratique, les consignes pour la puissance mécanique, $\bar{P}^o_{mi}$, sont choisies de telle sorte que, pour des charges de référence et à fréquence nominale, les Equations (9) et (10) ont une solution unique avec l'une des tensions $\bar{V}^{dc}_i$ égale à V^{dc}_{ref}.

2.3 Système de référence et perturbation

Le système de référence est constitué de cinq zones non-synchrones, reliées par un système HVDC à cinq terminaux. Le convertisseur de la zone 5 est choisi pour réguler la tension DC, dont la consigne est 100kV. La topologie du réseau en courant continu est représentée sur la Figure 2, où un cercle représente un noeud auquel un convertisseur est connecté, et une arête entre deux cercles représente une ligne à courant continu. Le graphe de communication coïncide avec la topologie du réseau, c'est à dire chaque arête sur la figure représente également un canal de communication bidirectionnel entre les deux zones qu'elle connecte. Les résistances en courant continu entre les zones AC sont les suivantes : $R_{12} = 1.39\Omega$, $R_{15} = 4.17\Omega$, $R_{23} = 2.78\Omega$, $R_{25} = 6.95\Omega$, $R_{34} = 2.78\Omega$, et $R_{45} = 2.78\Omega$. Contrairement à l'analyse de la stabilité dans la Section 3.2, les zones AC sont simulées avec des paramètres différents, tels que résumés dans le Tableau 1. Les zones AC sont simulées avec le modèle complet non-linéaire décrit par (2), (3), (4), (14c). Pour le réseau DC, nous utilisons (1) pour calculer le flux de charge DC.

3 Schéma de commande basé sur les puissances injectées

Ce chapitre présente un schéma de commande pour le partage des réserves primaires entre les zones non-synchrones. Nous l'appelons *schéma de commande basé sur les puissances injectées*

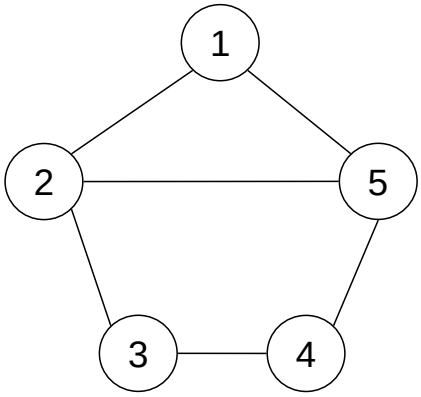

FIG. 2 – Topologie du réseau DC et graphe de communication du système de référence.

TAB. 1 – Valeurs des paramètres pour les zones AC du système de référence.

Paramètre	Zone					Unité
	1	2	3	4	5	
f_{nom}	50	50	50	50	50	Hz
P_m^o	50	80	50	30	80	MW
P_{nom}	50	80	50	30	80	MW
J	2026	6485	6078	2432	4863	kg m^2
D_g	48.4	146.3	140.0	54.9	95.1	$W \cdot s^2$
σ	0.02	0.04	0.06	0.04	0.03	(sans dimension)
T_{sm}	1.5	2.0	2.5	2	1.8	s
P_l^o	100	60	40	50	40	MW
D_l	0.01	0.01	0.01	0.01	0.01	Hz^{-1}

car il utilise les injections de puissance des zones AC vers le réseau DC comme les variables de commande.

Section 3.1 s'étend sur le schéma de commande. Section 3.2 analyse théoriquement la stabilité du système en boucle fermée. Section 3.3 présente des résultats de simulations.

Les résultats présentés dans ce chapitre ont été publiés dans [27, 28].

3.1 Loi de commande

Le partage des réserves primaires entre les zones AC signifie que toute zone soumise à un déséquilibre de puissance peut compter sur les réserves fournies non seulement par la production locale, mais aussi par des générateurs situés dans d'autres zones. Comme le réglage de la fréquence repose généralement sur des mesures de fréquence, qui reflètent l'équilibre de puissance d'une zone synchrone, une approche classique pour atteindre l'objectif ci-dessus est d'émuler une grande interconnexion AC pour que les déviations de fréquence de toutes les zones restent égales en permanence.

Pour rendre chaque générateur sensible à un déséquilibre de puissance à l'échelle du système, la fréquence de chaque zone AC doit tenir compte de l'équilibre globale entre la génération et la demande dans l'ensemble du système.

Dans le reste de cette section, nous donnons l'expression analytique du schéma de commande et nous expliquons son principe de fonctionnement. Nous discutons aussi les limites techniques imposées par les convertisseurs, ainsi que la présence du retard dans la mise en oeuvre pratique du schéma de commande.

Expression analytique

Le schéma de commande basé sur les puissances injectées modifie les injections de puissance des zones AC vers le réseau DC. Le schéma de commande est distribué par nature. Il consiste en $N-1$ sous-contrôleurs, un pour chaque convertisseur HVDC sauf le convertisseur N, ce dernier maintenant la tension du réseau DC. Le sous-contrôleur du convertisseur $i \in \{1, 2, \ldots, N-1\}$ modifie la valeur de P_i^{dc} telle que

$$P_i^{dc} = \bar{P}_i^{dc} + \alpha_i \sum_{k=1}^{N} b_{ik} \int (\Delta f_i - \Delta f_k) dt + \beta_i \sum_{k=1}^{N} b_{ik} (\Delta f_i - \Delta f_k) \ , \tag{11}$$

où

- $\Delta f_i = f_i - f_{nom,i}$ est la déviation de fréquence de la zone i.
- $\alpha_i \geq 0$ et $\beta_i \geq 0$ sont respectivement les gains intégral et proportionnel du sous-contrôleur i.
- b_{ik}'s sont les coefficients représentant le graphe de communication entre les zones AC. La valeur de b_{ik} est égale à 1 si le sous-contrôleur i reçoit des informations sur la fréquence de la zone k, et 0 autrement.

Les valeurs des gains du sous-contrôleur α_i et β_i ont un impact significatif sur la dynamique du système. Grosso modo, des valeurs plus grandes de α_i et β_i permettront à la déviation de fréquence de la zone i de rester près de ceux d'autres régions. Les valeurs des gains sont limitées

en pratique par (i) le taux de variation maximal du flux d'énergie dans le convertisseur, et (ii) des considérations de stabilité du système sous commande, par exemple, en prenant en compte le retard (voir plus tard).

Principe de fonctionnement

L'intuition derrière le schéma de commande défini par (11) est la suivante. Si la déviation de fréquence de la zone i est supérieure (inférieure, resp.) à la déviation de fréquence moyenne des autres zones, plus (moins, resp.) de puissance devrait être retirée de cette zone afin de faire revenir sa déviation de fréquence vers celle des autres zones. L'ajustement de cette puissance (P_i^{dc}) est déterminé par le sous-contrôleur i, ce dernier étant un régulateur PI dont le signal d'erreur est la somme des différences entre la déviation de fréquence de sa propre zone et celle des autres zones dont il obtient des informations. D'un point de vue global, le schéma de commande composé de tous les sous-contrôleurs prend la forme d'un algorithme tel que ceux développés pour résoudre les problèmes de consensus. Ce problème apparaît dans le contexte de la coordination des systèmes multi-agents : l'objectif est, pour les agents qui effectuent une tâche collective de manière distribuée (c'est à dire, sans un surveillant disant à tous ce qu'il faut faire), d'échanger des informations et les traiter afin de parvenir à un accord quant aux efforts respectifs de sorte à coordonner les actions individuelles [29, 30]. Ce cadre correspond bien à la création d'interconnexion HVDC. Les résultats théoriques sur le consensus fourniront donc des outils utiles pour l'étude de stabilité de notre schéma de commande.

Contraintes

Pour assurer le fonctionnement normal du système HVDC, les variables de commande doivent être modulés en fonction des contraintes suivantes

$$V_i^{dc,\min} \leq V_i^{dc} \leq V_i^{dc,\max}, \quad \forall i \in \{1, 2, \ldots, N\}\,, \tag{12a}$$

$$P_i^{dc,\min} \leq P_i^{dc} \leq P_i^{dc,\max}, \quad \forall i \in \{1, 2, \ldots, N\}\,, \tag{12b}$$

où $V_i^{dc,\min}$ et $V_i^{dc,\max}$ ($P_i^{dc,\min}$ et $P_i^{dc,\max}$, resp.) sont les valeurs minimale et maximale acceptable de V_i^{dc} (P_i^{dc}, resp.).

En pratique, ces valeurs devraient dépendre à la fois des caractéristiques techniques du convertisseur i et des tensions aux autres noeuds DC. En effet, avec un choix approprié de $V_i^{dc,\min}$ et $V_i^{dc,\max}$, on peut faire en sorte que les limites de courant des lignes DC et celles de la puissance du convertisseur i ne soient pas dépassées.

Temps de retard

Equation (11) devrait, en principe, déterminer l'évolution de P_i^{dc}, qui représente la puissance injectée de la zone i vers le réseau HVDC. Toutefois, un sous-contrôleur basé sur (11) conduirait dans un système réel à une variation de P_i^{dc} qui pourrait différer sensiblement de celle définie par cette équation.

En fait, l'information de fréquence d'une zone AC distante est généralement fournie par un système de mesure étendu (ou WAMS pour « wide area measurement system » en anglais). Dans

un tel système, les unités de mesure phaseur (ou PMU pour « phasor measurement units » en anglais) placés aux endroits où la fréquence d'intérêt est mesurée à partir de la forme d'onde de la tension, à partir de laquelle la fréquence est calculée en utilisant la transformée de Fourier discrète (TFD). Ensuite, les données de fréquence sont codées et transmises au moyen de lignes téléphoniques ou de fibres optiques, par exemple, avant de finalement atteindre la destination où elles sont recueillies et décodées [31]. Ainsi, dans l'étude et la mise en oeuvre du schéma de commande basé sur les puissances injectées, nous ne pouvons négliger la totalité du temps nécessaire pour mesurer les fréquences des zones AC, effectuer la TFD, coder et transmettre des données au sous-contrôleur i, décoder les données reçues par le sous-contrôleur i, calculer une valeur de consigne pour P_i^{dc}, et l'appliquer au convertisseur. Cela peut à son tour entraîner une variation effective de P_i^{dc} qui est retardée par rapport à celle prédite par (11).

Pour donner une valeur numérique de ce temps de retard, notons que cela prend au moins une période, qui est d'environ 20ms (17ms, resp.) pour mesurer une fréquence proche de 50Hz (60Hz, resp.). En ce qui concerne le temps nécessaire pour coder, transmettre et décoder les informations de fréquence, il est de l'ordre de quelques centaines de millisecondes [32, 31]. A titre d'exemple, l'Union pour la coordination du transport de l'électricité (UCTE) ne garantit pas un retard de moins de 2 secondes pour transmettre des informations à partir d'un poste à un système SCADA distant [3]. En ce qui concerne le temps nécessaire pour un convertisseur d'injecter effectivement vers le réseau HVDC une puissance calculée par son sous-contrôleur, il peut atteindre jusqu'à plusieurs dizaines de millisecondes.

3.2 Etude théorique

Cette section rapporte une étude théorique sur les propriétés de stabilité du système sous le schéma de commande basé sur les puissances injectées autour du point de fonctionnement de référence. Tout d'abord, certaines hypothèses sont faites pour l'étude théorique. Deuxièmement, le modèle en boucle fermée est linéarisé autour du point de fonctionnement de référence. Troisièmement, nous démontrons l'existence d'un point d'équilibre unique. Quatrièmement, nous utilisons une approche du domaine fréquentiel pour prouver la stabilité pour le cas particulier où toutes les zones AC ont des paramètres identiques. Enfin, nous mettons en évidence les effets des gains de contrôleur et la matrice laplacienne sur la vitesse de convergence. Les preuves mathématiques détaillées sont données dans le Chapitre 5.2 en anglais.

Hypothèses

L'analyse de stabilité sur le schéma de commande basé sur les puissances injectées repose sur les hypothèses suivantes :

Hypothèse 3.1. *Les pertes au sein du réseau DC ne varient pas avec le temps, c'est à dire*

$$\sum_{i=1}^{N} \frac{dP_i^{dc}}{dt} = 0 \,. \tag{13}$$

Hypothèses 3.1 se justifie par le fait que les pertes dans le réseau DC sont faibles par rapport à la puissance échangée dans le réseau, et que les variations de ces pertes sont encore plus petites par rapport aux pertes totales quand $P_1^{dc}, P_2^{dc}, \ldots, P_{N-1}^{dc}$ varient selon (11).

Hypothèse 3.2. *Le graphe de communication représentant la disponibilité des informations de fréquence à différents sous-contrôleurs a les propriétés suivantes :*

- *Le graphe de communication est non orienté, c'est à dire si une zone a l'accès à l'information de fréquence d'une autre zone, alors cette dernière a également l'accès à l'information de fréquence de la première, à savoir si $b_{ik} = 1$, alors $b_{ik} = 1$, $\forall i \neq k, i, k \in \{1, 2, \ldots, N-1\}$.*
- *Le graphe de communication est connecté, c'est à dire qu'il ne peut se composer de plusieurs parties qui ne sont pas reliées, à savoir si $b_{ik} = 0$, alors il doit exister des indices intermédiaires $k_1, k_2, \ldots, k_m$ tels que $b_{ik_1} = b_{k_1k_2} = \ldots = b_{k_mj} = 1$.*
- *Il est constant dans le temps.*

Notez que lorsqu'elle est combinée avec l'Hypothèse 3.1, la première propriété de l'Hypothèse 3.2 implique que la dérivée temporelle de P_N^{dc} satisfait aussi (11), où $b_{Ni} = b_{iN}, \forall i \in \{1, 2, \ldots, N\}$.

Hypothèse 3.3. *Pour simplifier l'étude, nous supposons que les retards sont les mêmes quel que soit le sous-contrôleur considéré et nous le notons par τ.*

Linéarisation du système en boucle fermée

Nous nous concentrons sur de petites variations de la charge, et nous considérons donc un système linéarisé autour du point de fonctionnement de référence. Pour mettre en évidence les effets du retard sur le schéma de commande, la dépendance temporelle des variables est rendue explicite dans la notation.

L'équation non-linéaire résultant de (2) et (3) représentant la dynamique électromécanique de la zone i est linéarisée autour du point de fonctionnement de référence comme

$$2\pi J_i \frac{df_i(t)}{dt} = \frac{P_{mi}(t) - P_{li}^o(t) - P_i^{dc}(t)}{2\pi f_{nom,i}} - 2\pi D_i(f_i(t) - f_{nom,i}) \,, \tag{14a}$$

où $D_i = D_{gi} + \bar{P}_{li}^o D_{li}/(4\pi^2 f_{nom,i})$. La dynamique du réglage primaire de la zone i est modélisée par

$$T_{smi} \frac{dP_{mi}(t)}{dt} = P_{mi}^o - P_{mi}(t) - \frac{P_{nom,i}}{\sigma_i} \frac{f_i(t) - f_{nom,i}}{f_{nom,i}} \,. \tag{14b}$$

Equations (14a) et (14b) décrivent la dynamique en boucle ouverte de la zone i. Pour que cette section soit autonome, on réécrit ici la loi de commande[1] sous l'Hypothèse 3.3

$$\begin{aligned} P_i^{dc}(t) = \bar{P}_i^{dc} &+ \alpha_i \sum_{k=1}^{N} b_{ik} \int (\Delta f_i(t-\tau) - \Delta f_k(t-\tau))dt \\ &+ \beta_i \sum_{k=1}^{N} b_{ik}(\Delta f_i(t-\tau) - \Delta f_k(t-\tau)) \,, \end{aligned} \tag{14c}$$

[1] Il est à noter que nous avons aussi introduit délibérément un retard pour l'information de fréquence locale, de sorte que l'information de fréquence à distance à un instant est comparée avec l'information locale *au même instant*. Ce choix est conforme à la pratique dans l'étude sur les algorithmes pour le problème du consensus par la communauté d'automatique [33].

avec $i = 1, 2, \ldots, N-1$. En outre, sous les Hypothèses 3.1 et 3.2, $P_N^{dc}(t)$ satisfait aussi (14c).

Dans cette section, nous nous concentrons sur le système en boucle fermée défini par (14) pour tout $i \in \{1, 2, \ldots, N\}$.

Point d'équilibre

Proposition 3.1. *Considérons que le système, initialement au point de fonctionnement de référence, est soudainement soumis à un changement radical de la charge de l'une des zones AC. Alors, sous les Hypothèses 3.1 et 3.2, le système linéarisé défini par* (14)*, pour tout* $i \in \{1, 2, \ldots, N\}$ *a un point d'équilibre unique, pour lequel les déviations de fréquence de toutes les zones AC sont égales.*

La stabilité du système avec des zones AC identiques

Il est particulièrement difficile de prouver théoriquement la stabilité du système pour le cas général. Nous présentons ci-après un résultat pour le cas particulier où toutes les zones AC sont identiques. Plus précisément, nous supposons que tous les paramètres, ainsi que les fréquences nominales $f_{nom,i}$ et les charges $\bar{P}_{li}^o$, sont indépendants de l'indice de zone i ; mais, $\bar{P}_{mi}^o$ et $\bar{P}_i^{dc}$ peuvent être différentes d'une zone à l'autre. Proposition 3.2 établit la stabilité du système linéarisé. Le système original non-linéaire hérite les propriétés de stabilité de son homologue linéarisé à condition que les perturbations de la charge autour de la référence soient suffisamment petites.

Nous abandonnons les indices des zones AC pour désigner leurs paramètres identiques. Définissons

$$h(s) = \frac{a_2(s + a_4)}{(s + a_1)(s + a_4) + a_2 a_3} , \tag{15}$$

où $a_1 = D/J$, $a_2 = 1/(4\pi^2 f_{nom} J)$, $a_3 = P_{nom}/(T_{sm}\sigma_i f_{nom})$, et $a_4 = 1/T_{sm}$.

Proposition 3.2. *Considérons que toutes les zones AC du système ont des paramètres identiques, et que les Hypothèses 3.1, 3.2, et 3.3 sont satisfaites. Notons par* λ_N *et* λ_2 *respectivement la plus grande et la plus petite des valeurs propres non-nulles de la matrice laplacienne associée au graphe de communication. Alors, le système est stable, et suite à un changement radical de la charge, il converge asymptotiquement vers le point d'équilibre unique de la Proposition 3.1, si le nombre de l'encerclement net de n'importe quel point sur le segment* $(-1/\lambda_2, -1/\lambda_N)$ *par la courbe de Nyquist de* $h(s)(\alpha + \beta s)e^{-\tau s}/s$ *est égal à zéro.*

La vitesse de convergence des déviations de fréquence

Dans ce qui suit, nous étudierons les facteurs qui déterminent la vitesse de convergence des déviations de fréquence. A cette fin, nous prouvons qu'un tel système est stable quand $\tau = 0$. Ensuite, nous commentons le rôle des gains du contrôleur et celui de la matrice laplacienne.

Proposition 3.3. *Considérons que toutes les zones AC du système HVDC sous les Hypothèses 3.1, 3.2 et 3.3 ont des paramètres identiques et que* $\tau = 0$*. Alors, le point d'équilibre unique avec des déviations de fréquence égales est stable pour tout* $\alpha > 0$ *et* $\beta \geq 0$*.*

Remarque 3.1. *Si nous choisissons $\beta = 0$, alors le système converge à un rythme lent dicté par la dissipation du système. Un choix de $\beta > 0$ introduit un terme de dissipation dans le contrôleur et donne donc lieu à une convergence beaucoup plus rapide et moins oscillatoire à des déviations de fréquence égales.*

Remarque 3.2. *En fait, le gains du contrôleur α et β sont toujours multipliés par la valeur propre de la connectivité graphique. La vitesse de convergence la plus lente sera donc dictée par la valeur propre non-nulle la plus petite de la matrice laplacienne. Ce dernier est un objet d'études approfondies de la théorie des graphes, où il est appelé* la connectivité algébrique du graphe. *Cela devrait permettre d'évaluer quels graphes sont plus ou moins favorables (c'est à dire exigent des gains plus ou moins grands dans notre contrôleur) pour la synchronisation des déviations de fréquence.*

3.3 Simulations

L'efficacité du schéma de commande est montrée ci-après sur le système de référence décrit dans le chapitre précédent. Pour observer la réponse du système à un déséquilibre de puissance, nous supposons que toutes les zones initialement fonctionnent dans un état stable à la fréquence nominale. Puis, à $t = 2$s, une augmentation sous forme d'un échelon de 5% de la valeur de P_{l2}^{o} (voir l'Equation (2)) est considérée. Les équations différentielles en temps continu sont intégrées en utilisant une méthode d'Euler avec un pas de discrétisation de 1ms. Pour montrer l'efficacité du schéma de commande ainsi que le rôle des gains du contrôleur, nous ne considérons pas dans un premier temps le retard et nous discutons de résultats de la simulation dans ce cas. Enfin, nous mettons en évidence les effets du retard sur la stabilité du système sous commande.

Résultats quand $\tau = 0$s

La Figure 3 décrit l'évolution des fréquences lorsque $\tau = 0$s et $\alpha = \beta = 2 \times 10^6$. A titre de comparaison, nous montrons également dans la même figure la fréquence de la zone 2 lorsque le schéma de commande n'est pas appliqué ($\alpha = \beta = 0$). Les simulations montrent que, sans le schéma de commande, la fréquence de la zone 2 subit une déviation avec un maximum transitoire de 0,196Hz et se stabilise à 49,927Hz. Lorsque le schéma de commande est appliqué, la déviation maximale transitoire de la zone 2 tombe à 0,136Hz, et les fréquences des cinq zones convergent vers une valeur commune qui s´établit finalement à 49,983Hz. La Figure 4 montre l'évolution de $P_1^{dc}, P_2^{dc}, \ldots, P_5^{dc}$ exprimées en MW. P_2^{dc} est l'injection de puissance qui varie le plus rapidement. En particulier, elle diminue de 8% dans la seconde suivant l'augmentation radicale de la charge.

Les résultats sur ces deux figures montrent que notre schéma de commande conduit à une amélioration significative de la déviation de fréquence de la zone 2 en régime permanent, qui passe de 0,073Hz à 0,017Hz. Toutefois, la performance transitoire est assez pauvre, puisque la déviation transitoire maximale n´est que légèrement réduit de 0,196Hz à 0,136Hz. Pour améliorer la performance transitoire, nous augmentons les gains du contrôleur. Par souci de simplicité, nous imposons que $\alpha = \beta$. La Figure 5 montre les fréquences lorsque les gains du contrôleur sont augmentés à $\alpha = \beta = 1 \times 10^7$. Par rapport à la Figure 3, le comportement transitoire est nettement amélioré avec les gains du contrôleur plus grands : les fréquences de toutes les zones convergent plus rapidement ; la déviation maximale transitoire de la zone 2 est réduite à 0,075Hz, tandis que le point d'équilibre en régime permanent ne change pas, comme le suggère

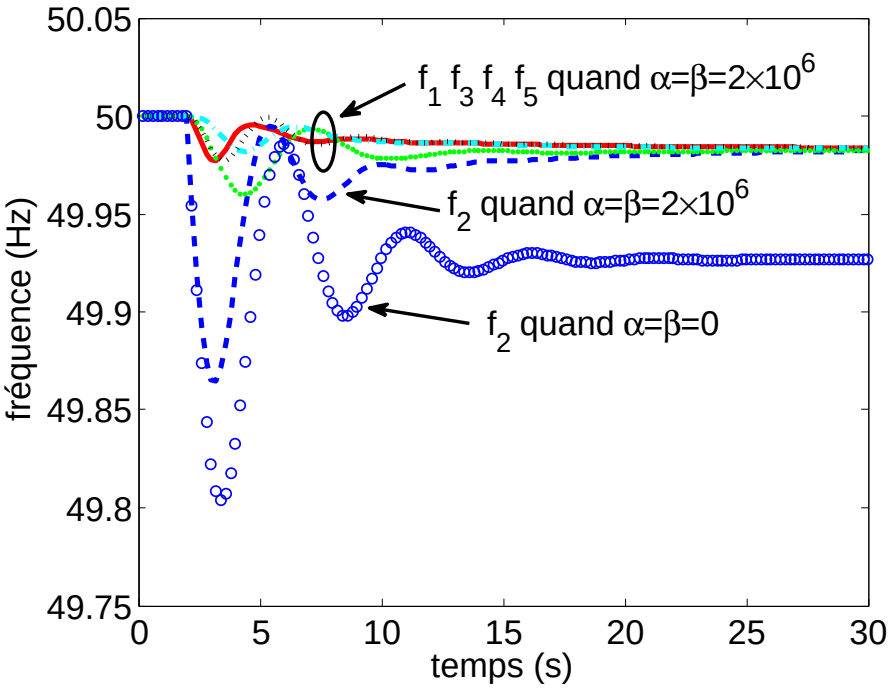

FIG. 3 – Fréquences des cinq zones AC sous le schéma de commande basé sur les puissances injectées lorsque $\tau = 0$s et $\alpha = \beta = 2 \times 10^6$. f_2 lorsque $\alpha = \beta = 0$ est aussi montrée.

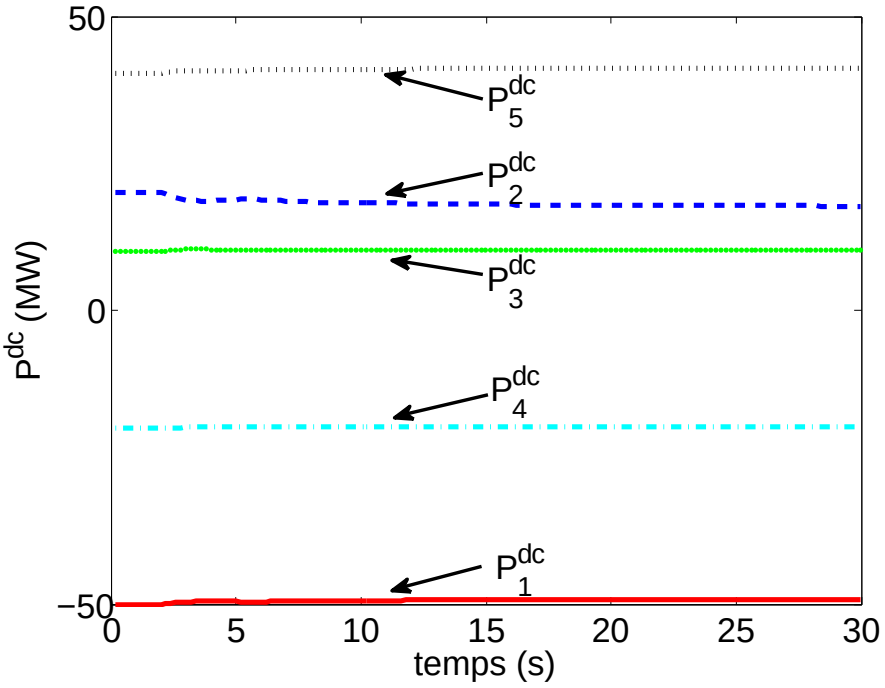

FIG. 4 – Injections de puissance à partir des cinq zones AC dans le réseau DC sous le schéma de commande basé sur les puissances injectées lorsque $\tau = 0$s et $\alpha = \beta = 2 \times 10^6$.

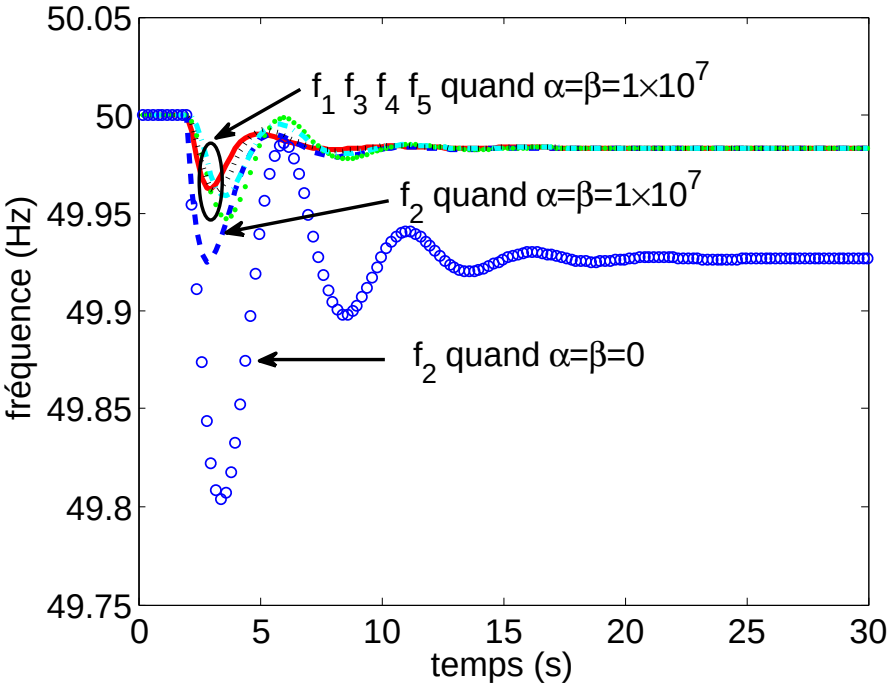

FIG. 5 – Fréquences des cinq zones AC sous le schéma de commande basé sur les puissances injectées lorsque $\tau = 0$s et $\alpha = \beta = 1 \times 10^7$. f_2 lorsque $\alpha = \beta = 0$ est aussi montrée.

la Proposition 3.1. L'amélioration dans le comportement transitoire se fait au prix de variations plus rapides des injections de puissance, qui sont représentées sur la Figure 6. Dans ce cas, P_2^{dc} diminue de 14% en une seconde après l'augmentation radicale de la charge. Néanmoins, même pour ces gains du contrôleur plus grands, les variations de P_i^{dc} restent modérées. D'un point de vue technique, les variations des injections de puissance représentées sur les figures sont inférieures aux limites de la vitesse de suivi des convertisseurs modernes, comme indiqué dans d'autres études telles que [34, 35].

Dans les simulations, nous avons considéré que la réserve primaire de chaque générateur était égale à sa puissance de sortie initiale. Pour le cas des réserves plus petites, les simulations supplémentaires non présentées ici montrent que les fréquences convergent toujours, même si certaines zones ont atteint leurs limites des réserves primaires. Toutefois, lorsque les réserves primaires de toutes les zones sont épuisées, les générateurs sont incapables de rétablir l'équilibre global d'énergie et toutes les fréquences diminuent constamment, jusqu'à ce qu'ils atteignent un certain seuil qui déclenche des mesures d'urgence telles que le délestage dans un système électrique réel.

3.4 Effets de la durée du temps de retard

Les simulations rapportées ci-dessus montrent que, pour $\tau = 0$s, le schéma de commande (14c) conduit les déviations de fréquence de toutes les zones à la même valeur. En outre, lorsque les fréquences sont stabilisées, la fréquence dans la zone 2 est égale à une valeur qui est plus

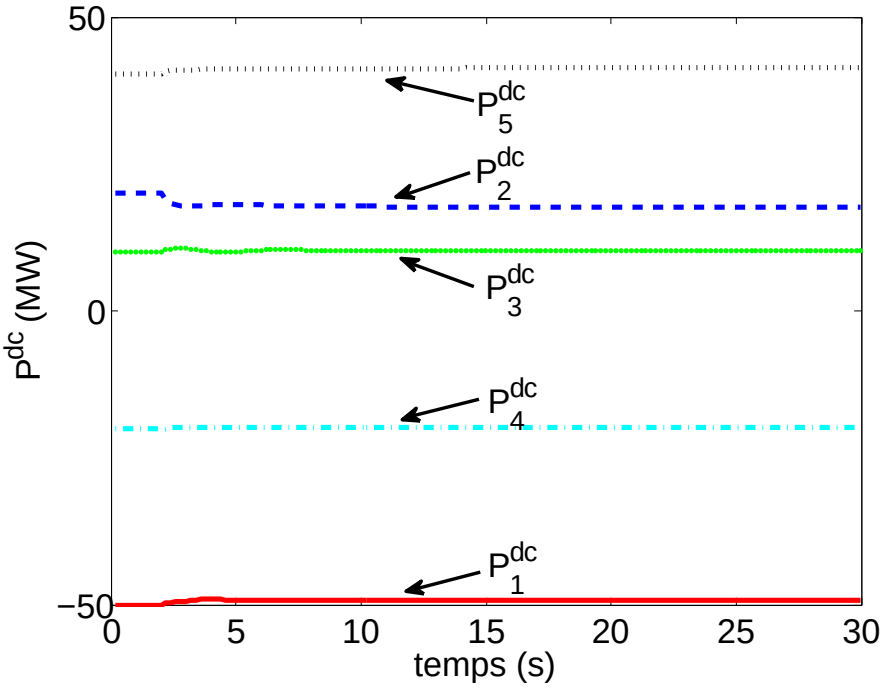

FIG. 6 – Injections de puissance à partir des cinq zones AC dans le réseau DC sous le schéma de commande basé sur les puissances injectées lorsque $\tau = 0$s et $\alpha = \beta = 1 \times 10^7$.

proche de $f_{nom,2}$ que le cas où les convertisseurs DC fonctionnent avec des injections de puissance constantes.

En revanche, en présence du temps de retard, des simulations montrent que les déviations de fréquence risquent de ne pas converger. En particulier, pour des valeurs données de α et β, il existe généralement une durée maximale acceptable du retard au-delà duquel les zones AC manifestent des oscillations des fréquences d'une grandeur de plus en plus importante. Par exemple, lorsque les gains du régulateur sont choisis comme 2×10^6, f_1 converge toujours en dépit des oscillations quand $\tau = 0,5$s et elle ne converge plus lorsque $\tau = 0,8$s, comme indiqué sur la Figure 7. A titre de comparaison, l'évolution de f_1 lorsque $\tau = 0$s est également indiquée dans la même figure.

Pour déterminer si les déviations de fréquence de toutes les zones AC convergent, nous définissons le critère suivant, similaire à la bande d'erreur utilisée dans la définition du temps d'établissement en automatique [36]. Notons par Δf^e la valeur commune à laquelle les déviations de fréquence des zones AC convergent lorsque $\tau = 0$ s. Nous classons le système comme pratiquement stable si, après $t > 22$s, soit 20 secondes après le changement radical de la charge, les déviations de fréquence de toutes les zones AC restent dans la bande de $\pm$ 50mHz autour de Δf^e, soit

$$|\Delta f_i(t) - \Delta f^e| \leq 50\text{mHz}, \forall i \text{ et } \forall t > 22\text{s} \ . \tag{16}$$

Nous définissons $\tau_{\max}$ comme la plus grande valeur du retard pour lequel (16) est satisfaite et nous recherchons une relation qui peut exister entre $\tau_{\max}$ et les gains du contrôleur. Pour faciliter l'analyse, nous imposons que $\alpha = \beta$. Nous calculons $\tau_{\max}$ pour différentes valeurs de

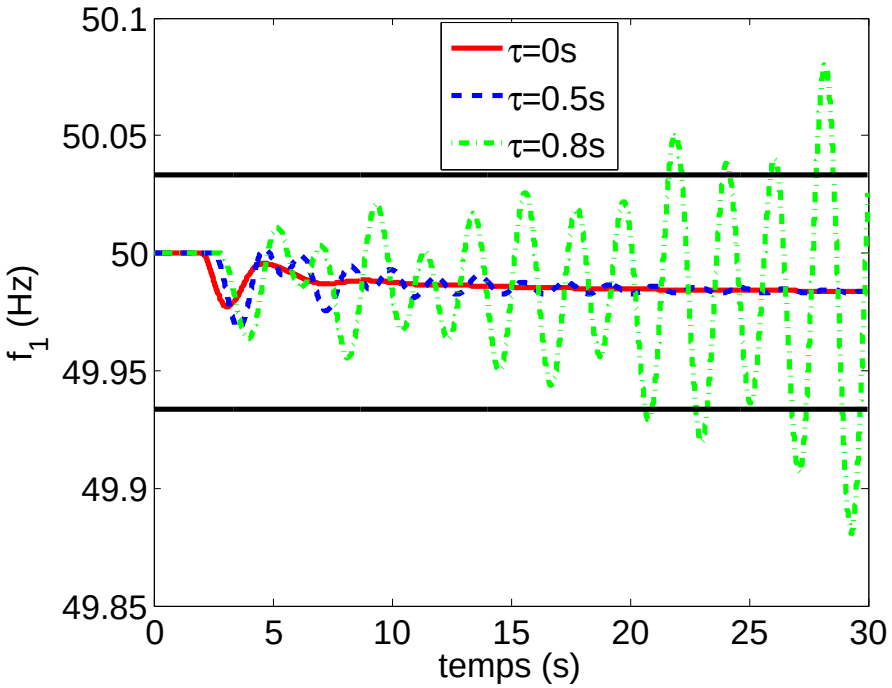

FIG. 7 – Fréquence de la zone 1 pour $\tau = 0$s, $\tau = 0.5$s, et $\tau = 0.8$s sous le schéma de commande basé sur les puissances injectées lorsque $\alpha = \beta = 2 \times 10^6$. Les deux lignes horizontales tracent la bande du critère de stabilié pratique, qui est ± 50mHz autour de Δf^e.

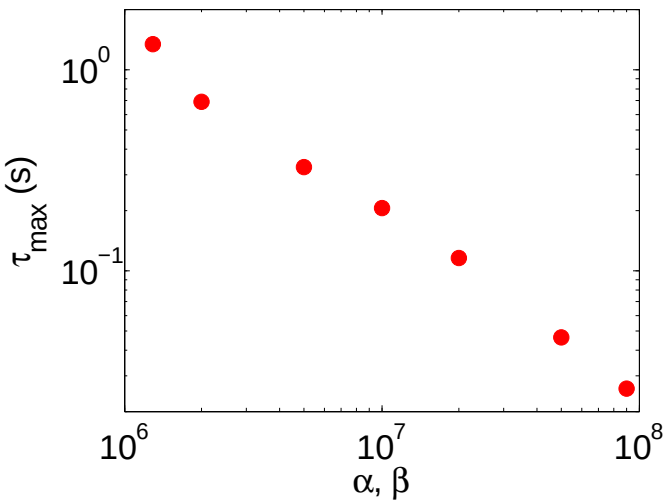

FIG. 8 – Valeurs de $\tau_{\max}$ pour divers valeurs de $\alpha = \beta$.

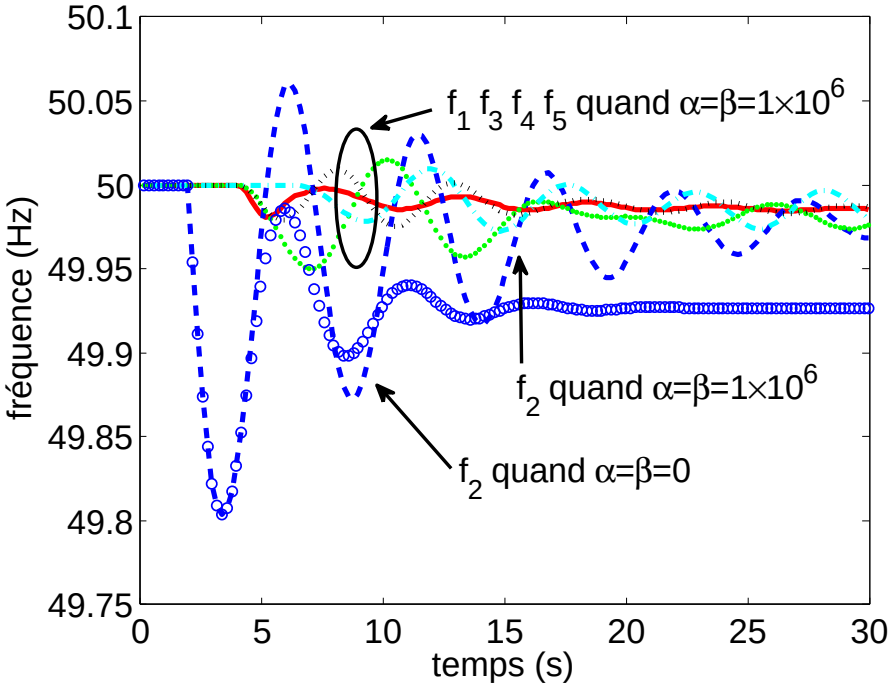

FIG. 9 – Fréquences des cinq zones AC sous le schéma de commande basé sur les puissances injectées lorsque $\tau = 2$s et $\alpha = \beta = 2 \times 10^6$. f_2 lorsque $\alpha = \beta = 0$ est aussi montrée.

$\alpha = \beta \in [1 \times 10^6, 1 \times 10^8]$ par une recherche binaire dans $\tau \in [0, 2]$s.

Les points sur la Figure 8 représentent les valeurs de $\tau_{\max}$ correspondant aux différentes valeurs de $\alpha = \beta$. Nous constatons que par la baisse des valeurs des gains du contrôleur, les oscillations nuisibles introduites par le retard peuvent être amorties. Par exemple, si τ est d'environ deux secondes pour notre système, nous devons diminuer les gains du contrôleur à une valeur d'environ 1×10^6 pour éviter les problèmes de stabilité. Toutefois, comme on l'a souligné plus tôt dans cette sous-section, avec des valeurs petites des gains du contrôleur, plus de temps est nécessaire pour faire converger les déviations de fréquence vers une valeur commune.

Ce phénomène est illustré ici pour $\tau = 2$s par les deux ensembles de courbes dans les Figures 9 et 10 qui représentent l'évolution des fréquences dans les cinq zones du système pour $\alpha = \beta = 1 \times 10^6$ et pour $\alpha = \beta = 1 \times 10^5$. Notez que nous avons également représenté sur ces figures l'évolution de f_2 lorsque le schéma de commande n'est pas mis en oeuvre (c'est à dire $\alpha = \beta = 0$).

4 Schéma de commande basé sur les tensions DC

4.1 Introduction

Dans le chapitre précédent, nous proposons un schéma de commande qui modifie les injections de puissance vers le réseau DC en fonction des mesures de fréquence d'autres zones afin de faire

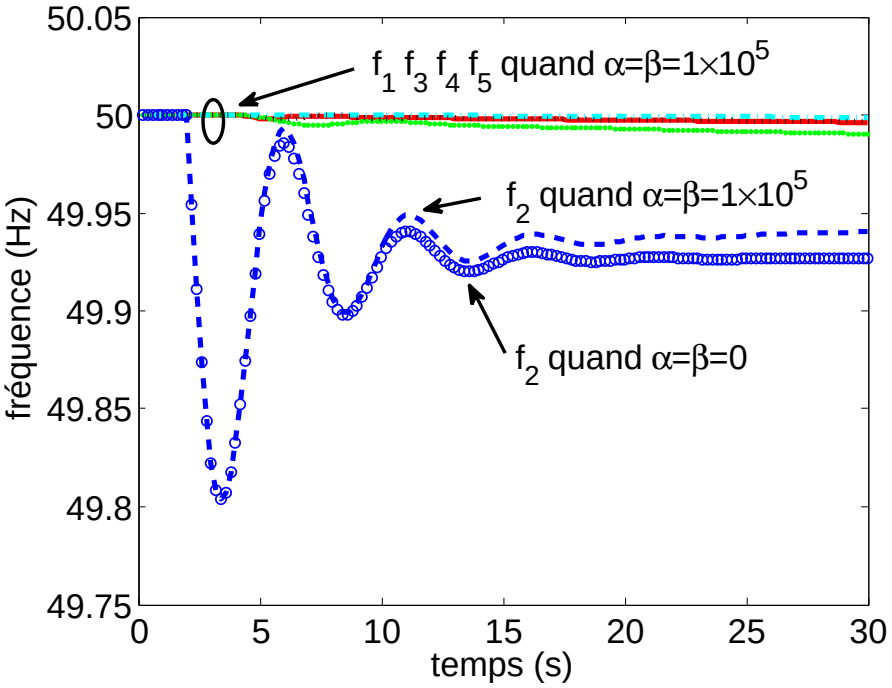

FIG. 10 – Fréquences des cinq zones AC sous le schéma de commande basé sur les puissances injectées lorsque $\tau = 2$s et $\alpha = \beta = 2 \times 10^5$. f_2 lorsque $\alpha = \beta = 0$ est aussi montrée.

évoluer leurs déviations de fréquence vers une même valeur. Ce schéma de commande fait réagir collectivement les zones AC aux déséquilibres de puissance. Puisque cette approche nécessite la transmission d'informations de fréquence entre les zones AC, un retard considérable (de l'ordre de quelques secondes) est à prévoir. Comme indiqué précédemment, un tel retard réduit l'efficacité du schéma de commande et peut même conduire à l'instabilité.

Dans cette chapitre, nous proposons un autre schéma de commande qui prend des décisions en fonction uniquement de la mesure de fréquence locale, éliminant ainsi le besoin de communication entre les zones AC situées à distance. Nous l'appelons *schéma de commande basé sur les tensions DC* car il utilise les tensions DC des convertisseurs HVDC comme les variables de commande.

Section 4.2 précise le nouveau schéma de commande. Section 4.3 analyse théoriquement la stabilité du système en boucle fermée. Section 4.4 présente les résultats de simulations.

Les résultats présentés dans ce chapitre ont été publiés dans [37].

4.2 Loi de commande

Nous continuons d'utiliser le modèle HVDC à plusieurs terminaux présenté dans la Section 2.1. Aussi, nous supposons que, préalablement à toute perturbation, le système est au point de fonctionnement de référence décrit dans la Section 2.2.

Expression analytique

Le schéma de commande basé sur les tensions DC est décentralisé par nature et il se compose de N sous-contrôleur, un pour chaque convertisseur HVDC. Le sous-contrôleur du convertisseur $i \in \{1, 2, \ldots, N\}$ modifie la valeur de V_i^{dc} tel que

$$V_i^{dc} = \bar{V}_i^{dc} + \alpha_i \Delta f_i \ , \tag{17}$$

où

- $\Delta f_i = f_i - f_{nom,i}$ est la déviation de fréquence de la zone i ;
- α_i est le gain du sous-contrôleur i.

La valeur du gain du sous-contrôleur α_i a un impact significatif sur la dynamique du système. De manière générale, une zone avec une valeur plus grande de α_i restera plus proche de sa fréquence nominale qu'une zone avec un α_i plus petit.

Principe de fonctionnement

L'intuition derrière la loi de commande définie par (17) est la suivante. Si par exemple le zone i a une production plus importante que la somme de la charge et l'injection vers le réseau DC, alors sa fréquence f_i va augmenter. Pour rétablir l'équilibre de la zone i, plus d'énergie doit être injectée de la zone i vers le réseau DC. Pour ce faire, la tension continue V_i^{dc} est augmentée de sorte que la différence de tension $V_i^{dc} - V_k^{dc}$ devienne plus élevée, avec V_k^{dc} inchangée, pour tout $k \neq i$. En vertu du flux de charge DC (1), cela donne lieu à une augmentation de l'injection de puissance de la zone i vers les autres zones. Ces dernières, qui injectent moins de puissance vers (ou de façon équivalente, retirent plus de puissance à partir de) le réseau DC, voient leurs fréquences augmenter et par conséquent élèvent également leurs tensions. En conclusion, le réseau dans son ensemble réagit au déséquilibre dans la zone i, en répartissant la déviation de fréquence sur toutes les zones.

Contraintes

Les contraintes sont les mêmes que celles dans le chapitre précédent. Pour le schéma de commande basé sur les tensions DC, les contraintes sur P_i^{dc} peuvent être *dynamiquement* assimilées aux contraintes sur V_i^{dc}. En particulier, si $P_i^{dc} = P_i^{dc,\max}$, nous pouvons exiger que V_i^{dc} n'augmente pas davantage, ou encore, qu'elle prenne la valeur actuelle de V_i^{dc} comme la nouvelle $V_i^{dc,\max}$. En outre, lorsque V_k^{dc}, $k \neq i$ baisse, $V_i^{dc,\max}$ (et donc V_i^{dc}) devrait également diminuer, afin de garantir que P_i^{dc} ne dépasse pas ses limites.

4.3 Etude théorique

Cette section rapporte une étude théorique sur les propriétés de stabilité du système sous le schéma de commande basé sur les tensions DC autour du point de fonctionnement de référence. Tout d'abord, le modèle linéarisé en boucle fermée utilisé dans l'étude théorique est présenté. Deuxièmement, nous démontrons l'existence d'un point d'équilibre unique. Troisièmement, nous démontrons la stabilité en utilisant une nouvelle approche dans le domaine fréquentiel. Enfin, le point d'équilibre unique pour ce cas est caractérisé pour mettre en évidence l'efficacité du

contrôleur et illustrer l'influence du gain du contrôleur. Les preuves mathématiques détaillées sont données dans le Chapitre 6.2 en anglais.

Linéarisation du système en boucle fermée

Nous nous concentrons sur de petites variations de la charge, et nous considérons donc un système linéarisé autour du point de fonctionnement de référence. Comme aucun retard est impliqué dans le schéma de commande basé sur les tension DC, nous omettons dans la notation la dépendance des variables vis-à-vis du temps.

Les équations différentielles décrivant la dynamique en boucle ouverte de la zone i sont les mêmes que dans le chapitre précédent, soit

$$2\pi J_i \frac{df_i}{dt} = \frac{P_{mi} - P_{li}^o - P_i^{dc}}{2\pi f_{nom,i}} - 2\pi D_i(f_i - f_{nom,i}) \,, \tag{18a}$$

$$T_{smi} \frac{dP_{mi}}{dt} = P_{mi}^o - P_{mi} - \frac{P_{nom,i}}{\sigma_i} \frac{f_i - f_{nom,i}}{f_{nom,i}} \,. \tag{18b}$$

Le flux de charge DC (1) est linéarisé autour du point de référence de fonctionnement comme

$$P_i^{dc} = \sum_{k=1}^{N} \frac{V_{ref}^{dc}(V_i^{dc} - V_k^{dc})}{R_{ik}} \,. \tag{18c}$$

Puisque $V_1^{dc}, V_2^{dc}, \ldots, V_N^{dc}$ sont toutes proche de V_{ref}^{dc} sous opération normale, nous faisons une approximation de (1) par

$$V_i^{dc} = \bar{V}_i^{dc} + \alpha_i \Delta f_i \,. \tag{18d}$$

Dans cette section, nous nous concentrons sur le système en boucle fermée définie par (18) pour tout $i \in \{1, 2, \ldots, N\}$.

Point d'équilibre

Proposition 4.1. *Considérons que le système, d'abord fonctionnant au point de fonctionnement de référence, est soudainement soumis à un changement radical dans la demande de la charge de l'une de ses zones AC. Alors, le système (linéarisé) définie par* (18) *pour tout* $i \in \{1, 2, \ldots, N\}$ *a un point d'équilibre unique.*

La stabilité du système

Pour le schéma de commande basé sur les tension DC, nous avons une proposition pour le cas général des zones hétérogènes AC.

Proposition 4.2. *Le système en boucle fermée défini par* (18) *pour tout* $i \in \{1, 2, \ldots, N\}$ *est stable.*

Caractérisation du point d'équilibre

L'analyse précédente prouve la stabilité du système. Cette sous-section se concentre sur l'objectif du schéma de commande, c'est à dire maintenir les déviations de fréquence des différentes zones AC proches les unes des autres. Par souci de simplicité, l'analyse théorique se concentre sur le cas particulier où toutes les zones AC ont des paramètres identiques.

Proposition 4.3. *Supposons que toutes les zones AC ont des paramètres identiques. Pour toute valeur donnée de* $\bar{V}_1^{dc}, \bar{V}_2^{dc}, \ldots, \bar{V}_N^{dc}$ *et pour toute variation de la charge, la différence entre les déviations de fréquence des zones AC au point d'équilibre du système (linéarisé) peut être rendue arbitrairement petite en prenant le gain du contrôleur suffisamment grand.*

4.4 Simulations

L'efficacité du schéma de commande proposée est illustrée ci-après dans le cadre du système de référence à cinq zones décrit dans le chapitre précédent. Les conditions de simulation sont également les mêmes que celles dans la Section 3.3.

La Figure 11 représente l'évolution des fréquences lorsque $\alpha = 2\times10^3$. A titre de comparaison, il montre également l'évolution de f_2 lorsque $\alpha = 0$ (c'est à dire $V_1^{dc}, V_2^{dc}, \ldots, V_5^{dc}$ DC sont maintenues constantes). Ces simulations montrent que, sans le contrôleur ($\alpha = 0$), la fréquence de la zone 2 subit une déviation avec un maximum transitoire de 0,196 Hz et se stabilise à 49,927Hz. Avec le contrôleur défini par (17), la déviation maximale transitoire de f_2 tombe à 0,055Hz, et les fréquences des cinq zones présentent le même comportement de variation et enfin s'installent dans une bande comprise entre 49,976Hz et 49,988Hz. Les courbes représentant l'évolution des variables de contrôle, $V_1^{dc}, V_2^{dc}, \ldots, V_5^{dc}$, sont présentées sur la Figure 12. Nous constatons que les variations de V_i^{dc} sont proportionnelles à la déviation de fréquence de la zone correspondante, et que ces variations restent inférieures à la grandeur des valeurs initiales $\bar{V}_i^{dc}$, ce qui indique que de telles variations ne donnent pas lieu à des tensions excessivement élevées ou faibles dans le réseau DC. La Figure 13 montre l'évolution des injections de puissance des zones AC vers le réseau DC, $P_1^{dc}, P_2^{dc}, \ldots, P_5^{dc}$, exprimées en MW. Les variations sont modérées dans la mesure où elles n'excèdent pas 10 % de la valeur initiale.

Ces résultats montrent que notre schéma de commande conduit à une amélioration significative dans les déviations de fréquence en régime permanent (de 0,073Hz à 0,024Hz) et les déviations maximales transitoires (de 0,196Hz à 0,055Hz) de la zone 2. Toutefois, les déviations de fréquence des différentes zones AC ne convergent pas l'unes vers les autres et elles restent dans une bande dont la largeur est 0,012Hz.

Les Figures 14-16 montrent les résultats lorsque α est doublé à 4×10^3. Nous constatons que la largeur de la bande de fréquences en régime permanent est réduite à 0,007Hz. Cela indique qu'une propriété similaire à la Proposition 4.3 semble encore tenir lorsque les zones AC ont des paramètres de valeurs différentes.

5 Coordination au niveau du réglage secondaire de la fréquence

Les deux schémas de commande proposés dans les chapitres précédents font réagir collectivement les zones AC à des déséquilibres de puissance au sein du système, mais comme il est indiqué

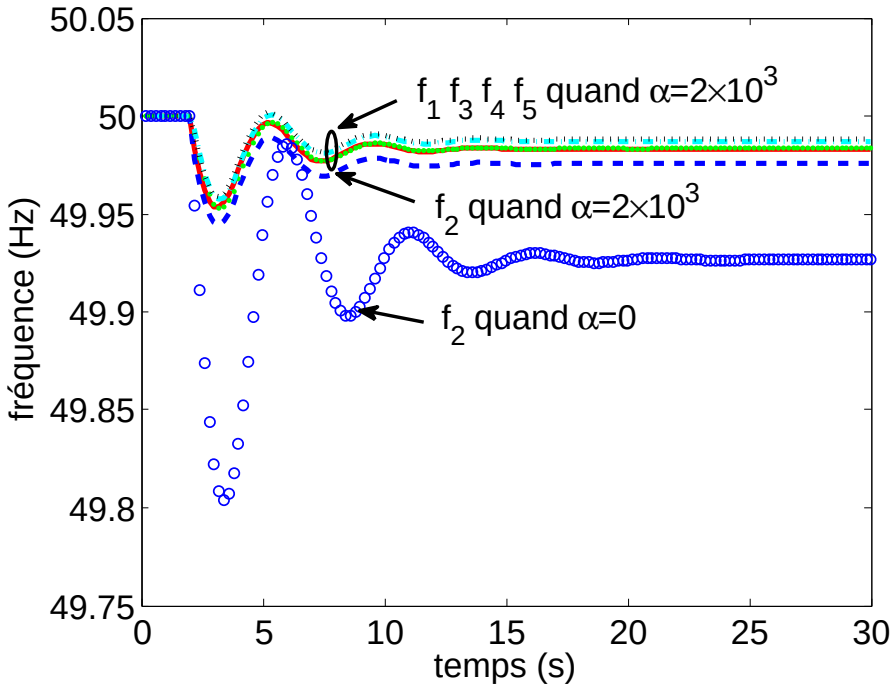

FIG. 11 – Fréquences des cinq zones AC sous le schéma de commande basé sur les tensions DC lorsque $\alpha = 2 \times 10^3$. f_2 lorsque $\alpha = 0$ est aussi montrée.

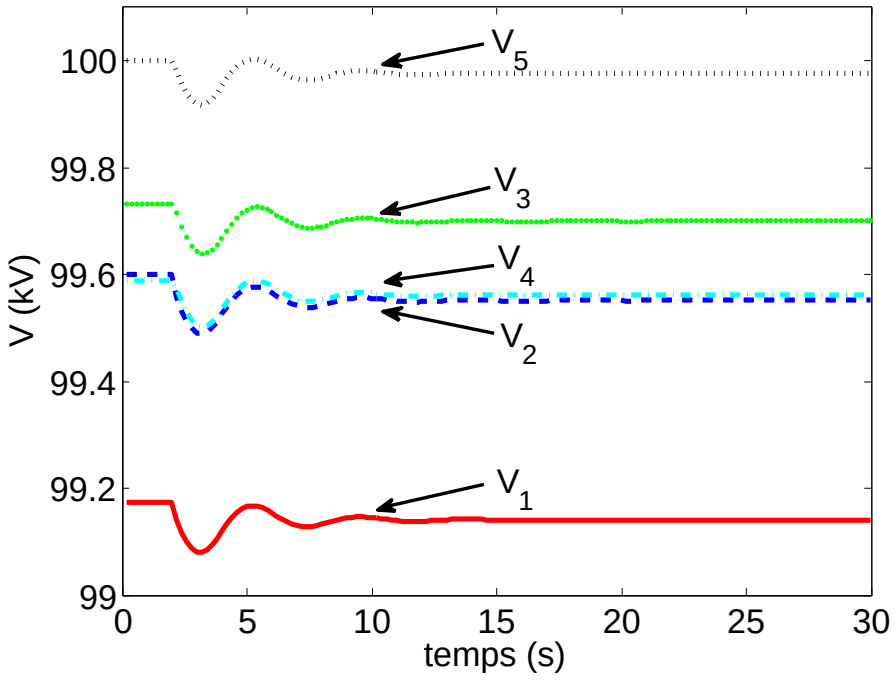

FIG. 12 – Les tensions DC des convertisseurs sous le schéma de commande basé sur les tensions DC lorsque $\alpha = 2 \times 10^3$.

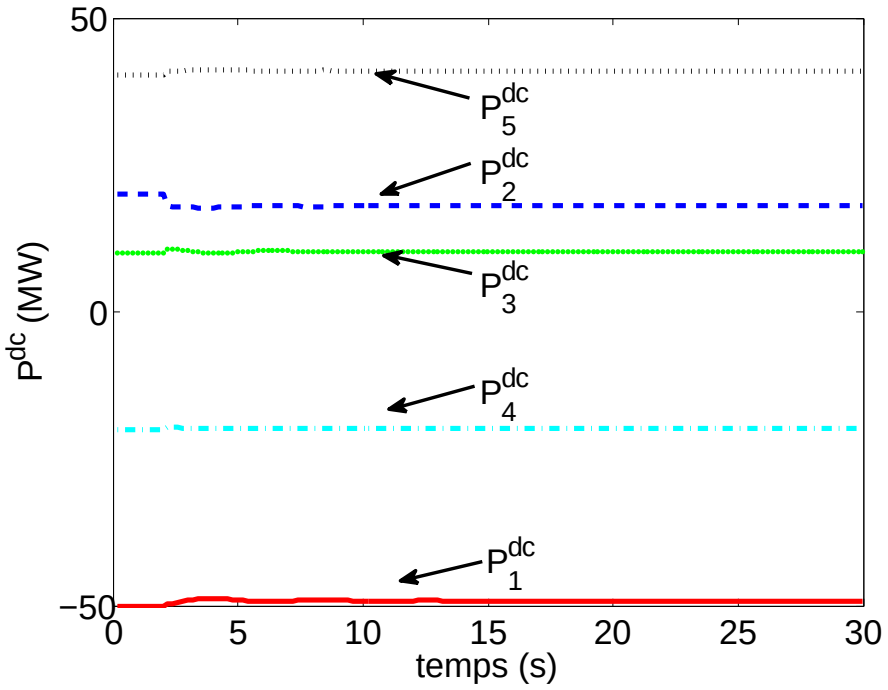

FIG. 13 – Injections de puissance à partir des cinq zones AC dans le réseau DC sous le schéma de commande basé sur les tensions DC lorsque $\alpha = 2 \times 10^3$.

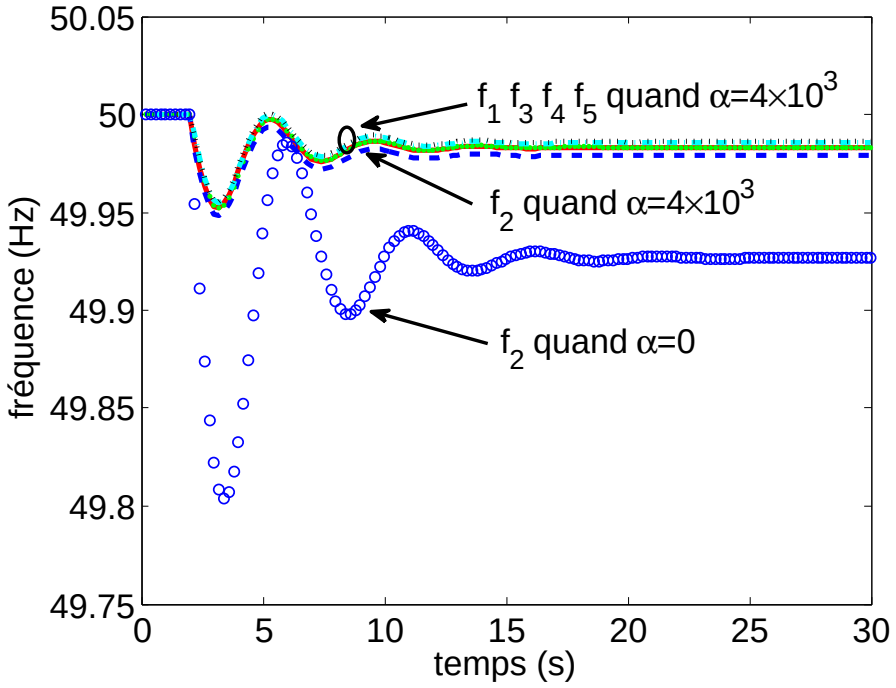

FIG. 14 – Fréquences des cinq zones AC sous le schéma de commande basé sur les tensions DC lorsque $\alpha = 4 \times 10^3$. f_2 lorsque $\alpha = 0$ est aussi montrée.

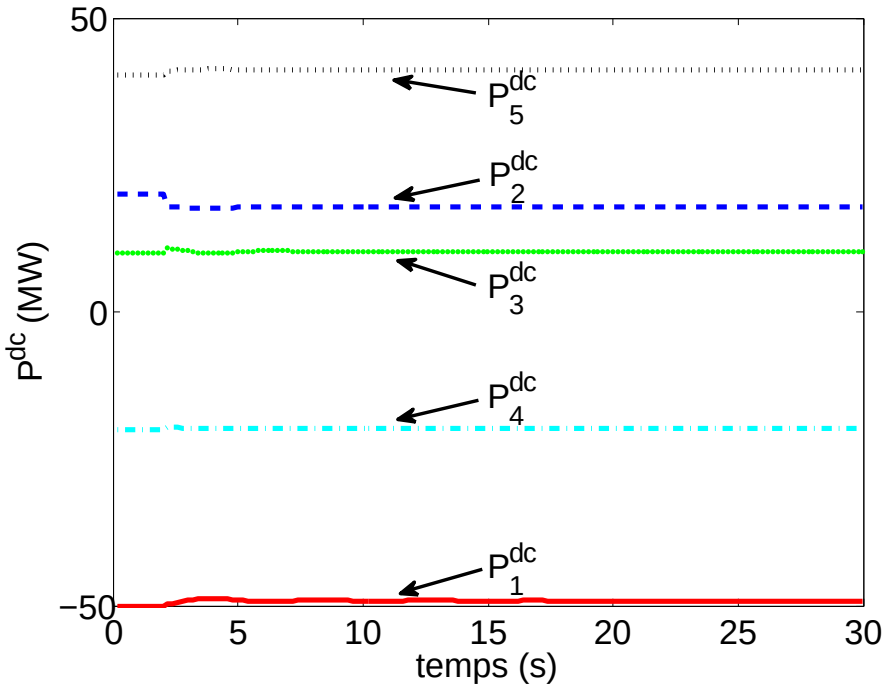

FIG. 15 – Les tensions DC des convertisseurs sous le schéma de commande basé sur les tensions DC lorsque $\alpha = 4 \times 10^3$.

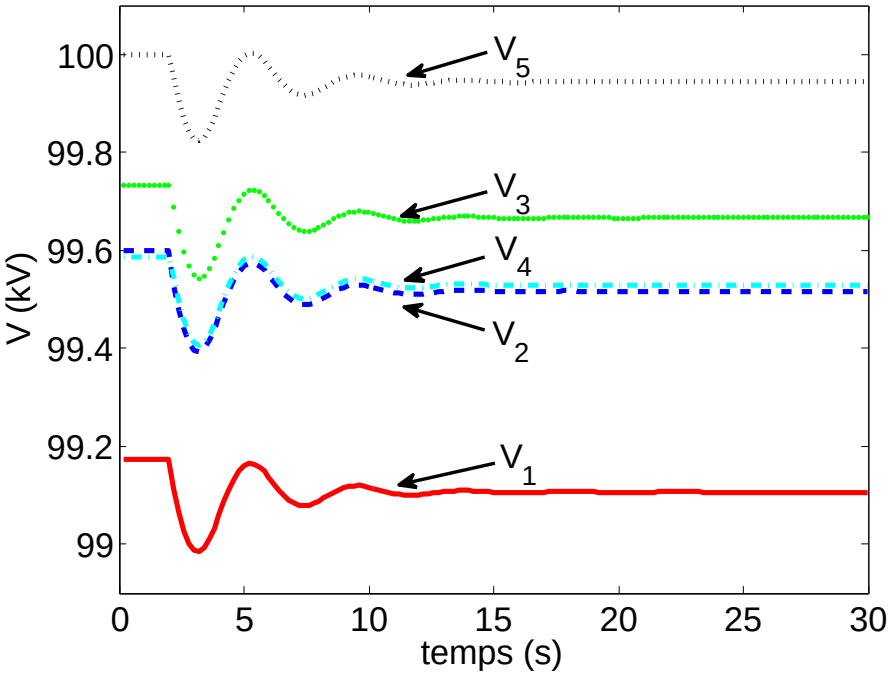

FIG. 16 – Injections de puissance à partir des cinq zones AC dans le réseau DC sous le schéma de commande basé sur les tensions DC lorsque $\alpha = 4 \times 10^3$.

dans les Propositions 3.1 et 4.1, les schémas de commande ne font revenir ni la fréquences, ni les échanges de puissance entre les zones à leurs valeurs nominales ou programmées. Pour restaurer les fréquences et les échanges de puissance, chaque zone doit recourir au réglage secondaire de la fréquence, qui agit sur la consigne de la puissance mécanique du générateur agrégé.

Pour discuter de la dynamique à long terme des zones AC reliés par un système MT-HVDC sous les deux schémas de commande proposés, nous présentons dans ce chapitre une solution pour les zones AC d'implémenter le réglage secondaire de la fréquence conformément aux recommandations de l'UCTE. Section 5.1 décrit le contrôleur secondaire de la fréquence, qui est inspiré par la pratique de l'UCTE pour le réglage secondaire de la fréquence dans une zone synchrone. Section 5.2 présente les résultats de simulations.

5.1 Schéma de commande du réglage secondaire de la fréquence

Le réglage secondaire de la fréquence a deux objectifs : (i) restaurer les fréquences de toutes les zones AC à leurs valeurs nominales, (ii) restaurer la puissance échangée entre les zones AC à leurs valeurs programmées. Ces objectifs ne peuvent être atteints que si tout déséquilibre de puissance est entièrement compensé par un changement de la consigne de la puissance mécanique des générateurs de la zone dont il est originaire.

L'énergie réglante de la zone i est définie comme

$$\lambda_i^{\mathrm{ER}} = \frac{-\Delta P_i^{dc*}}{\Delta f_i} \,, \tag{19}$$

où ΔP_i^{dc*} est la variation de l'injection de puissance de la zone i vers le réseau DC par rapport à sa valeur prévue suite à un déséquilibre de puissance provenant *à l'extérieur de la zone* i, et Δf_i est la déviation de fréquence de la zone i par rapport à sa valeur nominale. L'énergie réglante peut être utilisée pour évaluer l'erreur de réglage, qui est défini comme

$$E_i = \Delta P_i^{dc} + \lambda_i^{\mathrm{ER}} \Delta f_i \,, \tag{20}$$

où ΔP_i^{dc} est la variation *réelle* de l'injection de puissance de la zone i vers le réseau DC par rapport à sa valeur prévue, où que ce soit le déséquilibre de puissance.

Pour réaliser le réglage secondaire de la fréquence, chaque zone emploie un contrôleur intégral qui ajuste la consigne de la puissance mécanique des générateurs dans cette zone. La sortie du contrôleur secondaire de la fréquence pour la zone i est donnée comme

$$P_{mi}^o = \bar{P}_{mi}^o - \gamma_i \int E_i dt \,, \tag{21}$$

où $\bar{P}_{mi}^o$ est la valeur de P_{mi}^o au point de fonctionnement de référence défini dans la Section 2.2, et $\gamma_i > 0$ est le gain du contrôleur secondaire de la fréquence pour la zone i. La valeur de γ_i doit être choisie assez modérée pour que la dynamique de P_{mi}^o soit découplée du réglage primaire de la fréquence et que le réglage secondaire n'ait pas d'effet contradictoire au réglage primaire.

5.2 Résultats de simulations

Pour illustrer l'impact du réglage secondaire de la fréquence, nous effectuons des simulations dans les mêmes conditions que dans la Section 3.3. Les Figures 17 et 18 montrent l'évolution des

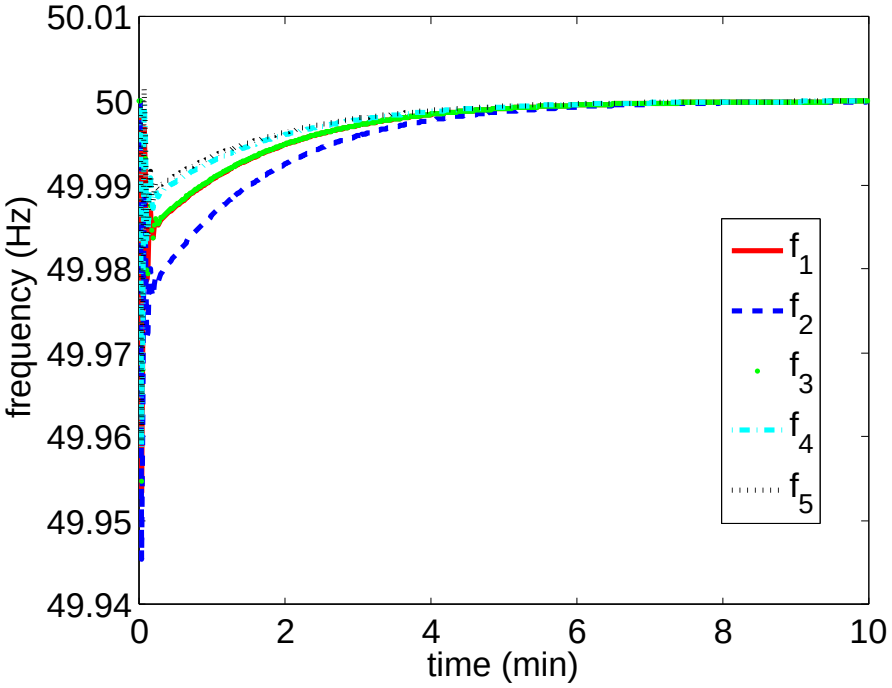

FIG. 17 – Fréquences des cinq zones AC sous le schéma de commande basé sur les tensions DC et schéma de commande pour le réglage secondaire.

fréquences et les consignes de puissance P_m^o des cinq zones AC lorsque le schéma de commande pour le réglage secondaire de la fréquence est mis en oeuvre en combinaison avec le schéma de commande basé sur les tensions DC. Les Figures 19 et 20 montrent l'évolution de ΔV^{dc} et ΔP^{dc} , qui sont les variations de V^{dc} and P^{dc} par rapport à leurs valeurs nominales ou programmées. Puisque le réglage secondaire de la fréquence a une échelle de temps de quelques minutes, nous étendons la fenêtre d'observation à 10 minutes. Les gains des contrôleurs sont choisis tels que $\alpha_1 = \alpha_2 = \ldots = \alpha_5 = 2 \times 10^3$ et $\gamma_1 = \gamma_2 = \ldots = \gamma_5 = 2$.

Le comportement pendant les premières secondes dans la figure 17 est essentiellement la même chose que dans la Figure 11 dans le chapitre précédent. Cela signifie que le réglage primaire de la fréquence domine, non perturbé par le réglage secondaire de la fréquence. Ce dernier agit comme prévu : seule la consigne de puissance pour la zone perturbée, P_{m2}^o, est modifiée de façon significative, et les fréquences convergent vers leurs valeurs nominales à long terme. L'évolution de P_i^{dc} indique que les injections de puissance vers le réseau DC sont également restaurées à leurs valeurs programmées. En outre, les tensions continues des convertisseurs V_i^{dc} reviennent à leurs valeurs initiales.

Les résultats ci-dessus montrent que notre schéma de commande pour le réglage secondaire de la fréquence atteint ses deux objectifs : rétablir les fréquences et les échanges de puissance à leurs valeurs nominales ou programmées. En outre, le réglage secondaire agit dans quelques minutes, donc les variations de P_m^o sont bien découplées du schéma de commande basé sur les tensions DC pour le réglage primaire de la fréquence.

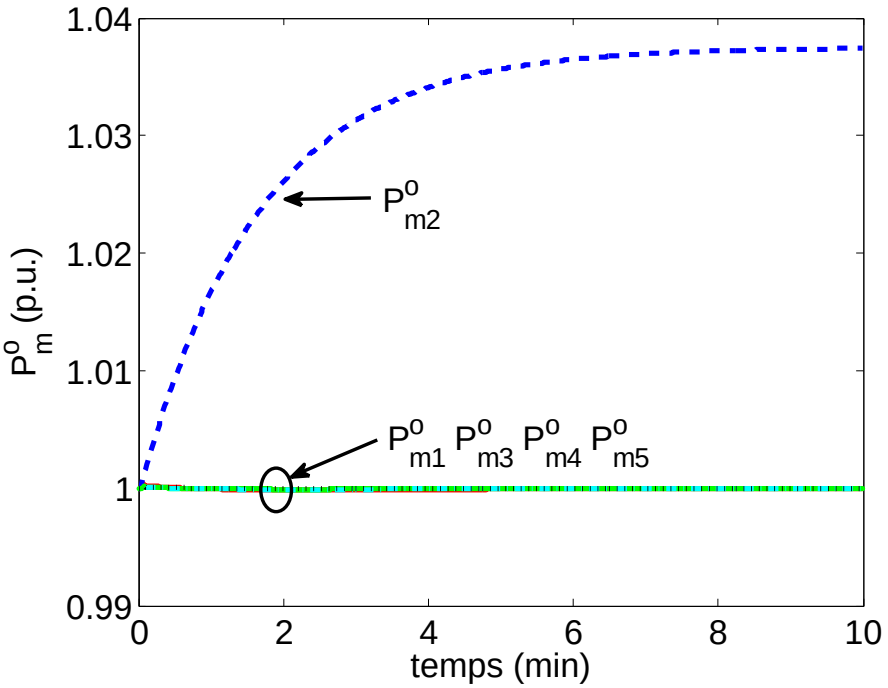

FIG. 18 – P^o_m des cinq zones AC sous le schéma de commande basé sur les tensions DC et schéma de commande pour le réglage secondaire.

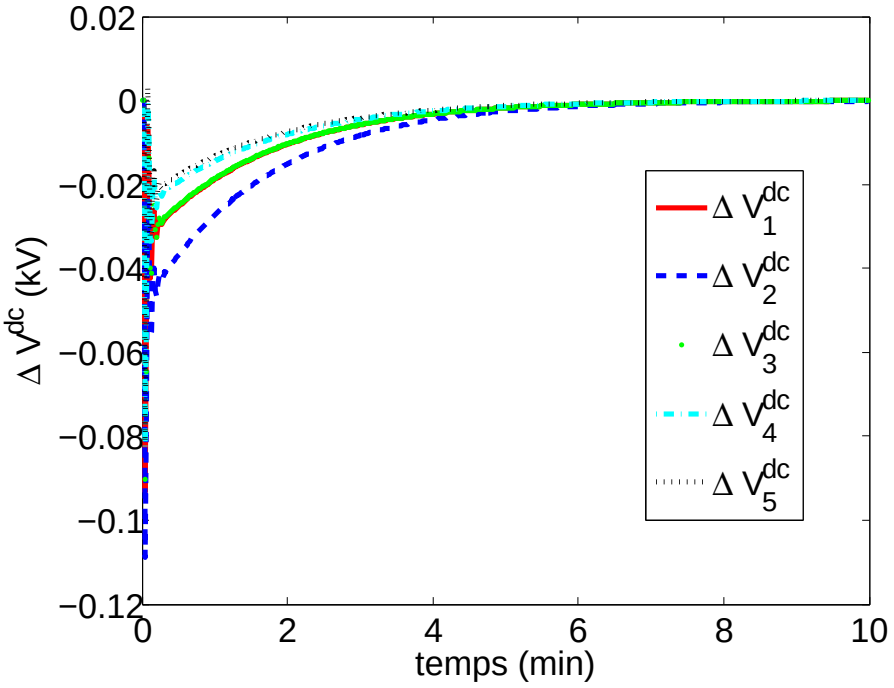

FIG. 19 – ΔV^{dc} des cinq zones AC sous le schéma de commande basé sur les tensions DC et schéma de commande pour le réglage secondaire.

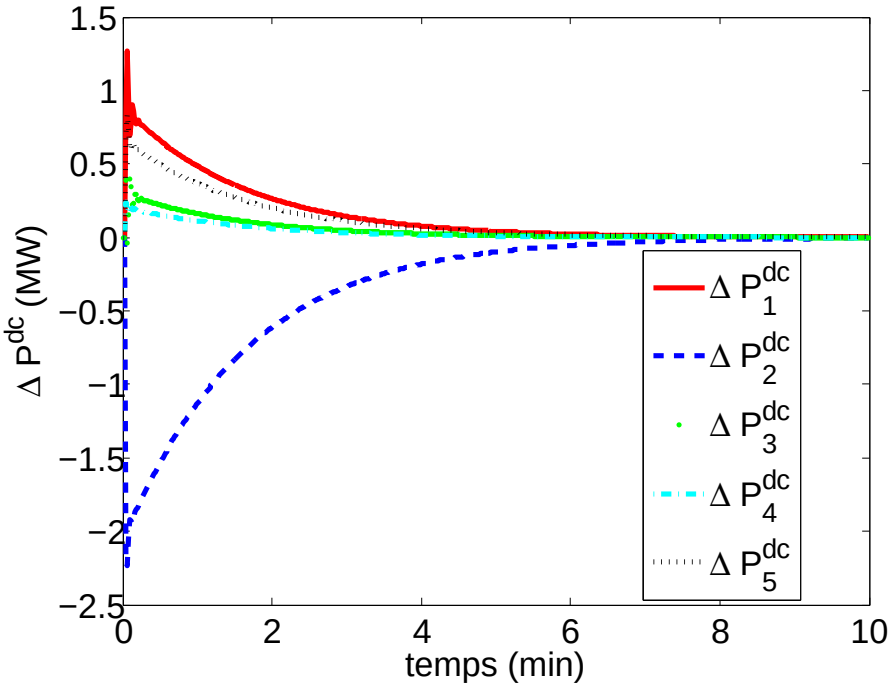

FIG. 20 – ΔP^{dc} des cinq zones AC sous le schéma de commande basé sur les tensions DC et schéma de commande pour le réglage secondaire.

6 Conclusion

6.1 Résumé des contributions

Dans cette thèse, nous avons proposé trois schémas de commande pour le réglage de la fréquence dans un système électrique composé de plusieurs zones AC non-synchrones reliées par un réseau HVDC à plusieurs terminaux.

Le premier schéma, appelé le schéma de commande basé sur les puissances injectées, est distribué par nature. En fonction des mesures à distance des fréquences des autres zones, ce schéma de commande modifie les injections de puissance des différentes zones AC vers le réseau DC de manière à faire réagir collectivement le système aux déséquilibres de puissance. Cette réaction collective permet à chaque zone de réduire leurs réserves primaires. La loi de commande est inspirée par des algorithmes pour le problème du consensus. Puisque les mesures à distance sont utilisées, les effets du retard sur l'efficacité du schéma de commande sont étudiés. Une analyse de la stabilité du système en boucle fermée montre que sous certaines hypothèses, tant que le retard ne dépasse pas une limite acceptable, le système converge vers un point d'équilibre pour lequel les déviations de fréquence des zones AC sont égales. Un critère de Nyquist permet de déterminer si le retard pourrait déstabiliser le système. Des simulations sur un système de référence à cinq zones AC non-identiques montrent que, en l'absence de temps de retard, les déviations de fréquence de toutes les zones convergent rapidement suivant un changement radical dans la demande de la charge. En revanche, nous avons constaté que pour un retard excédant une valeur critique, le schéma de commande peut entraîner des oscillations de fréquence

insuffisamment amorties, et que ces oscillations de fréquence insuffisamment amorties sont plus susceptibles d'apparaître lors de l'utilisation des valeurs élevées des gains du contrôleur. Les simulations mettent en évidence que ce schéma de commande basé sur les puissances injectées peut faire bon usage de la capacité de suivi rapide de puissance des convertisseurs HVDC afin de coordonner les efforts du réglage primaire de la fréquence entre les zones AC non-synchrones.

Pour éviter le problème du retard lié au schéma de commande basé sur les puissances injectées, un deuxième schéma de commande est introduit. Ce dernier a le même objectif que le premier, mais il agit sur les tensions continues des convertisseurs HVDC, d'où son nom le schéma de commande basé sur les tensions DC. En particulier, il modifie la tension continue de chaque convertisseur en fonction de la déviation de fréquence de la zone AC à laquelle il est connecté. Ce caractère décentralisé lui permet de se dégager du problème lié à la dépendance vis-à-vis des informations à distance. Une étude théorique montre que le réseau interconnecté est stable et il converge vers un point d'équilibre sur laquelle, pour des perturbations de la charge limitée, la différence entre les déviations de fréquence induites dans toutes les zones peut être rendue arbitrairement petite en choisissant un gain de contrôle suffisamment grand. Les résultats des simulations sur le même système de référence montrent que en utilisant l'information locale, le schéma de commande permet de réduire considérablement l'impact d'un déséquilibre de puissance en distribuant la déviation de fréquence associée dans toutes les zones.

Le dernier schéma de commande a pour objectif de restaurer les fréquences et les échanges de puissance à leurs valeurs nominales ou programmée suite à un déséquilibre de puissance. Il doit être combiné avec les deux autres schémas de commande. Les résultats de simulations sur le système de référence confirme sa bonne performance.

6.2 Perspectives

Les deux schéma de commande pour le réglage primaire de la fréquence peut être améliorés à plusieurs niveaux.

Tout d'abord, il serait intéressant d'étudier les effets du gain de chaque sous-contrôleur, de manière à trouver un moyen systématique de les choisir. En effet, ces gains influencent le degré de participation de chaque zone au réglage primaire, et, par une meilleure compréhension de leur influence, on devrait être capable de les choisir de manière à prendre en compte les caractéristiques techniques et économiques de chaque zone. Par exemple, la taille relative d'une zone par rapport aux autres peut être considérée, de sorte que, en réponse à un déséquilibre de puissance majeur dans une zone grande, une petite zone avec moins de réserves primaires puisse choisir d'arrêter de partager sa propre réserve si elle juge qu'une continuation de partage de sa réserve mettrait en péril sa propre stabilité. De cette façon, le système HVDC jouerait encore le rôle de « pare-feu » qui empêche des pannes en cascade à travers les zones AC. Ces gains pourraient probablement être réglés dynamiquement dans le cadre du temps du schéma de commande de la fréquence secondaire, de manière à refléter le changement du point de fonctionnement et de réduire la probabilité de congestions dans les lignes DC suite à une perturbation.

Deuxièmement, alors que les schémas de commande font appel simultanément aux réserves primaires de toutes les zones du système suite à un déséquilibre de puissance dans une zone, il serait également intéressant de vérifier si elle pouvait être adaptée au cas où les réserves primaires des différentes zones AC sont sollicitées de manière séquentielle, de sorte que les réserves des zones éloignées soient déployées uniquement lorsque les réserves locales ont été épuisées.

Troisièmement, l'étude théorique pourrait être étendue en assouplissant certaines des hypothèses faites pour établir les preuves.

Quatrièmement, il serait intéressant de tester ces schémas de commande sur des systèmes de référence plus sophistiqués qui négligent pas par exemple la régulation de tension dans les zones AC.

Enfin, l'utilisation d'un réseau HVDC à plusieurs terminaux pour le partage des réserves primaires de fréquence entre les zones AC peut avoir un effet négatif. En effet, les zones pourraient devenir plus vulnérables par rapport aux risques résultant d'une déconnexion du lien HVDC, parce que de telles éventualités peuvent créer un déséquilibre de puissance dans une zone vulnérable tout en réduisant simultanément la quantité de réserves primaires de fréquence sur laquelle la zone peut compter. C'est certainement une question à prendre en considération lorsqu'on a recours à un système HVDC pour offrir un tel type de service système.

Les schémas de commande proposés dans la thèse donnent un exemple de systèmes HVDC fournissant des services système au réseau électrique. Alors que l'effort de recherche sur les systèmes MT-HVDC est soutenu tant au niveau national, qu´international, nous espérons que ces travaux mettront en évidence les bénéfices potentiels des systèmes HVDC en tant qu´outil d'exploitation des systèmes électriques de grande dimension.

Chapter 1

Introduction

1.1 Background

To present the background of the dissertation on the use of HVDC systems for frequency control, the current chapter is divided into three parts. First, we briefly describe the issues of power system stability, of which frequency stability is a concern. Second, we present the HVDC technology, which offers new possibilities of enhancing power system stability. Third, we discuss the use of HVDC systems for frequency control in particular.

1.1.1 Power system stability and frequency control

Power system stability is defined as the ability of an electric power system to retain a state of equilibrium point after being subjected a physical disturbance [1]. It is classified into three categories: Rotor angle stability, frequency stability and voltage stability.

- Rotor angle stability deals with the ability of synchronous machines to remain in synchronism. Transient stability, as is commonly referred to, concerns rotor angle stability when the disturbance is so large that linearization of system equations is no longer permissible for analysis.
- Frequency stability refers to the ability of a power system to maintain steady frequency following a significant imbalance between generation and load.
- Voltage stability is concerned with the ability of a system to maintain steady voltages at all buses in the system after being subjected to a disturbance.

Measures are taken to enhance power system stability. Measures for enhancing transient stability aim at reducing the disturbing influence, increasing the synchronizing forces, and reducing the accelerating torque [2]. For frequency stability, control schemes to adjust generators' production are developed to keep the power balance and regulate the frequency [3]. The most common ways to improve voltage stability is to generate/consume reactive power at different buses of a system and to adjust the transformer tap-changers [4]. In practice, frequency stability and voltage stability are addressed by ancillary services, which include several types of service

aimed to support the basic functioning of generating capacity, energy supply, and power delivery [5].

The control schemes that the system operators have developed to regulate frequency are usually classified according to the time scale of their actions [6]. The actions corresponding to the shortest time scale are usually referred to as "primary frequency control". It consists of automatic adjustment, within a few seconds after a power imbalance, of the generators' power output based on locally measured frequency variations. To make it possible, the generators must have the so-called "primary reserves", i.e., power margins.

The frequency averaged over a few seconds can be considered identical in any part of a synchronous area. With a common frequency, every generator participating in primary frequency control adjusts its generation output in response to frequency excursions in the synchronous area, regardless of the location of the power imbalances. As the efforts of these generators sum up within the synchronous area, larger systems usually experience smaller frequency deviations. In addition, the provision of primary reserves accounts for non-negligible costs. For example, as of 2007, the average price for primary reserve is about 1.4 c€/kW/h in Germany [7]. Thus, one of the advantages of interconnecting several power systems to form a large synchronous area is to share their primary reserves, so that each system will deploy less primary reserves in response to a given power imbalance, and that the entire interconnected system will undergo a smaller frequency deviation. As the reserves are shared throughout the synchronous area, the requirement on the primary reserves of each power system is reduced [8, 9], which results in economic benefits [10].

1.1.2 HVDC technology and its stability benefits

High-Voltage Direct Current (HVDC) is a technology for bulk power transmission [11]. By using power electronic devices, AC power is converted into DC power for transmission, which yields less costs and lower electrical losses for long-distance power transfer. In addition, HVDC technology is also advantageous for asynchronous interconnections and long submarine cable crossings [12]. While conventional line-commutated current source converters (CSCs) need local reactive power generation, the state-of-the-art self-commutated voltage source converters (VSCs) are capable of controlling active power and reactive power independently [13].

The most common HVDC systems have two converters, one functioning as a rectifier while the other as an inverter. When more than two geographic zones need to be connected, a multi-terminal HVDC (MT-HVDC) system [14] can be used. Such a system with several converters gives rise to more challenges, as well as more flexibility in terms of control and stability improvement.

As a highly controllable device, HVDC technology opens new opportunities for improving power system reliability. A number of studies have shown the benefits of HVDC system to improve stability, in terms of transient stability [15, 16, 17, 18, 19, 20, 21], voltage stability [16, 17, 22, 18, 20], frequency stability [23, 21], and inter-area low frequency oscillations [16, 17, 23, 20].

In particular, the power transferred over the HVDC link is often made used of in order to improve stability. For example, to improve transient stability, three HVDC power modulation strategies are tested in [38], which add to the power flow order, a term depending on rotor

speeds, voltage phasors, and tie-line power, respectively. In addition to the above heuristically designed control schemes, Reference [39] proposes various control strategies, with a theoretical back on control Lyapunov function (CLF) [40] and modal analysis, to improve transient stability and low-frequency power oscillation damping. Also based on CLF, Reference [41] proposes a nonlinear control scheme to improve transient stability and oscillation damping, but this time for a parallel AC/DC power system. One difference between [39] and [41] is that, while the control scheme in [39] only uses CLF as a tool to justify its seemingly still heuristic control scheme, the *nonlinear* law in [41] is very sophisticatedly designed so that a CLF can be found to prove its stability. In addition, in a longer time scale, Reference [42] presents the solution to the security-constrained unit commitment problem, which is decomposed into a master problem for solving unit commitment problem and hourly transmission security check subproblems that evaluate branch flows and bus voltages of integrated AC/DC transmission systems.

1.1.3 Use of HVDC technology for frequency control

The development of the HVDC technology opens new perspectives for interconnecting non-synchronous areas. In this context, it is generally expected that the power flows through an HVDC system are set at scheduled values, while the frequencies of the AC areas remain independent. This type of HVDC control scheme may prevent the system from cascading outages by limiting the effects of a severe contingency within one area [12]. It also makes sense when the interconnected transmission utilities cannot agree on a common practice in terms of frequency control. However, this control scheme prevents the primary reserves from being shared among the non-synchronous AC areas, as the generators in one area are insensitive to frequency excursions in other areas. Since the supply of primary reserves represents a significant part of the operational transmission costs [24], it would be economically advantageous to share primary reserves among the non-synchronous areas by making use of the fast power-tracking capability of HVDC converters.

1.2 Literature review on use of the HVDC technology for frequency control

The use of HVDC systems for frequency control has been studied by a number of articles. Most papers focused on primary frequency control. For a two-terminal HVDC system, the basic idea is to modify the power transferred by the HVDC link using a PI/PID controller so that the frequencies of both AC areas connected by the HVDC link approach each other. This principle can be found in most of the papers, e.g. [43, 44, 45, 46, 47, 48, 49], where the control law is elaborated and simulation results are reported.

The above principle serves as the basis for other articles which treat more specific cases. For example, References [50, 51] study the case of an AC-DC parallel link, for which a frequency controller is synthesized using overlapping decomposition technique and eigenvalue assignment method, so that the transient frequency swing caused by large load disturbances is also eliminated. In [49], the idea is generalized to a multi-terminal HVDC system connecting more than two AC areas. In [48], the focus is placed on the modeling of an HVDC Link in Eastern Japan, for which the parameters of the frequency controller are estimated based on the measured fre-

quency deviations of the two areas connected by the HVDC link. The economic benefits of using HVDC for primary frequency control are studied in [43, 52].

A slightly different control law is found in [53], which treats the issue of primary frequency control as an optimization problem where the difference between the frequencies of two areas is to be minimized. Moreover, in addition to the frequencies, the mechanical power of both areas is also taken into consideration in the power modulation of the HVDC link. Two other control schemes are recently proposed in [54, 55], where droop controllers for the DC voltage control are made use of so that offshore wind turbines can provide frequency support to the main grid.

Concerning the secondary frequency control, in [56], a decentralized robust controller is designed for each AC area via a Riccati equation approach [57]. The parameter uncertainties are also taken into consideration in the controller design.

In addition to the above articles that are entirely dedicated to the use of HVDC systems for frequency control, there are also some articles where this usage is only conceptually mentioned in the larger context of frequency control and the HVDC technology, e.g. [58, 23].

1.3 Objective

The potentials of HVDC technology for frequency stability have not been investigated as extensively as for transient stability and voltage stability. This is partially due to the apparently simple control law as described in the previous section, which consists in adding to the scheduled power flow setting a term that is proportional to the frequency difference between two AC areas connected by the HVDC link. However, we believe that still more results are to be discovered in this aspect, especially for the case of multi-terminal HVDC systems.

Thus, the objective of this dissertation is to study the use of an MT-HVDC system for coordinating frequency control among the non-synchronous AC areas connected by it. Its main contributions are

- We propose three control schemes, two for primary frequency control and one for secondary frequency control.
- We prove stability of the three control schemes, where we use theoretical results from the control theory community on the consensus problem.
- We carry out simulations on a benchmark power system to test the control schemes.

1.4 Thesis outline

The rest of this thesis is organized as follows:

Chapter 2 elaborates the mechanisms of primary and secondary frequency control in a synchronous area, which serve as a basis of the control schemes introduced later.

Chapter 3 describes the HVDC technology and details the control strategies on the pole control level for two types of HVDC systems.

Chapter 4 models a power system with a multi-terminal HVDC link that serves as a reference for the following chapters where control schemes for frequency control will be introduced.

Chapter 5 introduces the first control scheme for primary frequency control of a multi-terminal HVDC system. This control scheme modifies the power injections from the different AC areas into the DC grid based on remote measurements of the other areas' frequencies, so as to make the system collectively react to power imbalances. A theoretical analysis proves its stability for a special case where all the AC areas have identical parameters. Simulation results on a benchmark power system with five AC areas show the effectiveness of the control scheme. In addition, as time-delays are inevitable in the communication of remote measurements, the effectiveness of the control scheme in the presence of the time-delays are investigated both theoretically and empirically.

Chapter 6 proposes the second control scheme for primary frequency control. In contrast to the first one, the second control scheme uses the DC voltages of the HVDC converters as the control variables. In particular, it modifies the DC voltage of each converter based on the frequency deviation of the AC area it is connected to. This decentralized nature frees it from the problems related to the dependence on remote information. By using an innovative frequency-domain approach, a theoretical analysis proves its stability for the general case of heterogeneous AC-area parameters. Simulation results on the same benchmark power system show its effectiveness.

Chapter 7 describes the last control scheme, which is designed for secondary frequency control. This control scheme is largely inspired by the practice of the UCTE for secondary frequency control in a synchronous area, and it is to be used in combination of one of the two control schemes introduced in the Sections 5 and 6. A theoretical analysis proves its stability. Simulation results on the same benchmark power system show its effectiveness.

Chapter 8 concludes the thesis and proposes future research directions.

The notations used in the thesis are summarized in the appendices. Also contained in the appendices are some mathematical and control-theory tools that we used in the chapters, including the graph theory, the consensus problem, the frequency-domain stability criterion used in Section 6.2, and the time-domain decomposition.

1.5 Publications

Most of the materials in this dissertation have been or will be published in the following articles:

- J. Dai, Y. Phulpin, A. Sarlette, and D. Ernst, "Coordinated primary frequency control among non-synchronous systems connected by a multi-terminal HVDC grid," *submitted to IET Generation, Transmission & Distribution*.
- J. Dai, Y. Phulpin, A. Sarlette, and D. Ernst, "Voltage control in an HVDC system to share primary frequency reserves between non-synchronous areas," in Proceedings of the 17th Power Systems Computation Conference, 2011 PSCC, (Stockholm, Sweden), August 2011.
- J. Dai, Y. Phulpin, A. Sarlette, and D. Ernst, "Impact of delays on a consensus-based

primary frequency control scheme for AC systems connected by a multi-terminal HVDC grid," in Proceedings of the IREP Symposium VIII, (Buzios, Brazil), August 2010.

Chapter 2

Frequency control in a synchronous area

This chapter presents general trends in actual practice of frequency control in a synchronous area. Section 2.1 describes generic organization of frequency control in a synchronous area, where three levels of actions are identified. Then, Sections 2.2 and 2.3 detail the first two levels of frequency control, which will be used in subsequent chapters. Finally, Section 2.4 briefly describes the coordinative and complementary relation between these different levels.

2.1 Introduction

The frequency of a synchronous area reflects the rotating speeds of the synchronized generators within the area. For a single generator, its rotating speed increases if its mechanical input power is greater than its electrical output power. The rotating speeds of all the generators collectively determine the frequency of the synchronous area. When measured in the time scale of a few seconds, the frequency can be considered identical in every part of the area, thus a *synchronous* area has a *unique* frequency throughout the area. This frequency reflects the power balance between demand and generation of the entire area. In particular, the frequency increases when the total generation is larger than the total demand within the area, and vice versa.

Power systems are subjected to disturbances and load variations resulting in power imbalances and thus frequency deviations. As a large number of electric devices are designed to operating at the nominal frequency, a large frequency deviation is hazardous to the normal operating of power systems. Thus, adequate measures must be taken to regulate the frequency at its nominal value. Hence the objective of frequency control. The latter is usually composed of three levels[1], corresponding to different time scales:

- Short-term frequency control consists of local automatic adjustment, within a few seconds, of generator power output based on rotor speed variations measured locally by each participating generating unit.

[1]This dissertation focuses on generation-side frequency control, with no consideration to the demand-side contribution such as described in [59] due to technical difficulties in its application. However, the dependency of load on frequency is taken into account, which does have some beneficial effect for frequency control.

- Mid-term frequency control, commonly called load-frequency control (LFC) in Europe [3] or automatic generation control (AGC) in North America [60], aims to bring the frequency back to its nominal value and restore the power exchanged between different control areas to their scheduled values. This level of control acts within several minutes, and is realized only by the control zone where the power imbalance originates.

- Long-term frequency control changes the commitment of generation units to restore primary and secondary reserves and manage congestions within the network. The response time of this level of control is greater than the above two.

In order to avoid ambiguity arising from the variety of terminologies used in different parts of the world [6, 61], we adopt the nomenclature convention of the Union for the Co-ordination of Transmission of Electricity (UCTE) [3], and refer to short-, mid-, and long-term frequency control as *primary*, *secondary*, and *tertiary frequency control*, respectively. In addition, we only consider primary and secondary frequency control in this thesis, with both assumed to implement the UCTE recommendations.

2.2 Primary frequency control

A generator that participates in primary frequency control is equipped with a speed governor, which observes the shaft's rotating speed, and uses a servomotor to control a throttle that determines the amount of fluid sent to the turbine. When the speed governor detects a deviation of the generator rotation speed ω, which is proportional to the stator electrical frequency f, its servomotor adjusts the opening of the throttle valve within a few seconds, thereby modifying the power input to the generator P_m.

2.2.1 Generator droop

When the frequency is equal to its nominal value f_{nom}, P_m equals the power setting P_m^o determined by the secondary frequency controller. When the frequency deviates from f_{nom} by Δf, the speed governor targets a variation in the mechanical power $\Delta P_m = P_m - P_m^o$. The magnitude of ΔP_m for a given Δf is determined by the *generator droop* σ, defined as

$$\sigma = -\frac{\Delta f / f_{nom}}{\Delta P_m / P_{nom}} , \tag{2.1}$$

where P_{nom} is the nominal power of the generator. Typical droop values range from 3% to 10% for a synchronous area of a national scale [6].

The limits on P_m, denoted by $P_m^{\min}$ and $P_m^{\max}$, are imposed by technical and economic attributes of the generator. The difference between $P_m^{\max}$ and P_m^o is referred to as *primary reserve*[2]. By way of example, the primary reserves of the UCTE are recommended to be 3000 MW [3].

[2]This is sometimes called *positive* primary reserves, in contrast to the *negative* primary reserves defined as the difference between P_m^o and $P_m^{\min}$ [3]. However, we do not make this distinction in this thesis.

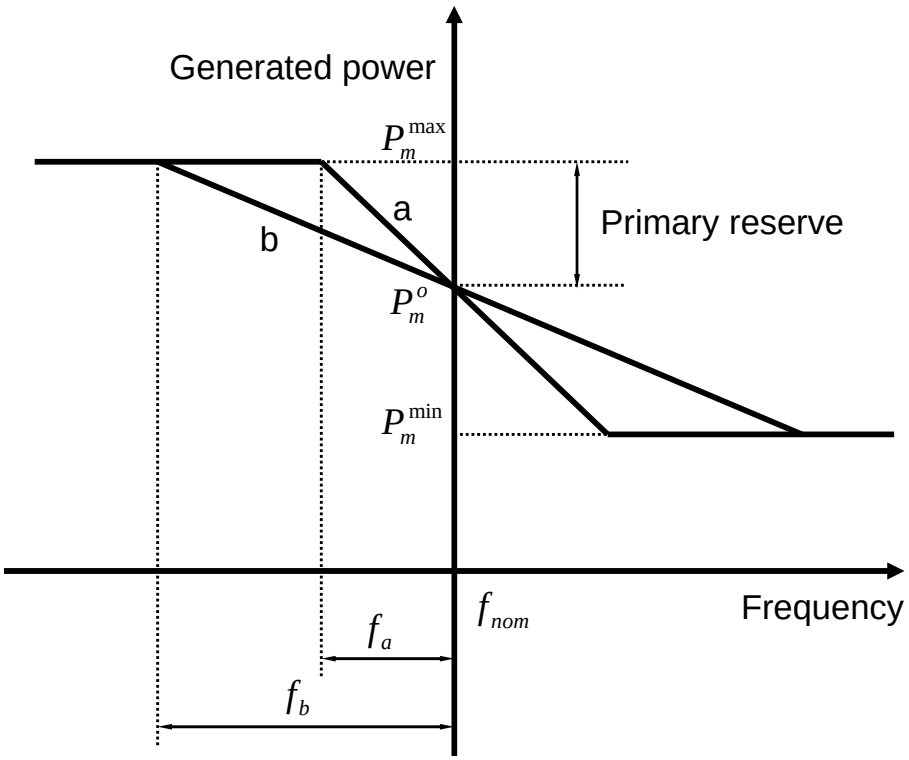

Figure 2.1: Steady-state power-frequency characteristics of two generator with the same primary reserves but different droop.

Figure 2.1 depicts the relation between P_m and f for two generators, which have identical primary reserves but different droops. The droop of Generator a is smaller than that of Generator b because for a given frequency deviation, when neither of them reaches the reserve limit, Generator a undergoes a larger variation in P_m than Generator b.

Primary frequency control dynamics

The dynamics of P_m under the influence of Δf is considered to be determined only by the speed governor, which is modeled by a first-order low-pass filter as shown in Figure 2.2 [2].

The differential equation representing this dynamics can be obtained from the Figure 2.2 as

$$T_{sm}\frac{dP_m}{dt} = P_m^o - P_m - \frac{P_{nom}}{\sigma}\frac{f - f_{nom}}{f_{nom}} , \tag{2.2}$$

where T_{sm} is the time constant of the servomotor, which is typically a few seconds [2].

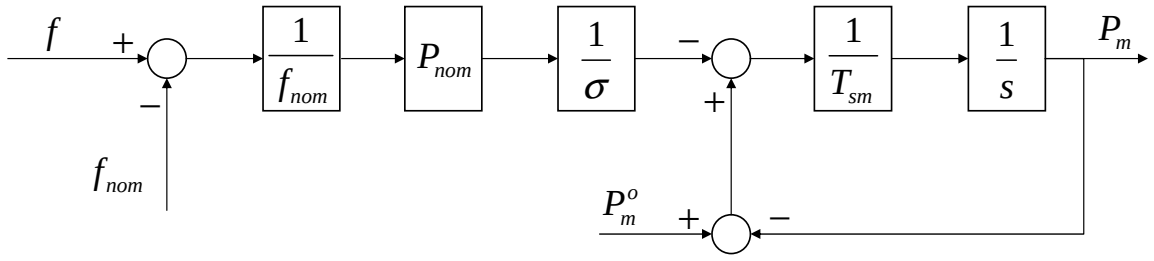

Figure 2.2: Dynamics model of the speed governor.

2.2.2 Generator aggregation

The generators in a power system usually have different droops and time constants. To facilitate our study, we use an aggregated model to represent the combined effects of all the generators within the system in terms of primary frequency control.

Suppose an AC area is composed of M generators. The corresponding symbols with no subscript represent the parameters of the aggregated generator representing these M generators. Since the mechanical power of the aggregated generator is the sum of the individual generators, we have

$$P_m = \sum_{i=1}^{M} P_{mi} \ , \tag{2.3}$$

$$P_m^o = \sum_{i=1}^{M} P_{mi}^o \ . \tag{2.4}$$

Then the droop and the time constant of the servomotor of the aggregated generator are given by [62] as

$$\sigma = \left(\sum_{i=1}^{M} P_{nom,i} \right) \Big/ \left(\sum_{i=1}^{M} \frac{P_{nom,i}}{\sigma_i} \right) \ , \tag{2.5}$$

$$T_{sm} = \left(\sum_{i=1}^{M} T_{smi} P_{nom,i} \right) \Big/ \left(\sum_{i=1}^{M} P_{nom,i} \right) \ . \tag{2.6}$$

2.3 Secondary frequency control

With the primary frequency control actions in response to a power imbalance, the frequency of a synchronous area will be different from its nominal value in the steady state. In addition, the power exchanged between the constituent parts of the synchronous area will be different from their scheduled values. To restore the frequency and the power exchanged to their nominal or scheduled values, secondary frequency control is used.

To describe the mechanism of secondary frequency control, we first show the effects of primary frequency control in a system composed of several control areas. Then we give the control law to realize this level of frequency control.

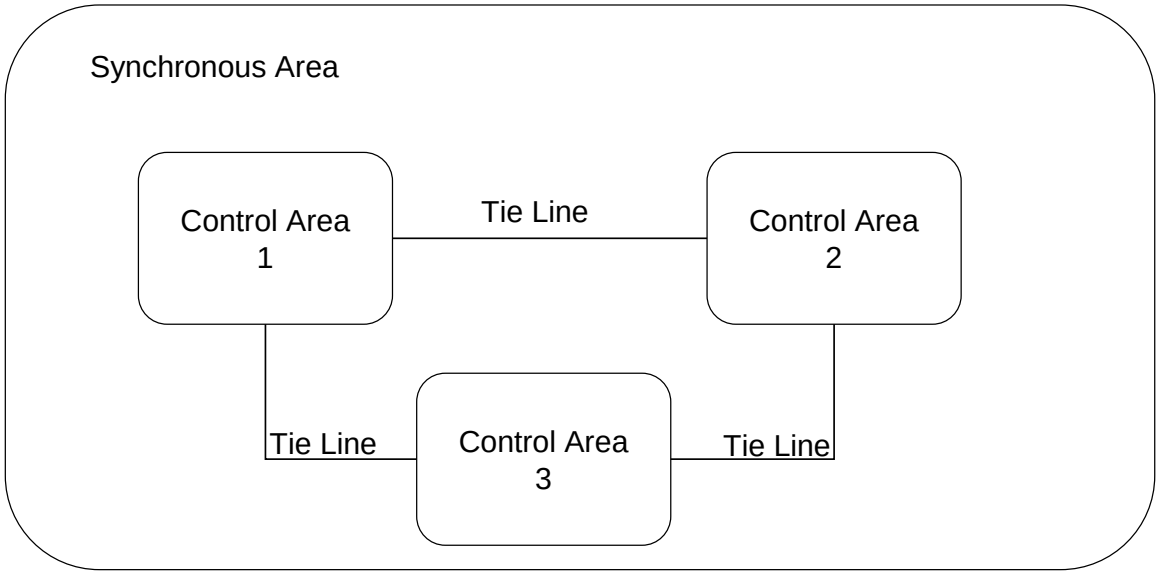

Figure 2.3: A synchronous area composed of three control areas connected by ties lines.

2.3.1 Interconnection of AC areas

A large synchronous system is usually composed of several control areas. By *control area* we mean a coherent part of an interconnected system, operated by a single transmission system operator (TSO) [3]. A control area usually coincides with the territory of a utility, a country or a geographical area, and it is connected to the rest of the system by tie lines, where the interchanged power between this control area and the others is measured. Figure 2.3 shows a synchronous area composed of three control areas, interconnected between themselves by tie lines.

The effects of primary frequency control on the power exchanged between the control areas can be measured by the *network power frequency characteristic*. Recall from (2.1) that the variation of a generator's output power due to primary frequency control actions (ΔP_m) is proportional to the frequency deviation (Δf). Therefore, on the control area level, the variation of the power exported from one control area due to primary control actions in response to a power imbalance *outside* that area is also proportional to the frequency deviation. The above observation leads to the following definition of the network power frequency characteristic for area i

$$\lambda_i^{\mathrm{NPFC}} = \frac{-\Delta P_i^{ex*}}{\Delta f} \,, \tag{2.7}$$

where ΔP_i^{ex*} is the change of the power exported from area i with respect to its scheduled value following a power imbalance originating *outside area i*. For a given interconnected system, the network power frequency characteristic of each control area is considered as a constant[3].

[3]Strictly speaking, the network power frequency characteristic does not remain constant, because of its dependency on the interconnected system, which itself continually varies over time. However, the variation of the network power frequency characteristic is very small compared to its absolute value, and moreover, its use for secondary frequency control does not require a precise measurement. Thus, we consider the network power frequency

The introduction of the network power frequency characteristic gives us a tool to locate a power imbalance. In particular, we define the *area control error* for area i as:

$$E_i = \Delta P_i^{ex} + \lambda_i^{\text{NPFC}} \Delta f \ , \tag{2.8}$$

where ΔP_i^{ex} is the *actual* change of the power exported from area i with respect to its scheduled value, irrespective of the location of the power imbalance. It can be seen from the definition of λ_i^{NPFC} that E_i differs from 0 in steady-state only if there is a power imbalance directly in area i itself, in which case ΔP_i^{ex} differ from ΔP_i^{ex*}. In particular, a positive E_i means that $\Delta P_i^{ex} > \Delta P_i^{ex*}$, i.e. the actual value of ΔP_i^{ex} is greater that the theoretical value of ΔP_i^{ex*} induced by a response to the same frequency deviation resulting from a power imbalance originating outside area i, which is an indication of a positive power imbalance originating in area i.

2.3.2 Secondary frequency controller

Secondary frequency control has two objectives: (i) to restore the frequency of the synchronous area back to its nominal value; (ii) to restore the power exchanged between the control areas back to their scheduled values. These objectives can be achieved if a power imbalance originating in one area i is fully compensated by a change in P_{mi}^o.

To realize secondary frequency control, each control area uses a PI controller that adjusts the power settings for the generators within that control area. The output of the secondary frequency controller for control area i is given as

$$\Delta P_{mi}^o = -K_{Ii} \int E_i dt - K_{Pi} E_i \ , \tag{2.9}$$

where ΔP_{mi}^o is the variation of P_{mi}^o with respect to its value prior to the disturbance, and K_{Ii} and K_{Pi} are the integral and proportional control gains, respectively. In practice, the controller gains should be chosen small enough so that P_{mi}^o can be considered constant in the time scale of primary frequency control. In some cases, only an integral controller is used in place of a PI controller, i.e. $K_{Pi} = 0$.

The reason behind (2.9) is that if control area i is not the area where the disturbance occurs, E_i is always zero, thus P_{mi}^o does not need to be adjusted. On the contrary, if control area i is the one where the disturbance originates, E_i is different from zero, thus the secondary frequency controller would modify P_{mi}^o to cover the power balance gap resulted from the disturbance so that the ΔP_i^{ex} tends to zero in the long run. The negative sign in (2.9) means that the secondary frequency controller should decrease P_{mi}^o if E_i is positive, since the latter indicates a positive power imbalance in area i.

The limits on P_m^o are imposed by technical and economic attributes of the generator. The difference between the upper limit and the current value of P_m^o is referred to as *secondary reserve*[4].

characteristic as a constant.

[4]This is sometimes called *positive* secondary reserves, in contrast to the *negative* secondary reserves defined as the difference between the current value of P_m^o and the lower limit. However, as before, we do not make this distinction in this thesis.

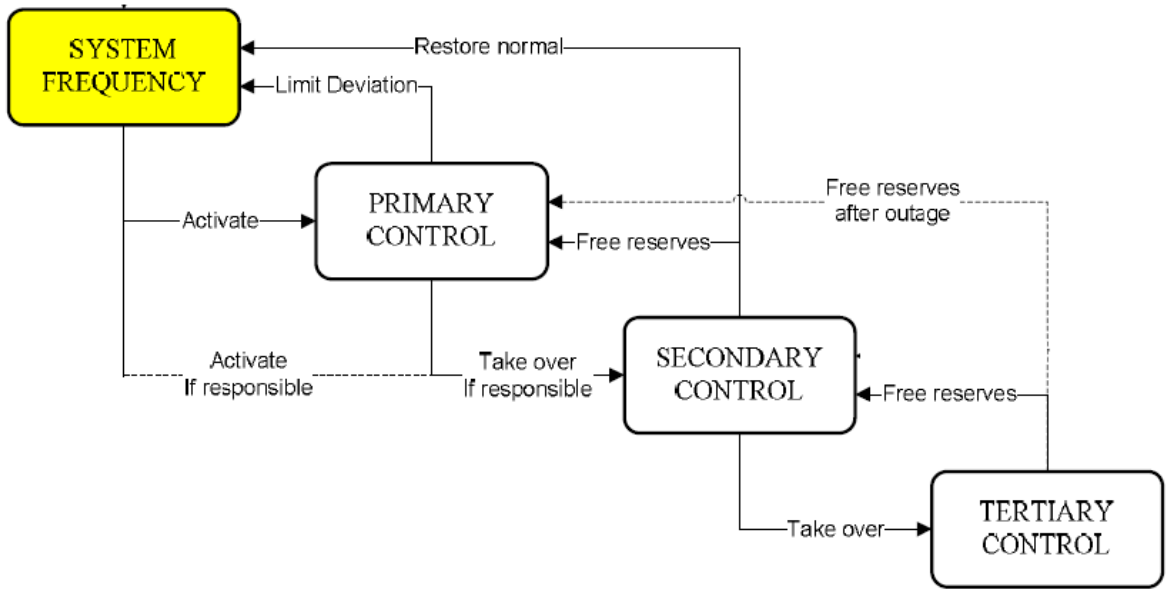

Figure 2.4: Frequency control hierarchy.

2.4 Frequency control hierarchy

As mentioned in Section 2.1, the three levels of frequency control actions differ in their time scales of deployment. This hierarchy can be schematically represented in Figure 2.4 [3].

This figure shows that, in response to a frequency deviation of the synchronous system, the primary control responds the fastest, where each control area deploys its primary reserves within a few seconds. For the particular control area where the power imbalance originates, the secondary frequency control of this area takes actions by adjusting the power settings of the generators within the area. This deployment of the secondary reserves by the responsible control area frees the primary reserves previously deployed by the synchronous area, and thus the interconnected system becomes ready again to cope with any new power imbalance by means of primary frequency control. A similar relation also exists between the secondary and the tertiary frequency control, where the latter frees the reserves of the former.

Chapter 3

HVDC technology

This thesis explores the possibility of using a high-voltage direct current (HVDC) system for frequency control. Given the importance of the HVDC technology itself, this chapter is entirely devoted to it. Section 3.1 gives a brief introduction. Section 3.2 describes the control hierarchy of an HVDC system. Sections 3.3 and 3.4 present the pole control strategies for two types of HVDC converters. For detailed general information on HVDC technology, the readers are referred to [11, 63, 64].

3.1 Introduction

An HVDC system is an electrical power transmission system that uses direct current for bulk power transmission. This section briefly describes its history, advantages, applications and configurations. Details of these aspects can be found in [12, 65].

3.1.1 History

The first long-distance power transmission in the world was achieved by using direct current in the 1880's at Miesbach-Munich Power Transmission. Despite the dominance of the three-phase AC systems as the common practice for the power generation, transmission, distribution and utilization ever since the late 19th century, attempts to use direct current for power transmission have never ceased [66, 67]. Following the early research endeavors in the 1930's and the 1940's, the 1950's witnessed the major progress in HVDC technology, probably because this technology seemed to be close to commercially feasible. In addition to the theoretical advancements, the first commercial HVDC project was also realized in the 1950's, which connects the Swedish mainland and the island of Gotland. Following this success, many HVDC links appeared in the 1960's, e.g. in New Zealand, Scandinavia and Japan, which accelerated the spreading of this technology throughout the world. In the 1970's, the progress in information technology gave rise to computer-controlled HVDC systems.

As HVDC systems use power electronics devices as converters, the technological development of the latter largely characterizes each generation of HVDC links. The earliest HVDC links used mercury arc valves, which were at the time one of the most efficient converters. How-

ever, since the 1970's, mercury arc converters were largely replaced by high-voltage solid-state semiconductor devices such as the thyristor, which offers better reliability and controllability. Thyristor valves constitute the conventional line-commutated current source converters (CSC), which remain today the solution for HVDC links of high power ratings. As the power electronics technology advances, the insulated-gate bipolar transistors (IGBT) have been used for HVDC systems since the 1990's. In contrast to the thyristor whose switching-off depends on the voltage bias of the external circuit[1], both the ignition and the extinction of the IGBT can be controlled. This feature makes it possible to synthesize complex waveforms when combined with the pulse width modulation (PWM) technology, thus allowing an independent control of the real and the reactive power of the converter. The IGBT valves comprise the self-commutated voltage source converters (VSC), which can be used for HVDC links of low power ratings. Both the line-commuted CSC and the VSC are the two basic converter technologies that are used in modern HVDC transmission systems.

After several decades of development, today, over 100 HVDC links have been built all over the world. The power rating of an HVDC system has reached the order of 1000 MW, while the distance of the DC line can be as long as 2000 km [69]. As there has been a renewed interest in the application of HVDC transmission schemes in recent years [65], one can expect further technological advancements and more projects in the coming years.

3.1.2 Advantages and applications

The principal advantage of HVDC is its ability to transmit large amounts of power over long distances with lower capital costs and with lower losses than AC. This economic incentive justifies its commercialization and its spreading. As a rule of thumb, an HVDC link of 5,000 MW at a voltage of 800 kV has its DC-line losses at less than 3% for every 1,000 kilometers, which is a saving of 30-40% with respect to an AC connection [70].

Thanks to the above advantage, the HVDC technology can be used in the following applications:

- Long-distance bulk power transmission: This is the main application of HVDC technology.
- Underground and submarine cable transmission [71, 72]: In addition to reduced losses, DC lines are free from the physical limits of AC lines in terms of the distance and the power level, an advantage that makes them a good alternative to AC links for underground and submarine transmission over long distances.
- Asynchronous ties [47]: As DC power serves as the intermediary between AC systems, these AC systems can possibly be asynchronous, e.g. between Nordic grid and UCTE, or even at different frequencies, e.g. in South America. Such an asynchronous HVDC link acts as an effective "firewall" against propagation of cascading outages from one network to another. Usually, this application uses a back-up-back connection, with no DC transmission line, e.g. in Japan.

[1]The gate turn-off thyristor (GTO), a special type of thyristor, can also be turned off at will, but it is not used for HVDC applications due to its high costs [68].

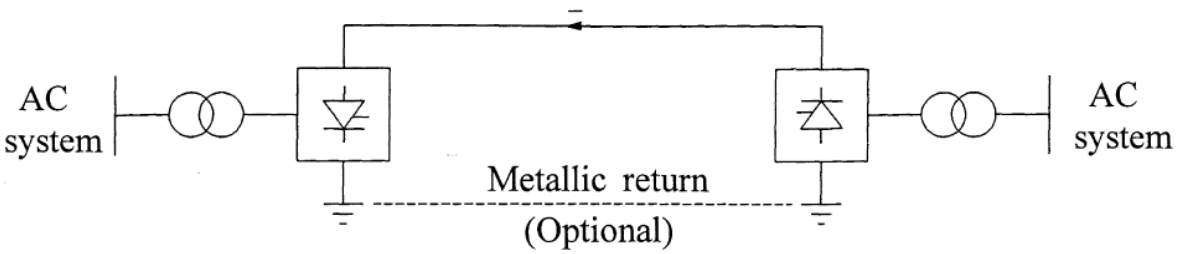

Figure 3.1: Monopolar HVDC link.

- Offshore transmission [71, 72, 73]: A VSC-based HVDC system can feed an isolated island or an offshore platform, thereby eliminating the need for local generation. For a remote wind generation array, an HVDC system also provides reactive power support.
- Multi-terminal (MT) systems [14, 74, 75]: In this application, an HVDC system connects more than two AC systems. Through sophisticated coordination between the converters, such an MT-HVDC system can achieve more flexibility in terms of power flows between the AC systems. This application enjoys several advantages over a combination of individual two-terminal HVDC links, such as minimized transmission losses, increased network availability, decreased number of converter units, and easy connection of a new offshore load/generation terminal. However, faster fault detection and protection systems are also needed to prevent contingencies from jeopardizing the entire system. Currently, multi-terminal systems are used in the SACOI three-terminal cable system between Italy, Corsica (France) and Sardinia (Italy), and the Quebec-New England three-terminal overland system in Canada/USA.
- Power delivery to large urban areas [76]: VSC-based underground transmission circuit can be used for power delivery to urban areas, where the requirement on voltage support and the environmental regulations must be met.

It should be noted that the above applications are not mutually exclusive. For example, the numerous links connecting offshore wind farms with continental Europe use submarine cables to realize offshore transmission.

3.1.3 Configurations

HVDC links can be broadly classified into three categories: monopolar links, bipolar links, and homopolar links.

- The basic configuration is the monopolar link, as shown in Figure 3.1 [2]. It uses a single conductor, usually of negative polarity, to transfer DC power, while the return path is provided by ground or water. This configuration is chosen mainly for its low costs. In situations where earth resistivity is too high or possible interference with underground or underwater metallic structures is objectionable, a metallic return may be used instead.
- The bipolar link, as shown in Figure 3.2 [2], uses two conductors, one positive and the other negative. The currents in the two poles are usually the same, resulting in considerable less

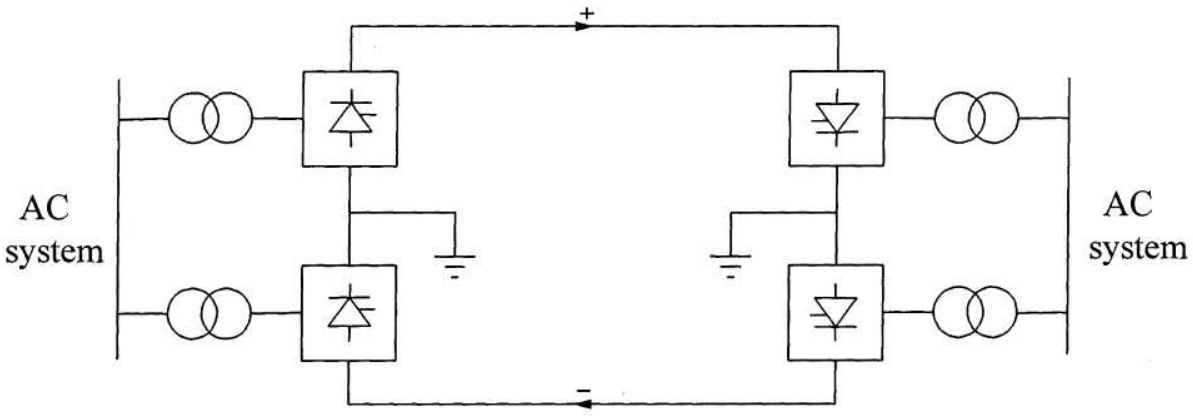

Figure 3.2: Bipolar HVDC link.

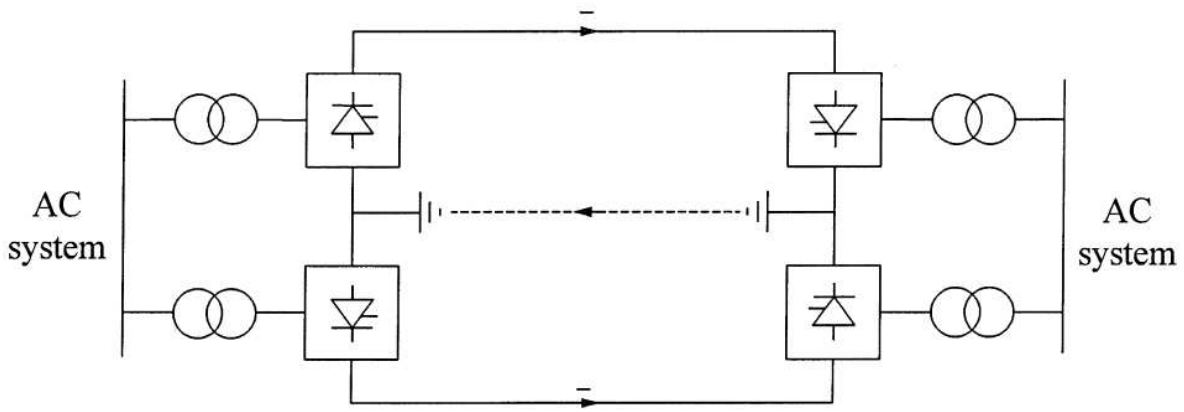

Figure 3.3: Homopolar HVDC link.

harmonic interference than the monopolar link. In addition, the two poles can operate independently. Thus, if one pole is isolated due to a fault, the other can carry half of the rated power or more using the overload capability.

- The homopolar link uses two or more conductors, all having the same polarity, and uses the ground as the return path, as shown in Figure 3.3 [2]. Similar to the bipolar link, if one pole is isolated due to a fault, the other poles can carry their shares of the rated power or more using the overload capability.

Each of the above three configurations can have cascaded groups of several converters, which are connected in parallel on the AC side and in series on the DC side, to reduce the voltage rating on each individual converter.

Finally, a special type is the back-to-back station, designed for a asynchronous ties where AC lines are used to connect both sides. No DC conductor is involved in this application.

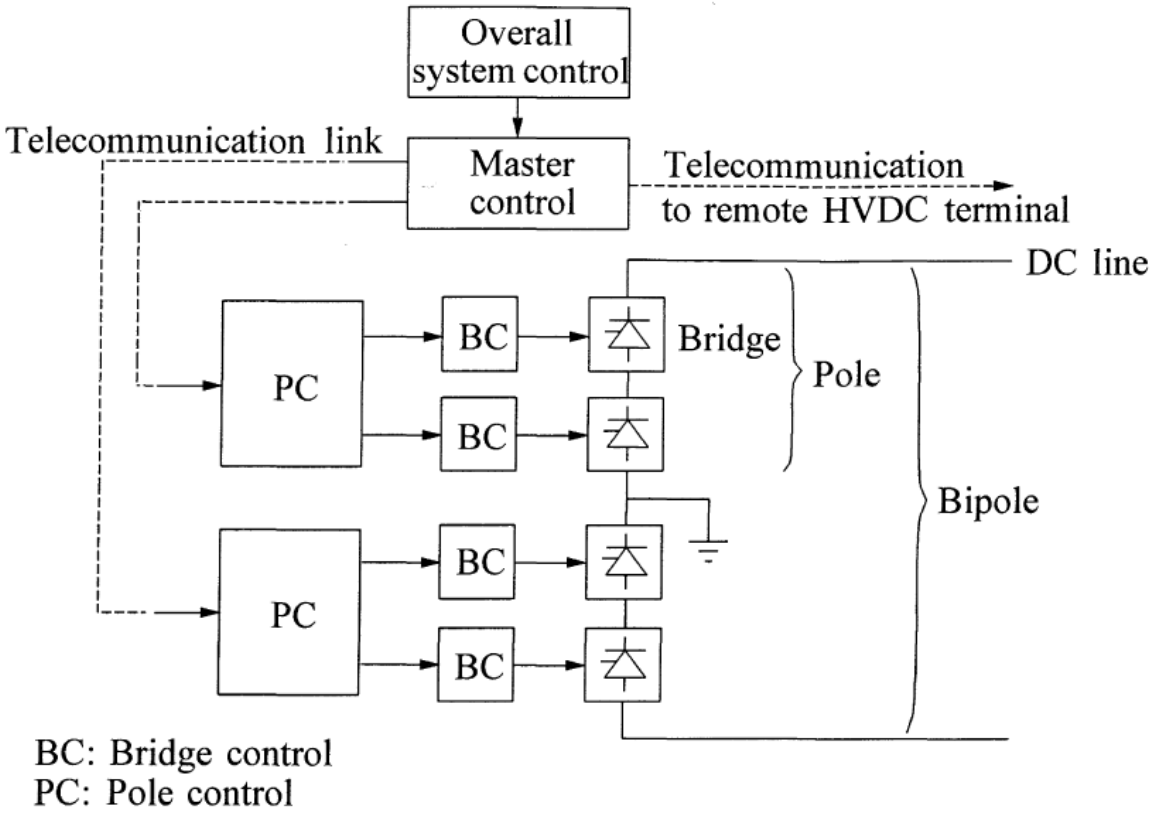

Figure 3.4: Control hierarchy of a bipolar HVDC link.

3.2 Control hierarchy of an HVDC system

Figure 3.4 [2] shows the control hierarchy of a typical bipolar HVDC link, where four levels of control can be identified:

- Bridge control: This level determines the firing instants of the valves of a bridge, and it has the fastest response time of the hierarchy.
- Pole control: This level coordinates the bridge control of a pole. It includes the conversion of the current order into firing angle order, tap change control of the transformer, etc. For this level, there exist mature control strategies for different types of converters, e.g. the *constant ignition angle control* and the *constant extinction angle control* for conventional CSC-based converters [2], and the vector control for the VSC-based converters [77, 78]. The remaining sections of the present chapter will detail this level of control for the two types of converters.
- Master control: The level determines the current order for each pole of the HVDC link in an coordinative manner. It interfaces between the overall system control and the pole control.
- Overall system control: At this level, the control center gives the HVDC link the power

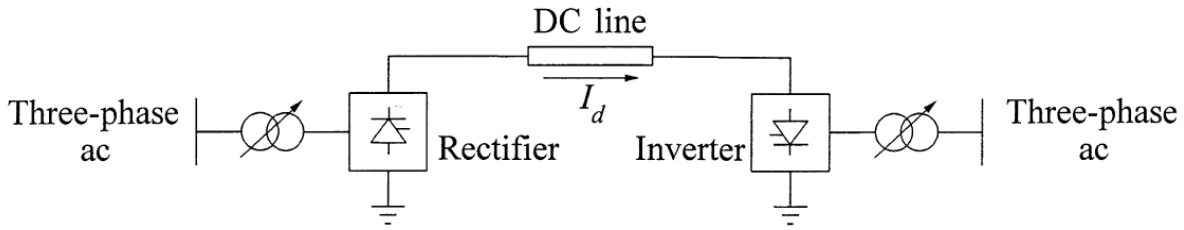

Figure 3.5: Diagram of a monopolar HVDC link.

flow order, which assumes the scheduled power transfer while maintaining AC systems stability. The control schemes proposed in this thesis focus on this level.

The following two sections describes in detail the pole control strategies for CSC-based and VSC-based HVDC converters. From the next chapter, the pole control will be considered as an underlying level of control for which the dynamics are neglected. In fact, with the modern power electronics technology, HVDC converters are capable of tracking a current order (and thus a power order) with a settling time of the order of a few milliseconds, as shown by simulation results in studies on HVDC systems [79, 80, 77, 81, 35, 78, 82, 83].

3.3 Control of a CSC-based HVDC system

As mentioned in Section 3.1.1, the line-commutated CSC-based HVDC (or simply, the conventional HVDC) composed of thyristors is still the technology used today for high power-rating projects. The fact that the thyristor can not be switched off at will implies that the control of a conventional HVDC link is different from that of a VSC-based HVDC system, where both the switching-on and the switching-off of the IGBT can be controlled.

The current section describes the pole control (i.e. how a current order is followed by the converter while the DC voltage is maintained at its nominal value) of a conventional HVDC system. The material in this section is largely borrowed from [2].

3.3.1 Diagram and equivalent circuit

Figure 3.5 [2] shows the diagram of a monopolar link or one pole of a bipolar link. In this system, two three-phase AC networks are connected by a DC line via transformers and converters. When the current (hence the power) flows from the left AC network to the right one, as is the case in the figure, the left converter works as a rectifier converting AC power to DC power, while the right converter works as an inverter converting DC power to AC power.

Figure 3.6 shows the equivalent circuit of the system shown in Figure 3.5, where

V_{d0r} (V_{d0i}, resp.): Ideal no-load direct voltage of the rectifier (the inverter, resp.).

V_{dr} (V_{di}, resp.): Actual direct voltage of the rectifier (the inverter, resp.).

α: Ignition delay angle of the rectifier.

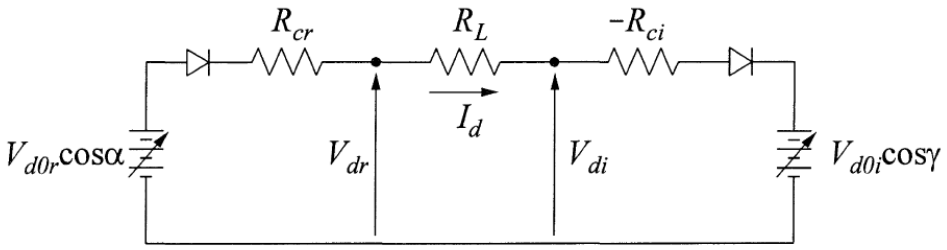

Figure 3.6: Equivalent circuit of Figure 3.5.

γ: Extinction angle of the inverter.

I_d: Direct current.

R_{cr} ($-R_{ci}$, resp.): Converter resistance of the rectifier (the inverter, resp.).

R_L: DC line resistance.

The power at the rectifier terminal is

$$P_{dr} = V_{dr} I_d \ . \tag{3.1}$$

The power at the inverter terminal is

$$P_{di} = V_{di} I_d = P_{dr} - R_L I_d^2 \ . \tag{3.2}$$

3.3.2 Expressions of I_d and V_d

The expressions of I_d and V_d to be given are obtained with the following assumptions on the system:

1. The AC system, including the converter transformer, may be represented by an ideal source of constant voltage and frequency in series with a lossless inductance.
2. The direct current (I_d) is constant and ripple-free.
3. The valves of the converters are ideal switches with zero resistance when conducting, and infinite resistance when not conducting.
4. There is no commutation overlap between valves.

The direct current flow from the rectifier to the inverter is

$$I_d = \frac{V_{d0r} \cos\alpha - V_{d0i} \cos\gamma}{R_{cr} + R_L - R_{ci}} \ . \tag{3.3}$$

The ideal no-load direct voltage of both converters can be expressed as:

$$V_{d0} = \frac{3\sqrt{2}}{\pi} BTE_{LL} \ , \tag{3.4}$$

where

B: Number of bridges in series.

T: Transformer ratio.

E_{LL}: RMS line-to-line primary voltage of the transformer.

The DC voltage, defined at the rectifier side, is:

$$V_d = V_{dc} = V_{d0i} \cos\gamma + (R_L - R_{ci}) I_d \; . \tag{3.5}$$

3.3.3 Basic pole control

The control of I_d and V_d must satisfy the following requirements:

- Large fluctuations in the direct current (I_d) must be prevented due to variations in the AC-side voltages (V_{d0r} and V_{d0i}).
- The direct voltage (V_d) must be maintained near its rated value.
- The power factors ($\cos\alpha$ and $\cos\gamma$) at both ends should be as high as possible.

As can be inferred from (3.3)-(3.5), there are two ways to control I_d and V_d, either by the internal voltages ($V_{d0r}\cos\alpha$ and $V_{d0i}\cos\gamma$) through grid/gate control of the valve ignition angle (α and γ), or by the tap changing of the converter transformer (T_r and T_i). These two types of control are used in a complementary manner, as the rapid grid/gate control has a response time in the order of several milliseconds while the slow tap changing are activated within several seconds. Thus, grid/gate control is used initially for rapid action, followed by tap changing to restore α and γ to the normal range.

Under normal operation, the rectifier maintains constant current (CC), while the inverter operates with constant extinction angle (CEA) so as to maintain an adequate commutation margin. The ideal steady-state $V - I$ characteristics are shown in Figure 3.7. In this figure, the rectifier characteristic is a vertical line, while the inverter characteristic a horizontal line with a slight slope due to the voltage drop by the resistances. The intersection of the two lines determines the operating point.

The rectifier's line can be shifted horizontally by adjusting the current order. If the measured current is less than the order, the regulator advances the firing by decreasing α. Similarly, the inverter characteristic line can be raised or lowered by its transformer tap changes. When the tap changer is moved, the CEA regulator quickly restores the desired γ. As a result, I_d changes, which is then quickly restored by the current regulator of the rectifier. The rectifier tap changer acts to bring α into the desired range to ensure a high power factor and adequate room for control.

The actual steady-state characteristics, where other factors such as the limit on α and the finiteness of the controller gains are taken into account, is not considered in this thesis.

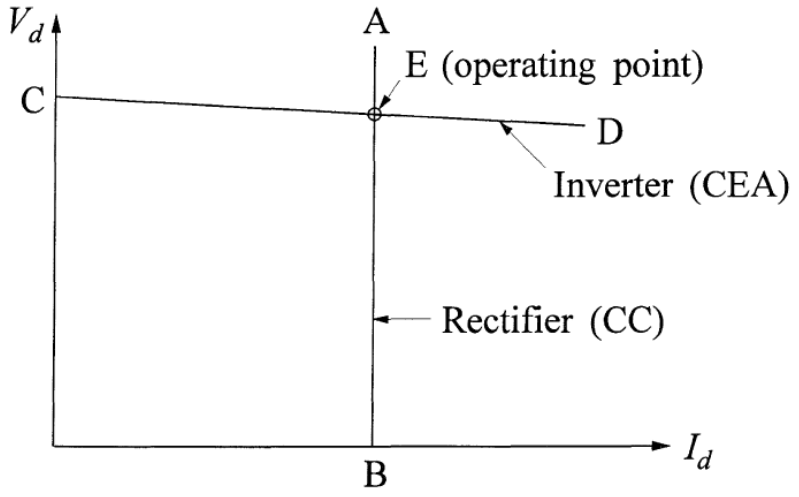

Figure 3.7: Rectifier and inverter ideal steady-state $V - I$ characteristics. V_d is measured at the rectifier. Thus the inverter characteristic includes $R_L I_d$ drop.

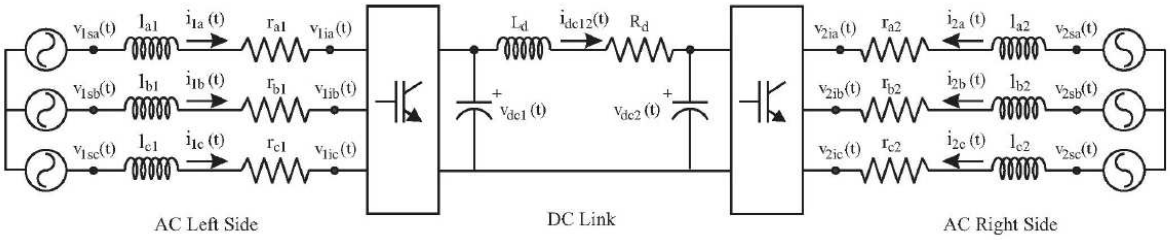

Figure 3.8: Three-phase diagram of a VSC-base HVDC link.

3.4 Control of a VSC-based HVDC system

This section describes the control of a VSC-based HVDC system. First, a state-space model is established in the synchronous *d-q* frame, which allows for a decoupled control on the real and the reactive power. Then, a double-loop control strategy is synthesized.

The material in this section is largely borrowed from [77, 82].

3.4.1 HVDC model

A VSC-based HVDC system is given in Figure 3.8.

We represent this system by an averaged model [84], where the high-frequency PWM characteristics are neglected. We only consider the balanced condition[2], i.e. the three phases have identical parameters and their voltages and currents have the same amplitude while phase-shifted 120° between themselves.

[2]For the unbalanced condition, the reader is referred to [81].

AC systems:

On the rectifier side, the Kirchhoff voltage law leads to

$$v_{1sa} - R_1 i_{1a} - L_1 \frac{di_{1a}}{dt} - v_{1a} = 0 \,, \tag{3.6a}$$

$$v_{1sb} - R_1 i_{1b} - L_1 \frac{di_{1b}}{dt} - v_{1b} = 0 \,, \tag{3.6b}$$

$$v_{1sc} - R_1 i_{1c} - L_1 \frac{di_{1c}}{dt} - v_{1c} = 0 \,, \tag{3.6c}$$

where

$$v_{1sa} = V_1 \sqrt{\frac{2}{3}} \sin(\omega t + \theta_1) \,, \tag{3.7a}$$

$$v_{1sb} = V_1 \sqrt{\frac{2}{3}} \sin(\omega t + \theta_1 - \frac{2\pi}{3}) \,, \tag{3.7b}$$

$$v_{1sc} = V_1 \sqrt{\frac{2}{3}} \sin(\omega t + \theta_1 + \frac{2\pi}{3}) \,, \tag{3.7c}$$

and

$$v_{1a} = \frac{M_1}{2} v_{dc1} \sin(\omega t + \theta_1 + \delta_1) \,, \tag{3.8a}$$

$$v_{1b} = \frac{M_1}{2} v_{dc1} \sin(\omega t + \theta_1 + \delta_1 - \frac{2\pi}{3}) \,, \tag{3.8b}$$

$$v_{1c} = \frac{M_1}{2} v_{dc1} \sin(\omega t + \theta_1 + \delta_1 + \frac{2\pi}{3}) \,. \tag{3.8c}$$

The electrical parameters in the above equations are shown in Figure 3.8. δ_1 is the angle of v_{1sa} and θ_1 the angle difference between v_{1sa} and v_{1a}. M_1 is the duty cycle. Both θ_1 and M_1 can be controlled by PWM technology.

Applying the Park's transformation

$$P = \frac{2}{3} \begin{bmatrix} \cos(\omega t) & \cos(\omega t - \frac{2\pi}{3}) & \cos(\omega t + \frac{2\pi}{3}) \\ -\sin(\omega t) & -\sin(\omega t - \frac{2\pi}{3}) & -\sin(\omega t + \frac{2\pi}{3}) \\ \frac{1}{2} & \frac{1}{2} & \frac{1}{2} \end{bmatrix} \,, \tag{3.9}$$

we obtain the relation in *d-q* synchronous reference frame

$$v_{1sd} - R_1 i_{1d} - L_1 \frac{di_{1d}}{dt} + \omega L_1 i_{1q} - v_{1d} = 0 \,, \tag{3.10a}$$

$$v_{1sq} - R_1 i_{1q} - L_1 \frac{di_{1q}}{dt} - \omega L_1 i_{1d} - v_{1q} = 0 \,, \tag{3.10b}$$

where

$$v_{1sd} = V_1 \sqrt{\frac{2}{3}} \sin\theta_1 \,, \tag{3.11a}$$

$$v_{1sq} = -V_1 \sqrt{\frac{2}{3}} \cos\theta_1 \,, \tag{3.11b}$$

and

$$v_{1d} = \frac{M_1}{2} v_{dc1} \sin(\theta_1 + \delta_1) \,, \tag{3.12a}$$

$$v_{1q} = -\frac{M_1}{2} v_{dc1} \cos(\theta_1 + \delta_1) \,. \tag{3.12b}$$

Let

$$M_{1d} = M_1 \sin(\theta_1 + \delta_1) \,, \tag{3.13a}$$

$$M_{1q} = -M_1 \cos(\theta_1 + \delta_1) \,. \tag{3.13b}$$

Then, (3.12) becomes

$$v_{1d} = \frac{M_{1d}}{2} v_{dc1} \,, \tag{3.14a}$$

$$v_{1q} = \frac{M_{1q}}{2} v_{dc1} \,. \tag{3.14b}$$

Similar reasoning for the inverter yields

$$v_{2sd} - R_2 i_{2d} - L_2 \frac{di_{2d}}{dt} + \omega L_2 i_{2q} - v_{2d} = 0 \,, \tag{3.15a}$$

$$v_{2sq} - R_2 i_{2q} - L_2 \frac{di_{2q}}{dt} - \omega L_2 i_{2d} - v_{2q} = 0 \,, \tag{3.15b}$$

where

$$v_{2sd} = V_2 \sqrt{\frac{2}{3}} \sin\theta_2 \,, \tag{3.16a}$$

$$v_{2sq} = -V_2 \sqrt{\frac{2}{3}} \cos\theta_2 \,, \tag{3.16b}$$

and

$$v_{2d} = \frac{M_{2d}}{2} v_{dc2} \,, \tag{3.17a}$$

$$v_{2q} = \frac{M_{2q}}{2} v_{dc2} \,, \tag{3.17b}$$

with

$$M_{2d} = M_2 \sin(\theta_2 + \delta_2) \,, \tag{3.18a}$$

$$M_{2q} = -M_2 \cos(\theta_2 + \delta_2) \,. \tag{3.18b}$$

The real and the reactive powers of both AC networks can be expressed as

$$P_1 = \frac{3}{2}(v_{1sd} i_{1d} + v_{1sq} i_{1q}) \,, \tag{3.19a}$$

$$Q_1 = \frac{3}{2}(v_{1sq} i_{1d} - v_{1sd} i_{1q}) \,, \tag{3.19b}$$

$$P_2 = \frac{3}{2}(v_{2sd} i_{2d} + v_{2sq} i_{2q}) \,, \tag{3.19c}$$

$$Q_2 = \frac{3}{2}(v_{2sq} i_{2d} - v_{2sd} i_{2q}) \,. \tag{3.19d}$$

DC line:

Applying the Kirchhoff voltage and current laws to the DC circuit yields

$$v_{dc1} - v_{dc2} - R_{dc} i_{dc12} + L_{dc} \frac{di_{dc12}}{dt} = 0 \,, \tag{3.20a}$$

$$i_{dc1} - i_{dc12} - C_1 \frac{dv_{c1}}{dt} = 0 \,, \tag{3.20b}$$

$$i_{dc2} + i_{dc12} - C_2 \frac{dv_{c2}}{dt} = 0 \,. \tag{3.20c}$$

AC-DC power coupling:

The real power balance on both sides of the converters yields

$$i_{dc1} v_{dc1} = \frac{3}{2}(v_{1d} i_{1d} + v_{1q} i_{1q}) \,, \tag{3.21a}$$

$$i_{dc2} v_{dc2} = \frac{3}{2}(v_{2d} i_{2d} + v_{2q} i_{2q}) \,. \tag{3.21b}$$

Global model:

The global state-space model of the HVDC system is summarized as follows

State variables: i_{1d}, i_{1q}, i_{2d}, i_{2q}, v_{dc1}, v_{dc2}, i_{dc12}.

Control variables: M_{1d}, M_{1q}, M_{2d}, M_{2q}.

Input variables: v_{1sd}, v_{1sq}, v_{2sd}, v_{2sq}.

Output variables: P_1, Q_1, P_2, Q_2.

The differential equations describing the evolution of the state variables are: (3.10), (3.15), (3.20).

The algebraic equations relating the variables are: (3.14), (3.17), (3.19), (3.21).

3.4.2 Pole control strategy

Control objective:

The objective of controlling a converter is to track a power order (P^*, Q^*) while the DC voltage of the HVDC link is maintained. To do this, we choose for both converters the d-axis such that it coincides with v_s, so $v_{sq} = 0$. Equation (3.19) thus becomes

$$P = \frac{3}{2} v_{sd} i_d \,, \tag{3.22a}$$

$$Q = -\frac{3}{2} v_{sd} i_q \,, \tag{3.22b}$$

where we omitted the converter index since the two equations in (3.22) apply to both the rectifier and the inverter. Thus, P and Q can be controlled independently by i_d and i_q, respectively.

On the other hand, the voltage of the DC line must be regulated at its nominal value so that the DC power balance is maintained. As the AC system fed by the inverter may potentially be a passive network where no generation resource is available, it is usually the rectifier that plays the role of regulating the DC voltage. As will be shown later, v_{dc1} can be controlled by i_{1d}.

Therefore, we consider that the rectifier tracks a reactive power order and regulates the DC voltage, while the inverter tracks a real power order and a reactive power order.

We design a double-loop control strategy to achieve the above control objectives. The inner loop with the fast dynamics deals with the current tracking problem, while the outer loop concerns the DC voltage regulating problem.

Inner loop:

As the inner loop applies to both the rectifier and the inverter, the converter index is omitted in this part. We introduce the following two new variables

$$u_d = \frac{di_d}{dt} \,, \tag{3.23a}$$

$$u_q = \frac{di_q}{dt} \,, \tag{3.23b}$$

which, when substituted into (3.15), yield

$$u_d = \frac{1}{L}v_{sd} - \frac{R}{L}i_d + \omega i_q - \frac{1}{L}\frac{M_d}{2}v_{dc} \,, \tag{3.24a}$$

$$u_q = \frac{1}{L}v_{sq} - \frac{R}{L}i_q - \omega i_d - \frac{1}{L}\frac{M_q}{2}v_{dc} \,. \tag{3.24b}$$

We use PI controllers to control i_d and i_q. Let i_d^* and i_q^* be the current orders. Then, u_d and u_q are the output of the PI controllers as:

$$u_d = K_{Pi}(i_d^* - i_d) + K_{Ii}\int (i_d^* - i_d)dt \,, \tag{3.25a}$$

$$u_q = K_{Pi}(i_q^* - i_q) + K_{Ii}\int (i_q^* - i_q)dt \,, \tag{3.25b}$$

where K_{Pi} and K_{Ii} are respectively the proportional and the integral current controller gains. These controller gains can be determined using any classic tuning methods [36]. The control variables M_d and M_q are calculated from (3.24).

Outer loop:

The outer loop is designed to regulate the DC voltage, thus it is only concerned with the rectifier. In this time scale, the currents in d-q axes are considered in their steady state, i.e. $i_{1d} = i_{1d}^*$ and $i_{1q} = i_{1q}^*$.

To regulate u_{dc1}, we introduce a new variable i_e as

$$i_e = \frac{du_{dc1}}{dt} \,, \tag{3.26}$$

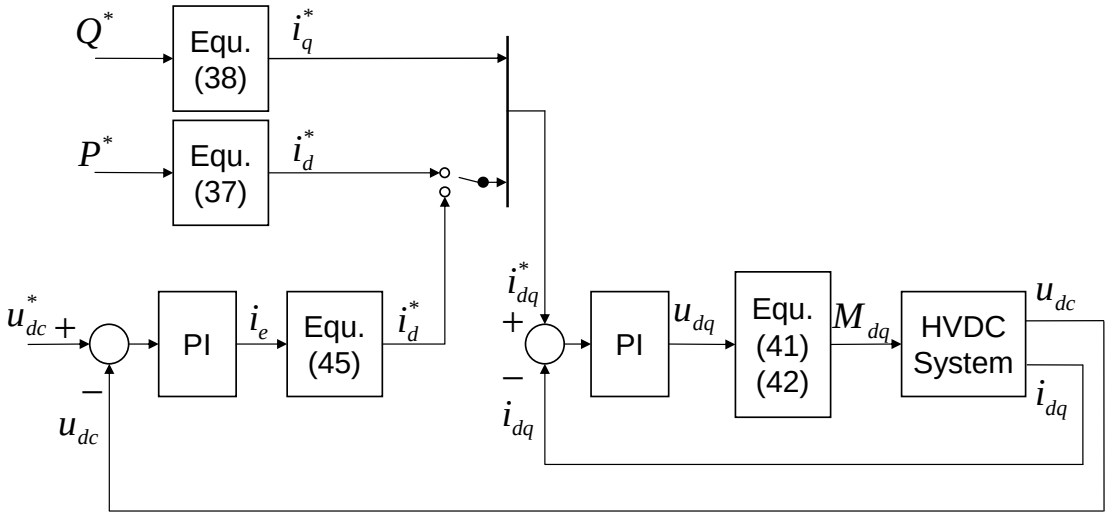

Figure 3.9: Control strategy diagram for a voltage source converter.

which, together with (3.20a) and (3.21a), yields

$$C_1 i_e + i_{dc12} - \frac{3}{4}(M_{1d} i_{1d} + M_{1q} i_{1q}) = 0 \; . \tag{3.27}$$

We use a PI controller to regulate u_{dc1}. Let u^*_{dc1} be the DC voltage orders. Then, i_e is the output of the PI controller as:

$$i_e = K_{Pu}(u^*_{dc1} - u_{dc1}) + K_{Iu} \int (u^*_{dc1} - u_{dc1}) dt \; , \tag{3.28}$$

where K_{Pu} and K_{Iu} are respectively the proportional and the integral DC voltage controller gains. The current order i^*_{1d} is then calculated from (3.27), where we assume that $i_{1d} = i^*_{1d}$, i.e. the actual current is well controlled at its order by the inner-loop controller.

Control diagram

The global control strategy is summarized in Figure 3.9.

Chapter 4

Multi-terminal HVDC system model and benchmark system

This chapter models a power system with a multi-terminal HVDC link that serves as a reference for the following chapters where control schemes for frequency control will be introduced.

Section 4.1 presents a multi-terminal HVDC system model, with respect to which the control schemes in the following chapters will be given. Section 4.2 defines the equilibrium point at which the system is assumed to be prior to any disturbance and which will be called the *reference operating point* in later chapters. Section 4.3 presents a benchmark system that will be used to test the control schemes.

4.1 Multi-terminal HVDC system model

We consider a system with three types of components: a DC grid, N non-synchronous AC areas, and N converters that interface the AC areas with the DC grid, as depicted in Figure 4.1. These components are detailed in this section.

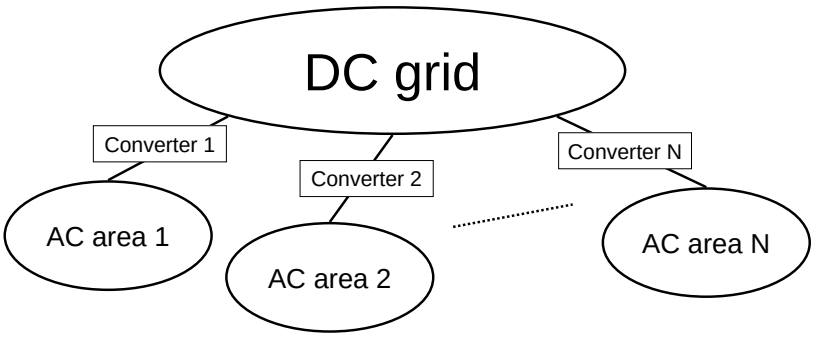

Figure 4.1: A multi-terminal HVDC system connecting N AC areas via N converters.

4.1.1 DC grid

As the electrical time constant of a DC grid is of the order of a few tens of milliseconds [4], transient dynamics of the DC grid are not considered.

We suppose that every node in the DC grid is connected to a converter. Each node inherits the index number of the AC area to which it is connected. Then, the power injection from area i into the DC grid, denoted as P_i^{dc}, satisfies

$$P_i^{dc} = \sum_{k=1}^{N} \frac{V_i^{dc}(V_i^{dc} - V_k^{dc})}{R_{ik}} , \tag{4.1}$$

where V_i^{dc} and V_k^{dc} are the voltages at nodes i and k, respectively, and R_{ik} is the resistance between these two nodes. V_i^{dc} is called the DC-side voltage of converter i in the following. Note that $R_{ik} = R_{ki}$. If nodes i and j are not directly connected, R_{ik} is considered equal to infinity. We consider a DC grid in which there is either a direct or an indirect connection between any two nodes, such that it is not made of several isolated parts.

Under normal operation conditions, a very small voltage difference between two nodes corresponds to a significant power flow. Therefore, $V_1^{dc}, V_2^{dc}, \ldots, V_N^{dc}$ are close to the rated voltage of the HVDC system, denoted as V_{ref}^{dc}.

4.1.2 Converters

We neglect the high-frequency characteristics of the converters, for the same reason as the DC transients. We assume that a converter can track instantaneously a reference signal for either the power injection into the DC grid via the converter P_i^{dc} or the converter's DC-side voltage V_i^{dc}.

4.1.3 AC areas

On the time scale of primary frequency control, the frequency can be considered identical in any part of an AC area. We use therefore an aggregated model to represent the loads and the generators within each area.

The sum of the loads within area i, denoted as P_{li}, is represented by a static load model [25]

$$P_{li} = P_{li}^{o} \cdot (1 + D_{li}(f_i - f_{nom,i})) , \tag{4.2}$$

where f_i is the frequency of area i, $f_{nom,i}$ is its nominal value, P_{li}^{o} is the power drawn by the load when $f_i = f_{nom,i}$, and D_{li} is the frequency sensitivity factor.

The mechanical dynamics of the generator for area i are described by the equation of motion

$$2\pi J_i \frac{df_i}{dt} = \frac{P_{mi} - P_{li} - P_i^{dc}}{2\pi f_i} - 2\pi D_{gi}(f_i - f_{nom,i}) , \tag{4.3}$$

where P_{mi}, J_i, and D_{gi} are respectively the mechanical power input, the moment of inertia, and the damping factor of the aggregated generator for area i. These parameters can be obtained by aggregation methods as in [26].

We assume that every AC area has the same type of primary frequency control, and we use the model given in Chapter 2 to represent its dynamics

$$T_{smi}\frac{dP_{mi}}{dt} = P^o_{mi} - P_{mi} - \frac{P_{nom,i}}{\sigma_i}\frac{f_i - f_{nom,i}}{f_{nom,i}} , \tag{4.4}$$

with P_{mi} bounded by

$$P^{\min}_{mi} \leq P_{mi} \leq P^{\max}_{mi} . \tag{4.5}$$

4.2 Reference operating point

The reference operating point of the system is a steady state defined by specific values of the input parameters (P^o_{li}, P^o_{mi}) and of the variables (f_i, P_{mi}, P_{li}, P^{dc}_i, V^{dc}_i). In the following, we denote as $\bar{P}^o_{li}$ and $\bar{P}^o_{mi}$ the values of P^o_{li} and P^o_{mi} at the reference operating point, respectively. We also denote the values of the variables at this point by their corresponding symbols with a bar overhead.

We take the frequencies at the reference operating point equal to their nominal values, i.e.

$$\bar{f}_i = f_{nom,i} , \quad \forall i \in \{1, 2, \ldots, N\} . \tag{4.6}$$

Then, (4.2) directly yields,

$$\bar{P}_{li} = \bar{P}^o_{li} , \quad \forall i \in \{1, 2, \ldots, N\} . \tag{4.7}$$

Since this reference operating point is an equilibrium point of each area, we get from (4.3) and (4.4)

$$\bar{P}_{mi} = \bar{P}^o_{mi} , \qquad \forall i \in \{1, 2, \ldots, N\} , \tag{4.8}$$

$$\bar{P}^{dc}_i = \bar{P}^o_{mi} - \bar{P}^o_{li} , \quad \forall i \in \{1, 2, \ldots, N\} . \tag{4.9}$$

The DC load flow equation (4.1) provides a final set of equations linking the voltage values to the other variables

$$\bar{P}^{dc}_i = \sum_{k=1}^{N} \frac{\bar{V}^{dc}_i(\bar{V}^{dc}_i - \bar{V}^{dc}_k)}{R_{ik}} , \quad \forall i \in \{1, 2, \ldots, N\} . \tag{4.10}$$

In practice, the values of power inputs $\bar{P}^o_{mi}$ are chosen such that, for reference loads and nominal frequencies, Equations (4.9) and (4.10) have a unique solution with one of the voltages $\bar{V}^{dc}_i$ equal to V^{dc}_{ref}.

4.3 Benchmark system

The benchmark system is made of five non-synchronous areas, connected by a five-terminal HVDC system. The converter of area 5 is chosen to regulate the DC voltage, whose setting is 100kV. The topology of the DC network is represented in Figure 4.2, where a circle represents a node to which a converter is connected, and an edge between two circles represents a DC line. The communication graph coincides with the network topology, i.e. each edge in the figure also

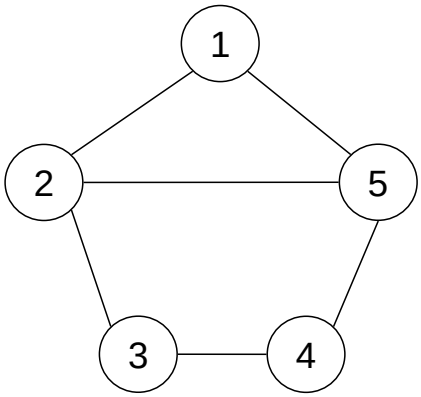

Figure 4.2: DC grid topology and communication graph of the benchmark system.

Table 4.1: Parameter values for the AC areas of the benchmark system.

Parameter	Area					Unit
	1	2	3	4	5	
f_{nom}	50	50	50	50	50	Hz
P_m^o	50	80	50	30	80	MW
P_{nom}	50	80	50	30	80	MW
J	2026	6485	6078	2432	4863	kg m^2
D_g	48.4	146.3	140.0	54.9	95.1	$W \cdot s^2$
σ	0.02	0.04	0.06	0.04	0.03	(dimensionless)
T_{sm}	1.5	2.0	2.5	2	1.8	s
P_l^o	100	60	40	50	40	MW
D_l	0.01	0.01	0.01	0.01	0.01	Hz^{-1}

represents a bi-directional communication channel between the two areas it connects. The DC resistances between the AC areas are: $R_{12} = 1.39\Omega$, $R_{15} = 4.17\Omega$, $R_{23} = 2.78\Omega$, $R_{25} = 6.95\Omega$, $R_{34} = 2.78\Omega$, and $R_{45} = 2.78\Omega$. The simulations consider AC areas with different parameters, as summarized in Table 4.1. The AC areas are simulated with the full nonlinear model described by (4.2), (4.3), (4.4). For the DC grid, we use (4.1) to calculate the DC load flow.

Chapter 5

Power-injection-based control scheme

This chapter presents a control scheme for sharing primary reserves among AC areas. We call it *power-injection-based control scheme* because it uses the power injections from the AC areas into the DC grid as the control variables.

Section 5.1 elaborates on the control scheme. Section 5.2 theoretically analyzes the stability of the controlled system. Section 5.3 presents simulation results.

The results reported in this chapter have been published in [28].

5.1 Control law

Sharing primary reserves between AC areas means that any area subjected to a power imbalance can rely on reserves provided not only by local generation but also by generators located in other areas. As primary frequency control usually relies on frequency measurements, which reflect the power balance of a synchronous area, a conventional way to achieve the above objective is to emulate a large AC interconnection so that the frequency deviations of all areas remain equal at all time.

To make every generator sensitive to a system-wide power imbalance, the frequency of every AC area must reflect the overall generation/demand balance of the entire system. This can be achieved by making the frequency deviations of all areas follow each other at any time.

In this section, we give the analytical expression of the control scheme and explain its working principle. We also discuss the technical limits imposed by the converters, as well as the presence of time-delays in the practical implementation of the control scheme.

5.1.1 Analytical expression

The power-injection-based control scheme modifies the power injections from the different AC areas into the DC grid. The control scheme is distributed by nature and is composed of $N-1$ subcontrollers, one for each HVDC converter except converter N which maintains the voltage

of the DC grid. The subcontroller assigned to converter $i \in \{1, 2, \ldots, N-1\}$ modifies the value of P_i^{dc} such that

$$P_i^{dc} = \bar{P}_i^{dc} + \alpha_i \sum_{k=1}^{N} b_{ik} \int (\Delta f_i - \Delta f_k) dt + \beta_i \sum_{k=1}^{N} b_{ik} (\Delta f_i - \Delta f_k) \,, \tag{5.1}$$

where

- $\Delta f_i = f_i - f_{nom,i}$ is the frequency deviation of area i.
- $\alpha_i \geq 0$ and $\beta_i \geq 0$ are respectively the integral control gain and the proportional control gain of subcontroller i.
- b_{ik}'s are the coefficients representing the communication graph between the AC areas. The value of b_{ik} equals 1 if subcontroller i receives frequency information of area k, and 0 otherwise.

The values of subcontroller gains α_i and β_i have a significant impact on the dynamics of the system. Roughly speaking, larger values of α_i and β_i will make the frequency deviation of area i stay closer to those of other areas. Gain values are limited in practice by (i) the maximal rate of change of power flows through the converter, and (ii) stability considerations of the controlled system, e.g., taking time-delays into account (see Section 5.1.4).

5.1.2 Working principle

The intuition behind the control scheme defined in (5.1) is as follows. If the frequency deviation of area i is higher (lower, resp.) than the average frequency deviation of the other areas, then more (less, resp.) power should be withdrawn from this area to drive its frequency deviation back towards the other areas'. The adjustment of this power (P_i^{dc}) is determined by subcontroller i, which is a PI controller whose error signal is the sum of the differences between its own frequency deviation and that of the AC areas from which it gets information. From a global point of view, the control scheme composed of all the subcontrollers takes the form of an algorithm for the consensus problem. This problem appears in the context of coordination of multi-agent systems: the objective is, for agents performing a collective task in a distributed way (that is, without a supervisor telling everyone what to do), to exchange and process information in order to reach agreement on quantities of interest that are necessary to coordinate their actions [29, 30]. This framework indeed corresponds to the HVDC interconnection setting. Theoretical results on consensus will therefore provide useful tools for the stability study of our control scheme.

5.1.3 Constraints

To ensure normal operation of the HVDC system, the control variables should be modulated subject to the following constraints

$$V_i^{dc,\min} \leq V_i^{dc} \leq V_i^{dc,\max}, \quad \forall i \in \{1, 2, \ldots, N\} \,, \tag{5.2a}$$

$$P_i^{dc,\min} \leq P_i^{dc} \leq P_i^{dc,\max}, \quad \forall i \in \{1, 2, \ldots, N\} \,, \tag{5.2b}$$

where $V_i^{dc,\min}$ and $V_i^{dc,\max}$ ($P_i^{dc,\min}$ and $P_i^{dc,\max}$, resp.) are the minimum and the maximum acceptable values of V_i^{dc} (P_i^{dc}, resp.).

In practice, these values should depend on both the technological features of converter i and the voltages at the other DC buses. Indeed, with an appropriate choice of $V_i^{dc,\min}$ and $V_i^{dc,\max}$, one can make sure that the transmission limits of the DC lines and the power rating of converter i are not exceeded.

5.1.4 Time-delays

Equation (5.1) should in principle determine the evolution of P_i^{dc}, which represents the power injection from area i into the HVDC grid. However, a subcontroller based on (5.1) would lead in a real power system to a variation of P_i^{dc} that may differ significantly from the one defined by this equation.

In fact, the frequency information of a remote AC area is usually provided by a wide area measurement system (WAMS). In such a system, phasor measurement units (PMU) are placed at the locations where the frequency information of interest is measured via the waveform of the voltage, based on which the frequency is calculated using discrete Fourier transform (DFT). Then, the frequency data is coded and transmitted over a certain medium, e.g. telephone lines or optical fibers, before finally reaching the destination where it is collected and decoded [31]. Thus, in the study and the implementation of the power-injection-based control scheme, the sum of the time necessary to measure the frequencies of the AC areas by the voltage transducers of the PMU, perform the DFT, code and transmit the data to subcontroller i, decode the received data at subcontroller i, compute a reference value for P_i^{dc}, and apply it to the converter can not be neglected. This may in turn lead to an effective variation of P_i^{dc} that is delayed with respect to the one predicted by (5.1).

To give numerical values for these time-delays, let us note that it takes at least one period, which is around 20ms (17ms, resp.), to measure a frequency close to 50Hz (60Hz, resp.). Concerning the time necessary to encode, transmit, and decode the frequency information, it is of the order of several hundreds of milliseconds [32, 31]. By way of example, the UCTE does not guarantee time-delays less than 2 seconds for transmitting information from a substation to a remote SCADA system [3]. As to the time necessary for a converter to effectively inject into the HVDC grid a power setting computed by its subcontroller, it can reach up to tens of milliseconds.

5.2 Theoretical study

The present section reports a theoretical study on the stability properties of the system under the power-injection-based control scheme around the reference operating point. First, some assumptions are made for the theoretical study. Second, the closed-system model is linearized around the reference operating point. Third, we prove the existence of a unique equilibrium point. Fourth, we use a frequency-domain approach to prove stability for the particular case where all the AC areas have identical parameters. Finally, we highlight the effects of the controller gains and the Laplacian matrix on the convergence speed using an algebraic approach.

5.2.1 Assumptions

The stability analysis on the power-injection-based control scheme relies on the following assumptions:

Assumption 5.1. *The losses within the DC grid do not vary with time, i.e.*

$$\sum_{i=1}^{N} \frac{dP_i^{dc}}{dt} = 0 \, . \tag{5.3}$$

Assumption 5.1 is justifiable for the reason that the losses in the DC grid are small compared to the power exchanged in the grid, and that the variations of these losses are still smaller compared to the total losses when $P_1^{dc}, P_2^{dc}, \ldots, P_{N-1}^{dc}$ vary according to (5.1).

Assumption 5.2. *The communication graph that represents the frequency information availability at different subcontrollers has the following properties:*

- *The communication graph is undirected, i.e. if the subcontroller of one area has access to the information on another area's frequency, then the subcontroller of this second area also has access to the information on the first area's frequency, i.e. if* $b_{ik} = 1$, *then* $b_{ki} = 1, \forall i \neq k, i, k \in \{1, 2, \ldots, N-1\}$.
- *The communication graph is connected, i.e. it can not be made of several parts which are not connected to each other, i.e. if* $b_{ik} = 0$, *then there must exist some intermediate indices* $k_1, k_2, \ldots, k_m$ *such that* $b_{ik_1} = b_{k_1k_2} = \ldots = b_{k_mj} = 1$.
- *It is constant in time.*

Observe that when combined with Assumption 5.1, the first property of Assumption 5.2 implies that P_N^{dc} also satisfies (5.1), where $b_{Ni} = b_{iN}, \forall i \in \{1, 2, \ldots, N\}$.

Assumption 5.3. *To simplify the study, we assume that the overall time-delays are the same regardless of the subcontroller considered and we denote it as* τ.

5.2.2 Linearized closed-loop system

We focus on small variations of the load, and consider thus a system linearized around the reference operating point. To highlight the effects of time-delays involved in the power-injection-based control scheme, the time-dependency of the variables is made explicit in notation.

The nonlinear equation resulting from (4.2) and (4.3) representing the electromechanical dynamics of area i is linearized around the reference operating point as

$$2\pi J_i \frac{df_i(t)}{dt} = \frac{P_{mi}(t) - P_{li}^o(t) - P_i^{dc}(t)}{2\pi f_{nom,i}} - 2\pi D_i(f_i(t) - f_{nom,i}) \, , \tag{5.4a}$$

where $D_i = D_{gi} + \bar{P}_{li}^o D_{li}/(4\pi^2 f_{nom,i})$. The dynamics of primary frequency control of with area i are modeled by

$$T_{smi} \frac{dP_{mi}(t)}{dt} = P_{mi}^o - P_{mi}(t) - \frac{P_{nom,i}}{\sigma_i} \frac{f_i(t) - f_{nom,i}}{f_{nom,i}} \, . \tag{5.4b}$$

Equations (5.4a) and (5.4b) describe the open-loop dynamics of area i. For this section to be self-contained, we rewrite here the control law[1] under Assumption 5.3

$$P_i^{dc}(t) = \bar{P}_i^{dc} + \alpha_i \sum_{k=1}^{N} b_{ik} \int (\Delta f_i(t-\tau) - \Delta f_k(t-\tau))dt + \beta_i \sum_{k=1}^{N} b_{ik}(\Delta f_i(t-\tau) - \Delta f_k(t-\tau)) \,, \tag{5.4c}$$

with $i = 1, 2, \ldots, N-1$. In addition, under Assumptions 5.1 and 5.2, $P_N^{dc}(t)$ also satisfies (5.4c).

In the present section, we focus on the close-loop system defined by (5.4) for all $i \in \{1, 2, \ldots, N\}$.

5.2.3 Equilibrium point

Proposition 5.1. *Consider that the system, initially operating at the reference operating point, is suddenly subjected to a step change in the load demand of one of its AC areas. Then, under Assumptions 5.1 and 5.2, the linearized system defined by* (5.4) *for all $i \in \{1, 2, \ldots, N\}$ has a unique equilibrium point, at which the frequency deviations of all AC areas are equal.*

Proof. We introduce the following variables: $x_i(t) = \Delta f_i(t)$, $y_i(t) = P_{mi}(t) - \bar{P}_{mi}$, $u_i(t) = P_i^{dc}(t) - \bar{P}_i^{dc}$, and $v_i(t) = P_{li}^{o}(t) - \bar{P}_{li}^{o}$. Denote the values of the variables at the equilibrium point by their corresponding symbols with a superscript e. With these notations and taking (4.6)-(4.10) into account, the equilibrium conditions associate to Equations (5.4) become

$$0 = -a_{1i}x_i^e + a_{2i}y_i^e - a_{2i}u_i^e - a_{2i}v_i^e \,, \tag{5.5}$$

$$0 = -a_{3i}x_i^e - a_{4i}y_i^e \,, \tag{5.6}$$

$$0 = \alpha_i \sum_{k=1}^{N} b_{ik}(x_i^e - x_k^e) \,, \tag{5.7}$$

where $a_{1i} = D_i/J_i$, $a_{2i} = 1/(4\pi^2 f_{nom,i} J_i)$, $a_{3i} = P_{nom,i}/(T_{smi}\sigma_i f_{nom,i})$, and $a_{4i} = 1/T_{smi}$. Note that a_{1i}, a_{2i}, a_{3i}, and a_{4i} are all positive constants. Define the column-vector $\mathbf{x}^e = [x_1^e, x_1^e, \ldots, x_N^e]^T$ and the matrices $A_\alpha = \mathrm{diag}(\alpha_1, \alpha_2, \ldots, \alpha_N)$ and L with

$$[L]_{ik} = \begin{cases} -b_{ik} & \text{for } i \neq k \,, \\ \sum_{k \neq i} b_{ik} & \text{for } i = k \,. \end{cases} \tag{5.8}$$

Then, (5.7) can be written in matrix form as

$$0 = A_\alpha L \mathbf{x}^e \,. \tag{5.9}$$

In graph theory, L is well-known as the Laplacian matrix associated to a communication graph. For a communication graph satisfying Assumption 5.2, L is symmetric positive semidefinite and its only zero eigenvalue corresponds to the eigenvector $\mathbf{1}_N$. Therefore, equilibrium

[1] It should be noted that we also deliberately introduce time-delays for the local frequency information, so that the remote frequency information at one instant is compared with the local information *at the same instant*. This choice conforms to the practice in the study on the algorithms for the consensus problem by the control engineering community [33].

requires that the frequency deviations of all AC areas be equal. Let x^e be the value of this common frequency deviation at the equilibrium point. From (5.5) and (5.6), we obtain

$$y_i^e = -\frac{a_{3i}}{a_{4i}} x^e \,, \tag{5.10}$$

$$u_i^e = -\left(\frac{a_{1i}}{a_{2i}} + \frac{a_{3i}}{a_{4i}}\right) x^e - v_i^e \,. \tag{5.11}$$

We see in the above expressions that if x^e can be uniquely determined, then the equilibrium point exists and is unique. In fact, Assumption 5.1 implies that $\sum_{i=1}^N u_i(t)$ remains constant, and the initial conditions at the reference operating point yield that $\sum_{i=1}^N u_i(0) = 0$. Thus,

$$\sum_{i=1}^N u_i^e = 0 \,. \tag{5.12}$$

From (5.11), we see that x^e is uniquely determined as

$$x^e = -\left(\sum_{i=1}^N v_i^e\right) \cdot \left(\sum_{i=1}^N \frac{a_{1i}a_{4i} + a_{2i}a_{3i}}{a_{2i}a_{4i}}\right)^{-1} \,. \tag{5.13}$$

□

Remark 5.1. *We consider in Proposition 5.1 that the step change in the load occurs in only one AC area. However, the expressions of the equilibrium values are also valid for the general case where $v_i(t)$ changes in more than one area and eventually settles at v_i^e different from* 0.

Remark 5.2. *A physical interpretation for the different components of the equilibrium point can be found. Indeed, from* (5.10) *and* (5.11)*, we have*

$$\sum_{i=1}^N y_i^e = \sum_{i=1}^N v_i^e + \sum_{i=1}^N u_i^e - \left(\sum_{i=1}^N \frac{a_{1i}}{a_{2i}}\right) x^e \,, \tag{5.14}$$

where

- $\sum_{i=1}^N y_i^e$ *is the total change in the mechanical power due to primary frequency control of all areas;*
- $\sum_{i=1}^N v_i^e$ *is the total change in the load demand;*
- $\sum_{i=1}^N u_i^e$ *is the total change in the losses within the DC grid, and it equals* 0 *(see* (5.12)*);*
- $(\sum_{i=1}^N a_{1i}/a_{2i})x^e$ *contains the damping effects of the generators and the loads resulted from non-zero frequency deviations.*

In practice, the order of magnitude of $(\sum_{i=1}^N a_{1i}/a_{2i})x^e$ is much smaller than that of $\sum_{i=1}^N v_i^e$, which means that the final variation in mechanical power induced by primary frequency control of all the areas is approximately equal to the total variation in the load.

Remark 5.3. *The equilibrium point, which is a static quantity, is of course independent of time-delay τ. However, time-delays play a crucial role in the system's convergence towards the equilibrium or not, which we study next.*

5.2.4 Stability of the system with identical AC areas

Theoretically proving stability of the system for the general case is particularly difficult. We present hereafter a result for the particular case where all AC areas are identical. More precisely, we assume that all system parameters, as well as the nominal frequencies $f_{nom,i}$ and the loads $\bar{P}^o_{li}$, are independent of area index i; however, $\bar{P}^o_{mi}$ and $\bar{P}^{dc}_i$ can be different from one AC area to the other. Proposition 5.2 establishes stability of the linearized system. The original nonlinear system inherits the stability properties of its linearized counterpart provided that the load perturbations around reference are sufficiently small.

Proposition 5.2. *Consider that all AC areas of the system have identical parameters, and that Assumptions 5.1, 5.2, and 5.3 are satisfied. Denote as λ_N and λ_2, respectively the largest and smallest non-zero eigenvalues of the Laplacian associated to the communication graph (see (5.8)). Then the system is stable, and following a step change in the load it asymptotically converges to the unique equilibrium point of Proposition 5.1, if the net encirclement of any point on the segment $(-1/\lambda_2, -1/\lambda_N)$ by the Nyquist plot of $h(s)(\alpha+\beta s)e^{-\tau s}/s$ is zero.*

Proof. We drop AC area index i when referring to the parameters of the areas that have the same values. With the notations introduced in Section 5.2.3, applying the Laplace transform to (5.4a) and (5.4b) yields

$$x_i(s) = \frac{a_2}{s+a_1} y_i(s) - \frac{a_2}{s+a_1}(u_i(s) + v_i(s)) \,, \tag{5.15}$$

$$y_i(s) = -\frac{a_3}{s+a_4} x_i(s) \,, \tag{5.16}$$

where $a_1 = D/J$, $a_2 = 1/(4\pi^2 f_{nom} J)$, $a_3 = P_{nom,i}/(T_{sm}\sigma f_{nom})$, and $a_4 = 1/T_{sm}$. Replacing $y_i(s)$ in (5.15) by (5.16) yields

$$x_i(s) = \frac{-a_2(s+a_4)}{(s+a_1)(s+a_4)+a_2 a_3}(u_i(s) + v_i(s)) \,, \tag{5.17}$$

Define the transfer function

$$h(s) = \frac{a_2(s+a_4)}{(s+a_1)(s+a_4)+a_2 a_3} \,. \tag{5.18}$$

Then, Equation (5.17) can be written in matrix form as

$$\mathbf{x}(s) = -h(s) I_N(\mathbf{u}(s) + \mathbf{v}(s)) \,, \tag{5.19}$$

where $\mathbf{x} = [x_1, x_2, \ldots, x_N]^T$, $\mathbf{u} = [u_1, u_2, \ldots, u_N]^T$, $\mathbf{v} = [v_1, v_2, \ldots, v_N]^T$. By following the same procedure, the dynamics of P^{dc}_i defined by (5.4c) can be expressed in the frequency domain as

$$u_i(s) = \left(\frac{\alpha}{s} + \beta\right) e^{-\tau s} \sum_{k=1}^{N} b_{ik}(x_i(s) - x_k(s)) \,, \tag{5.20}$$

which can be written in matrix form for $i = 1, 2, \ldots, N$ as

$$\mathbf{u}(s) = \left(\frac{\alpha}{s} + \beta\right) e^{-\tau s} L\mathbf{x}(s) \,. \tag{5.21}$$

By replacing $\mathbf{u}(s)$ in (5.19) by (5.21), we have

$$\mathbf{x}(s) = -s\ h(s)\ (sI_N + h(s)(\alpha + \beta s)e^{-\tau s}L)^{-1}\mathbf{v}(s)\ . \tag{5.22}$$

Define

$$G_\tau(s) = -s\ h(s)\ (sI_N + h(s)(\alpha + \beta s)e^{-\tau s}L)^{-1}\ . \tag{5.23}$$

Then, $G_\tau(s)$ is the MIMO transfer function between $\mathbf{v}(s)$, the load change vector, and $\mathbf{v}(s)$, the frequency deviation vector.

The system defined by (5.22) is asymptotically stable if all the poles of its transfer function $G_\tau(s)$ are on the open left half-plane. Since $h(s)$ is itself a stable transfer function because of the positiveness of a_1, a_2, a_3, and a_4, we only have to investigate the zeros of $Z_\tau(s) = sI_N + h(s)(\alpha + \beta s)e^{-\tau s}L$.

Under Assumption 5.2, the Laplacian L of the communication graph is positive semidefinite and has a single zero eigenvalue. Thus, $L = VDV^T$ where V is an orthogonal matrix (containing eigenvectors of L) and D is diagonal (containing eigenvalues $0 = \lambda_1 < \lambda_2 \leq \lambda_3 \leq \ldots \leq \lambda_N$). Now $V^T Z_\tau(s)V = sI_N + h(s)(\alpha + \beta s)e^{-\tau s}D$ has the same zeros as $Z_\tau(s)$. A single zero at $s = 0$ is obtained with eigenvector of $\lambda_1 = 0$. The latter however cancels with the zero at $s = 0$ in the numerator[2] of $G_\tau(s)$. To ensure input-output stability, $Z_\tau(s)$ must be positive definite in the subspace spanned by all other eigenvectors (which we denoted as ω_k), for s in the closed right half-plane. This means that

$$\begin{aligned}(sI_N + h(s)(\alpha + \beta s)e^{-\tau s}L)\omega_k &= s\omega_k + \lambda_k h(s)(\alpha + \beta s)e^{-\tau s}\omega_k \\ &= (s + \lambda_k h(s)(\alpha + \beta s)e^{-\tau s})\omega_k \\ &= 0\ ,\end{aligned} \tag{5.24}$$

with $k > 1$ may not have solutions in the closed right half-plane. The Nyquist criterion says that this holds if the net encirclement of the point $(-1/\lambda_k, 0)$ by the Nyquist plot of $h(s)(\alpha+\beta s)e^{-\tau s}/s$ is zero. Hence the proposition's requirement. Because the whole system's state is observable from the frequency deviation signals, output (i.e. frequency deviation) stability implies stability of the whole state.

The output corresponding to zero initial conditions and a step input

$$\mathbf{v}(t) = \begin{cases} 0 & \text{for } t < 0\ , \\ \bar{\mathbf{v}}^e & \text{for } t > 0\ , \end{cases} \tag{5.25}$$

is then given by

$$\mathbf{x}(s) = G_\tau(s)\mathbf{v}(s) = \frac{1}{s}G_\tau(s)\ \bar{\mathbf{v}}^e\ . \tag{5.26}$$

As before, we can diagonalize (5.26) in the basis of eigenvectors of L. From the previous analysis/conditions, components corresponding to λ_k, $k > 1$, have negative poles and therefore, according to linear systems theory, exponentially decay to zero. The term $1/s$ in (5.26) introduced by $v(s)$ is the only term that does not decay away in the output, and in time-domain it corresponds to a step change which represents the shift by x_e of all frequency deviations at equilibrium. □

[2]This does not correspond to the pole cancellation control. As a matter of fact, the "s" factors in denominator and numerator also cancel for the open-loop system, which is stable. The factors "s" come from rewriting our dynamics, so the pole and zero at $s = 0$ always cancel exactly.

Corollary 5.1. *The above criterion yields that the system defined by* (5.22) *is always stable for* $\tau = 0$.

Proof. To show this, we define

$$J(s) = \lambda_k h(s)(\alpha + \beta s)/s = \frac{\lambda_k a_2 (s + a_4)(\beta s + \alpha)}{s[(s + a_1)(s + a_4) + a_2 a_3]} \, . \tag{5.27}$$

The argument of $J(s)$ can be calculated as

$$\arg(J(s)) = \arg(s + a_4) + \arg(\beta s + \alpha) - 90^\circ - \arg((s + a_1)(s + a_4) + a_2 a_3) \, . \tag{5.28}$$

With the definition of all the coefficients in $J(s)$, we have

$$\arg((s + a_1)(s + a_4) + a_2 a_3) < \arg((s + a_1)(s + a_4)) = \arg(s + a_1) + \arg(s + a_4) \, , \tag{5.29}$$

from which

$$\arg(J(s)) > \arg(\beta s + \alpha) - 90^\circ - \arg(s + a_1) > -180^\circ \, . \tag{5.30}$$

On the other hand, it is straightforward to see that $\arg(J(s)) < 180^\circ$. Thus, the Nyquist plot of $J(s)$ can not intersect with the negative real axis as s grows from $j0$ to $j\infty$. Therefore, the points on the segment $(-1/\lambda_2, -1/\lambda_N)$ are never encircled, which, according to Proposition 5.2, implies that the system is always stable for $\tau = 0$. □

5.2.5 Convergence speed of the frequency deviations

In the following, we investigate the factors determining the convergence speed of the frequency deviations. To this end, we first use an algebraic approach to prove that such a system is stable when $\tau = 0$. Then, we comment on the role of the controller gains and the Laplacian matrix.

Proposition 5.3. *Consider that all the AC areas of the HVDC system under Assumptions 5.1, 5.2 and 5.3 have identical parameters and that* $\tau = 0$. *Then, the unique equilibrium with equal frequency deviations given by Equations* (5.10), (5.11), *and* (5.13) *is stable for any* $\alpha > 0$ *and* $\beta \geq 0$.

Proof. With the notations introduced earlier in the current section, Equations (5.4a)-(5.4c) can be written in matrix form as

$$\begin{aligned} \frac{d}{dt} \begin{bmatrix} \mathbf{x}(t) - \mathbf{x}^e \\ \mathbf{y}(t) - \mathbf{y}^e \\ \mathbf{u}(t) - \mathbf{u}^e \end{bmatrix} &= \begin{bmatrix} -A_1 & A_2 & -A_2 \\ -A_3 & -A_4 & 0 \\ \alpha L - \beta L A_1 & \beta L A_2 & -\beta L A_2 \end{bmatrix} \begin{bmatrix} \mathbf{x}(t) - \mathbf{x}^e \\ \mathbf{y}(t) - \mathbf{y}^e \\ \mathbf{u}(t) - \mathbf{u}^e \end{bmatrix} \\ &\doteq M \begin{bmatrix} \mathbf{x}(t) - \mathbf{x}^e \\ \mathbf{y}(t) - \mathbf{y}^e \\ \mathbf{u}(t) - \mathbf{u}^e \end{bmatrix} \, , \end{aligned} \tag{5.31}$$

where $\mathbf{y} = [y_1, y_2, \ldots, y_N]^T$, and $\mathbf{u}^e$ and $\mathbf{y}^e$ are defined in a similar manner.

The stability of this system – and thus the convergence property of the system towards equal frequency deviations when subjected to small load variations – can be inferred from the

eigenvalues of M. It is not difficult to see that M will always have one zero eigenvalue, associated to the eigenvector $[\mathbf{x}^e, \mathbf{y}^e, \mathbf{u}^e + \mathbf{v}]^T$ defined above. This strict zero eigenvalue corresponds to an equilibrium shift: there is a priori a continuum of equilibria for M. However, the addition of Assumption 5.1 ensures that there is only one possible equilibrium for a given contingency – see the preceding Proposition 5.1. As a conclusion, M has one 0 eigenvalue which is irrelevant given Assumption 5.1, and stability is dictated by its $3N - 1$ remaining eigenvalues.

Under Assumption 5.2, the Laplacian L of the communication graph is positive semidefinite and has a single zero eigenvalue. Thus, $L = VDV^T$ where V is an orthogonal matrix (containing eigenvectors of L) and D is diagonal (containing eigenvalues $0 = \lambda_1 < \lambda_2 \leq \lambda_3 \leq \ldots \leq \lambda_N$). Then we have

$$(I_3 \otimes V^{-1})M(I_3 \otimes V) = \begin{bmatrix} -a_1 I_N & a_2 I_N & -a_2 I_N \\ -a_3 I_N & -a_4 I_N & 0 \\ \alpha D - \beta a_1 D & \beta a_2 D & -\beta a_2 D \end{bmatrix} \doteq \tilde{M} \, . \tag{5.32}$$

$\tilde{M}$ has the same eigenvalues as M. By simple reordering of rows and columns, $\tilde{M}$ can further be brought into block-diagonal form where each block takes the form

$$\tilde{M}_i = \begin{bmatrix} -a_1 & a_2 & -a_2 \\ -a_3 & -a_4 & 0 \\ \alpha\lambda_i - \beta a_1 \lambda_i & \beta a_2 \lambda_i & -\beta a_2 \lambda_i \end{bmatrix} , \tag{5.33}$$

one for each eigenvalue of L.

For $i = 1$, we have $\lambda_1 = 0$, which gives the zero eigenvalue associated to equilibrium shift, and covered by Assumption 5.1. The two remaining eigenvalues of $\tilde{M}_1$ are those of the matrix $\begin{bmatrix} -a_1 & a_2 \\ -a_3 & -a_4 \end{bmatrix}$. Since the constants a_1, a_2, a_3, a_4 are all positive as defined earlier, the eigenvalues associated to $\tilde{M}_1$ must have negative real part.

Let ξ_k denote an eigenvalue of $\tilde{M}_i$ for $i > 1$. To find it, we write

$$\begin{aligned} &\det(\xi_k I_3 - \tilde{M}_i) \\ &= \xi_k^3 + (a_1 + a_4 + \beta a_2 \lambda_i)\xi_k^2 + (a_1 a_4 + a_2 a_3 + \alpha a_2 \lambda_i + \beta a_2 a_4 \lambda_i)\xi_k + \alpha a_2 a_4 \lambda_i \, . \end{aligned} \tag{5.34}$$

By the Routh-Hurwitz stability criterion for negativity of polynomial roots, all ξ_k will have negative real part if, for all $i > 1$,

$$(a_1 + a_4 + \beta a_2 \lambda_i) > 0 \, , \tag{5.35a}$$

$$(a_1 + a_4 + \beta a_2 \lambda_i)(a_1 a_4 + a_2 a_3 + \alpha a_2 \lambda_i + \beta a_2 a_4 \lambda_i) - \alpha a_2 a_4 \lambda_i > 0 \, , \tag{5.35b}$$

$$\alpha a_2 a_4 \lambda_i > 0 \, . \tag{5.35c}$$

Given the positiveness of the efficients a_1, a_2, a_3, a_4 defined in Section 5.2.3, the above inequalities are satisfied for all $\lambda_i > 0$ as long as $\alpha > 0$ and $\beta \geq 0$. □

Remark 5.4. *If we choose $\beta = 0$, then the system will converge at a slow pace dictated by the system's dissipation. Taking $\beta > 0$ introduces a dissipation-like term in the controller and therefore allows much faster and less oscillatory convergence to equal frequency deviations.*

Remark 5.5. *Note that the controller gains α and β are always multiplied by the graph connectivity eigenvalue λ_i in Equation* (5.34)*. The slowest convergence speed will therefore be dictated by the smallest Laplacian eigenvalue, λ_2. The latter is an extensively studied object of graph theory, where it is called the* algebraic graph connectivity*. This should allow evaluating which graphs are more or less favorable (i.e. requiring smaller or larger gains in our controller) for synchronization of frequency deviations.*

5.3 Simulations

The effectiveness of the proposed control scheme is illustrated hereafter in the context of the five-area benchmark system described in the previous chapter. To observe the system's response to a power imbalance, we assume that all the areas initially operate in steady state at the nominal frequency. Then at time $t = 2$s, a step increase by 5% of the value of P_{l2}^o (see Equation (4.2)) is considered. The continuous-time differential equations are integrated using a Euler method with a time-discretization step of 1ms.

To show the effectiveness of the control scheme as well as the role of the controller gains, we consider no time-delay and discuss simulation results under this assumption. Then, we highlight the effects of the time-delays on the stability of the controlled system.

5.3.1 Results when $\tau = 0$s

Figure 5.1 gives the evolution of the frequencies when $\tau = 0$s and $\alpha = \beta = 2 \times 10^6$. For comparison, we also show in the same figure the frequency of area 2 when the control scheme is not applied (i.e. $\alpha = \beta = 0$). The simulations show that without the control scheme, the frequency of area 2 undergoes a deviation with transient maximum of 0.196Hz and stabilizes at 49.927Hz. When the control scheme is applied, the maximum transient deviation of area 2 drops to 0.136Hz, and the frequencies of the five areas converge to each other to finally settle at 49.983Hz. Figure 5.2 shows the evolution of $P_1^{dc}, P_2^{dc}, \ldots, P_5^{dc}$ expressed in MW. P_2^{dc} is the power injection which varies the fastest. In particular, it decreases by 8% within 1 second following the load step increase.

The above results show that our control scheme leads to a significant improvement in the steady-state frequency deviation of area 2, from 0.073Hz to 0.017Hz. However, the transient performance is quite poor, since the maximum transient deviation is just slightly reduced from 0.196Hz to 0.136Hz. To improve the transient performance, we increase the controller gains. For the sake of simplicity, we impose that $\alpha = \beta$. Figure 5.3 shows the frequencies when the controller gains are increased to $\alpha = \beta = 1 \times 10^7$. Compared to Figure 5.1, the transient behavior is significantly improved with the larger controller gains: the frequencies of all the areas converge to each other more quickly; the maximal transient deviation of area 2 is reduced to 0.075Hz, while the steady-state equilibrium does not change, as suggested by Proposition 5.1. The improvement in the transient behavior comes at the price of faster variations of the power injections, which are shown in Figure 5.4. In this case, P_2^{dc} decreases by 14% within 1 second after the load step increase. Nevertheless, even for these larger controller gains, the variations in P_i^{dc} remain moderately small. From an engineering point of view, the power injection variations shown in the figures are within modern converters' power-tracking speed limit, as shown in other

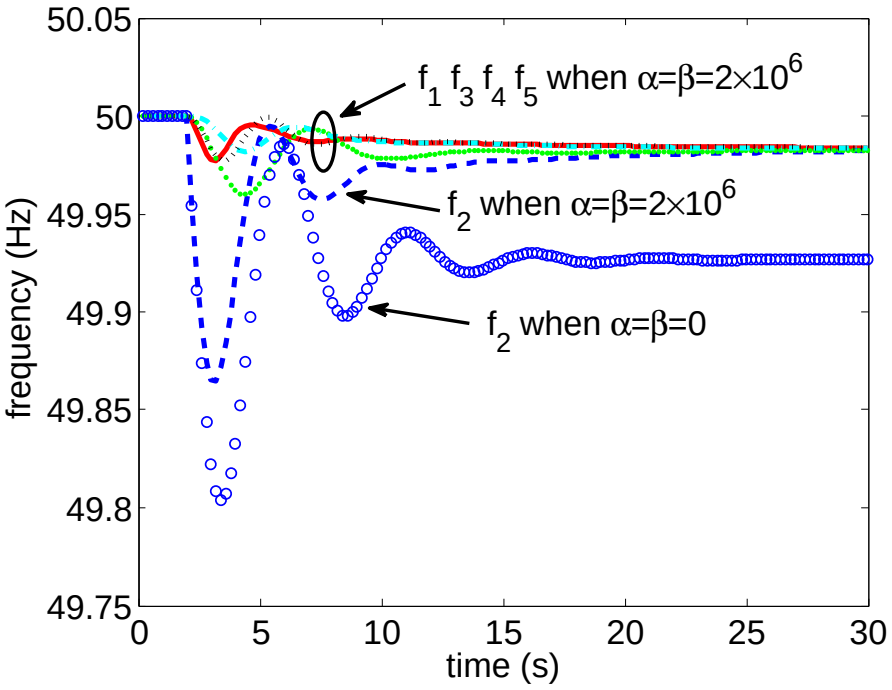

Figure 5.1: Frequencies of the five AC areas under the power-injection-based control scheme when $\tau = 0$s and $\alpha = \beta = 2 \times 10^6$. The evolution of f_2 when $\alpha = \beta = 0$ is also shown.

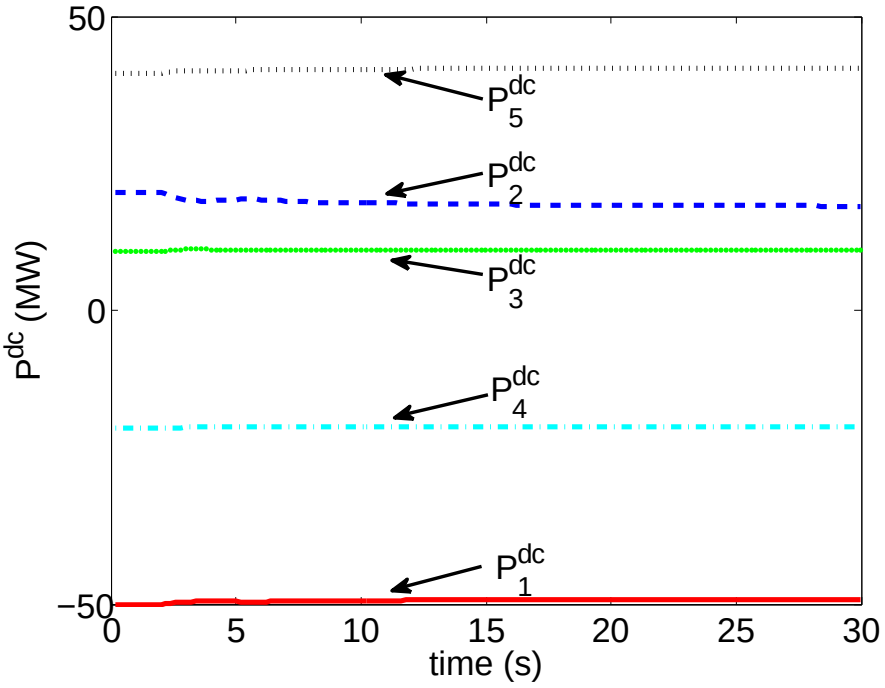

Figure 5.2: Power injections from the five AC areas into the DC grid under the power-injection-based control scheme when $\tau = 0$s and $\alpha = \beta = 2 \times 10^6$.

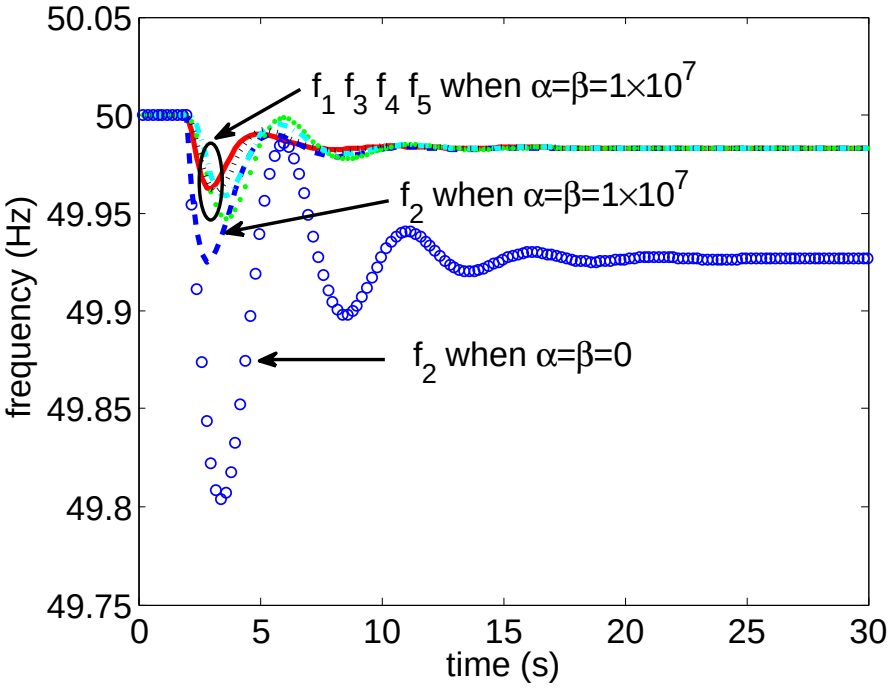

Figure 5.3: Frequencies of the five AC areas under the power-injection-based control scheme when $\tau = 0$s and $\alpha = \beta = 1 \times 10^7$. The evolution of f_2 when $\alpha = \beta = 0$ is also shown.

studies such as [34, 35].

In the simulations, we have considered that the primary reserve of each generator were equal to its initial power output. For the case of smaller reserves, additional simulations not reported here show that the frequencies still converge even if some areas have reached their primary reserve limits. However, when the primary reserves of all areas are depleted, generators are unable to restore the overall power balance and all the frequencies would keep decreasing, until they reach a certain threshold that triggers emergency control actions such as load-shedding in a real power system.

5.3.2 Effects of the time-delays

The simulations reported above show that for $\tau = 0$s, the control scheme (5.1) drives the frequency deviations of all the areas to the same value. Additionally, when the frequencies are stabilized, the frequency in area 2 is equal to a value which is closer to $f_{nom,2}$ than when the DC converters are operated with constant power injection.

In contrast, in the presence of time-delays, simulations show that the frequency deviations may fail to converge to each other. In particular, for given values of α and β, there generally exists a maximum acceptable time-delay beyond which the AC areas' frequencies exhibit oscillations of increasingly large magnitude. For example, when the controller gains are chosen to be 2×10^6, f_1 still converges despite oscillations when $\tau = 0.5$s and fails to converge when $\tau = 0.8$s, as shown in Figure 5.5. For comparison, the evolution of f_1 when $\tau = 0$s is also shown in the same

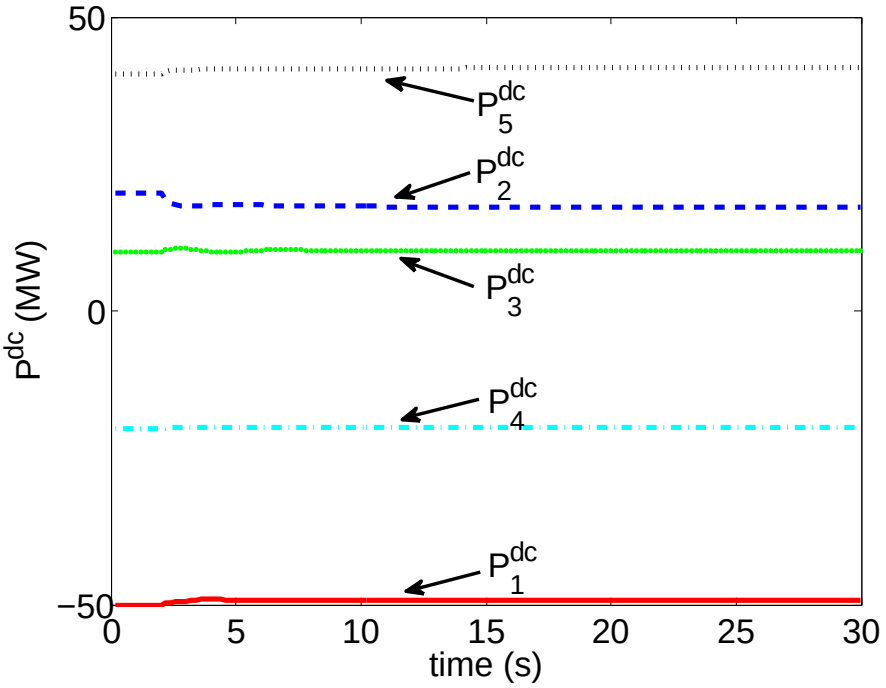

Figure 5.4: Power injections from the five AC areas into the DC grid under the power-injection-based control scheme when $\tau = 0$s and $\alpha = \beta = 1 \times 10^7$.

figure.

To determine whether the frequency deviations of all the AC areas converge to each other, we define the following criterion, similar to the error band used in the definition of settling time in control theory [36]. Let us denote by Δf^e the common value to which the frequency deviations of all AC areas converge when $\tau = 0$s. We classify the system as practically stable as long as after $t > 22$s, i.e. 20 seconds after the step change in the load, all the AC areas' frequency deviations remain within $\pm$ 50mHz around Δf^e, i.e.

$$|\Delta f_i(t) - \Delta f^e| \leq 50\text{mHz}, \ \forall i \text{ and } \forall t > 22\text{s} \ . \tag{5.36}$$

We define $\tau_{\max}$ as the largest value of the time-delay for which (5.36) is satisfied and we search for a relation that may exist between $\tau_{\max}$ and the controller gains. To ease the analysis, we impose that $\alpha = \beta$. We compute $\tau_{\max}$ for different $\alpha = \beta \in [1 \times 10^6, 1 \times 10^8]$ by a binary search in $\tau \in [0, 2]$s.

The points in Figure 5.6 represent values of $\tau_{\max}$ corresponding to different $\alpha = \beta$. We can see that by decreasing the values of the controller gains, the harmful oscillations introduced by time-delays can be curbed. For example, if τ is around two seconds for our system, then we have to decrease the controller gains to a value around 1×10^6 to avoid stability problems. However, as pointed out earlier in the current section, with lower values of the controller gains, more time is needed for the frequency deviations to converge to similar values.

This phenomenon is illustrated here for $\tau = 2$s by the two sets of curves in Figures 5.7 and 5.8 that represent the evolution of the frequencies in the five areas of the system for $\alpha = \beta = 1 \times 10^6$

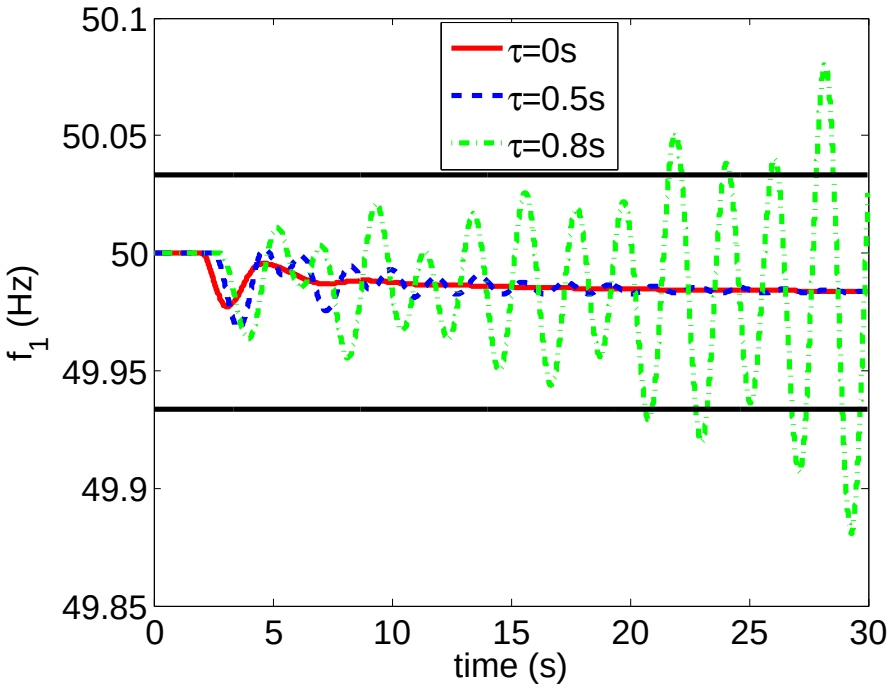

Figure 5.5: Frequency of AC area 1 for $\tau = 0$s, $\tau = 0.5$s, and $\tau = 0.8$s under the power-injection-based control scheme when $\alpha = \beta = 2 \times 10^6$. The two horizontal lines draw the band of the practical stability criterion, which is ± 50mHz around Δf^e.

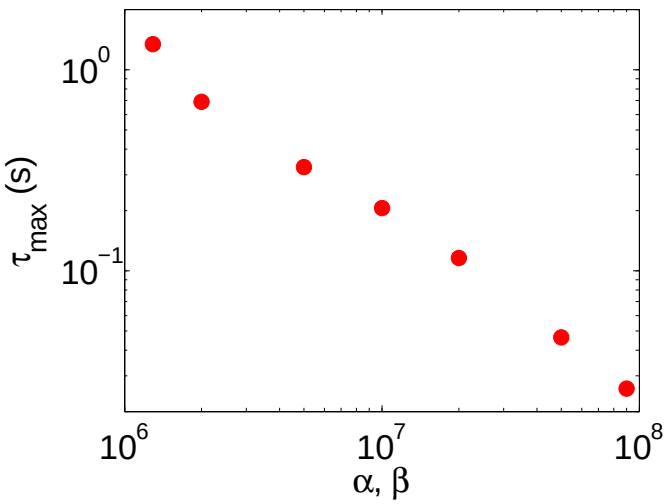

Figure 5.6: Values of $\tau_{\max}$ for several values of $\alpha = \beta$.

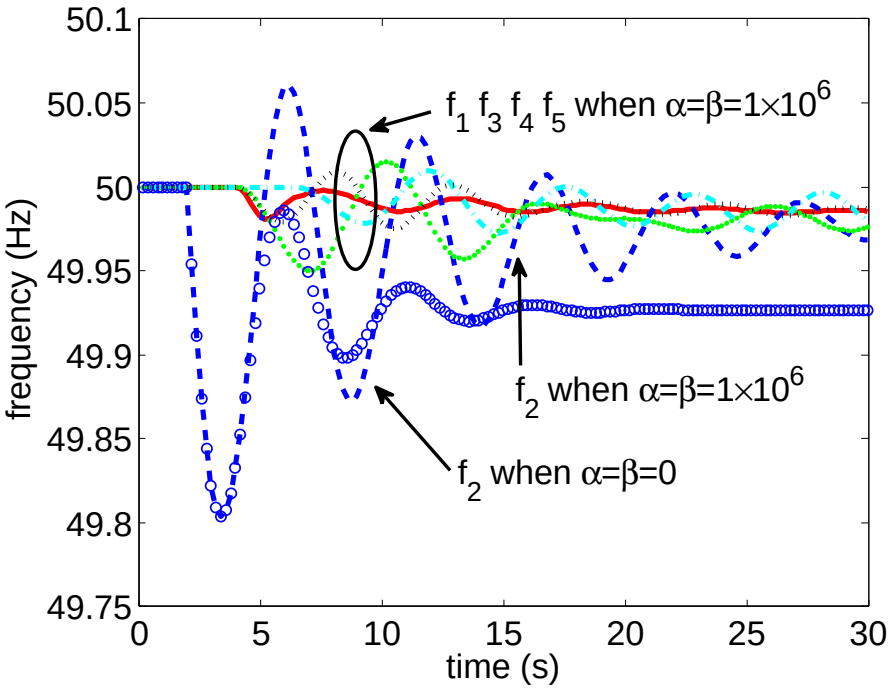

Figure 5.7: Frequencies of the five AC areas under the power-injection-based control scheme when $\tau = 2$s and $\alpha = \beta = 1 \times 10^6$. The evolution of f_2 when $\alpha = \beta = 0$ is also shown.

and for $\alpha = \beta = 1 \times 10^5$. Note that we also represent in these figures the evolution of f_2 when the control scheme is not implemented (i.e. $\alpha = \beta = 0$).

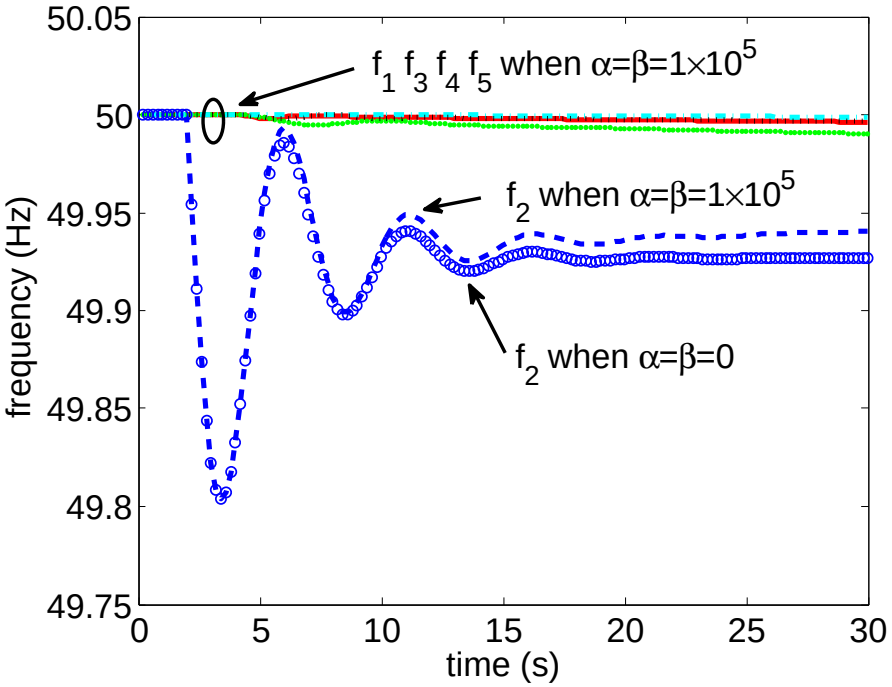

Figure 5.8: Frequencies of the five AC areas under the power-injection-based control scheme when $\tau = 2$s and $\alpha = \beta = 1 \times 10^5$. The evolution of f_2 when $\alpha = \beta = 0$ is also shown.

Chapter 6

DC-voltage-based control scheme

In the previous chapter, we propose a control scheme that modifies the power injections into the DC grid based on frequency measurements of other areas so as to make their frequency deviations evolve towards the same value. That control scheme makes the AC areas collectively react to power imbalances. Since this approach requires transmission of frequency information among the AC areas, considerable delays (of the order of a few seconds) can be involved. As shown earlier, such delays reduce the efficiency of the control scheme and may even lead to instability.

In the present chapter, we propose another control scheme that makes decisions based only on local frequency measurement, thus eliminating the need of communication between remotely located AC areas. We call it *DC-voltage-based control scheme* because it uses the DC-side voltages of the HVDC converters as the control variables.

Section 6.1 elaborates on the new control scheme. Section 6.2 theoretically analyzes the stability of the controlled system. Section 6.3 presents simulation results. Section 6.4 theoretically studies the case when the control scheme is applied to some but not all of the converters. Section 6.5 discusses the practical implementation of the control scheme.

The results reported in the first three sections of the current chapter have been published in [37].

6.1 Control law

We continue to use the multi-terminal HVDC model given in Section 4.1. Also, we assume that prior to any disturbance, the system is at the reference operating point described in Section 4.2.

6.1.1 Analytical expression

The DC-voltage-based control scheme is decentralized by nature and is composed of N subcontrollers, one for each HVDC converter. The subcontroller assigned to converter $i \in \{1, 2, \ldots, N\}$ modifies the value of V_i^{dc} such that

$$V_i^{dc} = \bar{V}_i^{dc} + \alpha_i \Delta f_i \ , \tag{6.1}$$

where

- $\Delta f_i = f_i - f_{nom,i}$ is the frequency deviation of area i;
- α_i is the gain of subcontroller i.

The value of subcontroller gain α_i has a significant impact on the dynamics of the system. Roughly speaking, an area with a larger value of α_i will stay closer to its nominal frequency than an area with a smaller α_i.

6.1.2 Working principle

The intuition behind the control law defined in (6.1) is as follows. If for instance area i has more generation than the sum of the load and the injection into the DC grid, then its frequency f_i will increase. To restore the balance of area i, more power should be injected from area i into the DC grid. To achieve this, the DC voltage V_i^{dc} is increased so that the voltage difference $V_i^{dc} - V_k^{dc}$ becomes higher, under unchanged V_k^{dc}, for all $k \neq i$. By virtue of the DC flow equation (4.1), this yields increased power injected from area i to the other areas. The other areas, injecting less power into (or equivalently, withdrawing more power from) the DC grid, see their frequencies increase and as a consequence also raise their voltages. In conclusion, the network as a whole reacts to the imbalance in area i, distributing the voltage and the frequency deviation over the whole network.

6.1.3 Constraints

The constraints are the same as in the previous chapter. For the DC-voltage-based control scheme, the constraints on P_i^{dc} can be *dynamically* assimilated by the constraints on V_i^{dc}. In particular, if $P_i^{dc} = P_i^{dc,\max}$, we can require that V_i^{dc} should not further increase, or alternatively, take the current value of V_i^{dc} as the new $V_i^{dc,\max}$. In addition, when V_k^{dc}, $k \neq i$ decrease, $V_i^{dc,\max}$ (and thus V_i^{dc}) should also decrease, to guarantee that P_i^{dc} does not exceed its limit.

6.2 Theoretical study

The present section reports a theoretical study on the stability properties of the system under the DC-voltage-based control scheme around the reference operating point. First, the linearized closed-system model used in the theoretical study is presented. Second, we prove the existence of a unique equilibrium point. Third, we prove stability using a new frequency-domain approach. Finally, the unique equilibrium point for this case is characterized to highlight the effectiveness of the controller and illustrate the influence of the controller gain.

6.2.1 Linearized closed-loop system

We focus on small variations of the load, and consider thus a system linearized around the reference operating point. Since no delay is involved with the DC-voltage-based control scheme, we omit in notation the time-dependency of the variables.

The differential equations describing the open-loop dynamics of area i are the same as in the previous chapter, i.e.

$$2\pi J_i \frac{df_i}{dt} = \frac{P_{mi} - P_{li}^o - P_i^{dc}}{2\pi f_{nom,i}} - 2\pi D_i(f_i - f_{nom,i}) \ , \tag{6.2a}$$

$$T_{smi}\frac{dP_{mi}}{dt} = P_{mi}^o - P_{mi} - \frac{P_{nom,i}}{\sigma_i}\frac{f_i - f_{nom,i}}{f_{nom,i}} \ . \tag{6.2b}$$

As $V_1^{dc}, V_2^{dc}, \ldots, V_N^{dc}$ are all close to V_{ref}^{dc} under normal opeartion, we approximate DC power flow (4.1) by

$$P_i^{dc} = \sum_{k=1}^{N} \frac{V_{ref}^{dc}(V_i^{dc} - V_k^{dc})}{R_{ik}} \ . \tag{6.2c}$$

For this section to be self-contained, we rewrite here the control law

$$V_i^{dc} = \bar{V}_i^{dc} + \alpha_i \Delta f_i \ . \tag{6.2d}$$

In the present section, we focus on the closed-loop system defined by (6.2) for all $i \in \{1, 2, \ldots, N\}$.

6.2.2 Equilibrium point

Proposition 6.1. *Consider that the system, initially operating at the reference operating point, is suddenly subjected to a step change in the load demand of one of its AC areas. The (linearized) system defined by* (6.2) *for all* $i \in \{1, 2, \ldots, N\}$ *has a unique equilibrium point.*

Proof. We introduce the following variables: $x_i = \Delta f_i$, $y_i = P_{mi} - \bar{P}_{mi}$, $z_i = V_i^{dc} - \bar{V}_i^{dc}$, $u_i = P_i^{dc} - \bar{P}_i^{dc}$ and $v_i = P_{li}^o - \bar{P}_{li}^o$. Denote the values of the variables at the equilibrium point by their corresponding symbols with a superscript e. With these notations and taking into account the equations describing the reference operating point (4.6)-(4.10), the equilibrium conditions associated to (6.2) become

$$0 = -a_{1i}x_i + a_{2i}y_i - a_{2i}u_i - a_{2i}v_i \ , \tag{6.3a}$$

$$0 = -a_{3i}x_i - a_{4i}y_i \ , \tag{6.3b}$$

$$z_i = \alpha_i x_i \ , \tag{6.3c}$$

$$u_i = \sum_{k=1}^{N} b_{ik}(z_i - z_k) + b_i \ , \tag{6.3d}$$

where $a_{1i} = D_i/J_i$, $a_{2i} = 1/(4\pi^2 f_{nom,i} J_i)$, $a_{3i} = P_{nom,i}/(T_{smi}\sigma_i f_{nom,i})$, $a_{4i} = 1/T_{smi}$, $b_i = \sum_k (V_{ref}^{dc} - \bar{V}_i^{dc})(\bar{V}_i^{dc} - \bar{V}_k^{dc})/R_{ik}$, and $b_{ik} = V_{ref}^{dc}/R_{ik}$. Note that a_{1i}, a_{2i}, a_{3i}, a_{4i}, and b_{ik} are all positive constants. Replacing z_i in (6.3d) by (6.3c) yields

$$u_i = \alpha_i \sum_{k=1}^{N} b_{ik}(x_i - x_k) + b_i \ . \tag{6.4}$$

Define the vectors $\mathbf{x} = [x_1, x_2, \ldots, x_N]^T$, $\mathbf{y} = [y_1, y_2, \ldots, y_N]^T$, $\mathbf{u} = [u_1, u_2, \ldots, u_N]^T$, $\mathbf{v} = [v_1, v_2, \ldots, v_N]^T$, $\mathbf{b} = [b_1, b_2, \ldots, b_N]^T$ and the matrices $A_i = \text{diag}(a_{i1}, a_{i2}, \ldots, a_{iN})$, $i = 1, 2, 3, 4$, $A_\alpha = \text{diag}(\alpha_1, \alpha_2, \ldots, \alpha_N)$, and L

$$[L]_{ik} = \begin{cases} -b_{ik} & \text{for } i \neq k \ , \\ \sum_{k \neq i} b_{ik} & \text{for } i = k \ . \end{cases} \tag{6.5}$$

Then, (6.3a), (6.3b), (6.4) can be written in matrix form as

$$0 = -A_1\mathbf{x} + A_2\mathbf{y} - A_2\mathbf{u} - A_2\mathbf{v} \ , \tag{6.6a}$$
$$0 = -A_3\mathbf{x} - A_4\mathbf{y} \ , \tag{6.6b}$$
$$\mathbf{u} = LA_\alpha\mathbf{x} + \mathbf{b} \ . \tag{6.6c}$$

Introducing (6.6b), (6.6c) in (6.6a) yields

$$(LA_\alpha + A_1A_2^{-1} + A_3A_4^{-1})\mathbf{x} = -(\mathbf{v} + \mathbf{b}) \ . \tag{6.7}$$

In graph theory, L is well-known as the Laplacian matrix associated to an undirected weighted graph. It is symmetric positive semidefinite, with the number of zero eigenvalues equal to the number of connected components, which here is just one as the whole DC grid is assumed to be connected. Since a_{1i}, a_{2i}, a_{3i}, and a_{4i} are all strictly positive, and L and A_α are positive semidefinite, $(LA_\alpha + A_1A_2^{-1} + A_3A_4^{-1})$ is invertible. So a fixed value $\mathbf{v} = \mathbf{v}^e$ defines a single equilibrium value of $\mathbf{x}$

$$\mathbf{x}^e = -(LA_\alpha + A_1A_2^{-1} + A_3A_4^{-1})^{-1}(\mathbf{v}^e + \mathbf{b}) \ . \tag{6.8a}$$

From (6.3c), (6.6b), and (6.6c), we then readily obtain the equilibrium values of the other vectors

$$\mathbf{y}^e = -A_3A_4^{-1}\mathbf{x}^e \ , \tag{6.8b}$$
$$\mathbf{z}^e = A_\alpha\mathbf{x}^e \ , \tag{6.8c}$$
$$\mathbf{u}^e = LA_\alpha\mathbf{x}^e + \mathbf{b} \ . \tag{6.8d}$$

□

Remark 6.1. *The equilibrium point defined by* (6.8) *for* $\mathbf{v}^e = 0$ *differs from the reference operating point by a term of order* $\mathbf{b}$*, due to approximation* (6.2c)*. If the latter is valid to first order, then* $\mathbf{b}$ *is a second-order perturbation that can be neglected.*

6.2.3 Stability of the system

By following the same procedure as in the proof in the previous chapter, we can prove the stability of the interconnected system under the DC-voltage-based control scheme for the particular case where all AC areas are identical.

In the present subsection, we use a new frequency-domain approach, which is introduced in [85] and is summarized in Appendix D to prove for the general case of heterogeneous AC areas.

Proposition 6.2. *The closed-loop system defined by* (6.2) *for all* $i \in \{1, 2, \ldots, N\}$ *is stable.*

Proof. We first reformulate the model to reach a representation that satisfies the prerequisite conditions for the application of the Proposition D.2 in Appendix D. Then we apply that proposition.

We continue to use the notations introduced in Section 6.2.2. Let $w_i = v_i + b_i$ and $u'_i = u_i - b_i$. Then, Equation (6.2) becomes

$$\frac{dx_i}{dt} = -a_{1i}x_i + a_{2i}y_i - a_{2i}u'_i - a_{2i}w_i \ , \tag{6.9a}$$

$$\frac{dy_i}{dt} = -a_{3i}x_i - a_{4i}y_i \ , \tag{6.9b}$$

$$z_i = \alpha_i x_i \ , \tag{6.9c}$$

$$u'_i = \sum_{k=1}^{N} b_{ik}(z_i - z_k) \ . \tag{6.9d}$$

Applying the Laplace transform to (6.9) and eliminating $x_i(s)$ and $y_i(s)$ yields

$$z_i(s) = -h_i(s)(u'_i(s) + w_i(s)) \ , \tag{6.10a}$$

$$u'_i(s) = \sum_{k=1}^{N} b_{ik}(z_i(s) - z_k(s)) \ , \tag{6.10b}$$

where

$$h_i(s) = \frac{\alpha_i a_{2i}(s + a_{4i})}{(s + a_{1i})(s + a_{4i}) + a_{2i}a_{3i}} \ . \tag{6.11}$$

For the interconnected system described by (6.10) with $i = 1, 2, \ldots, N$, $w_i(s), i = 1, 2, \ldots, N$ are external inputs. To study the stability of the interconnected system, we assume that $w_i(s) = 0, i = 1, 2, \ldots, N$.

In order to satisfy all the prerequisites for the application of the Proposition D.2 in Appendix D, we reformulate the model (6.10) with $w_i(s) = 0$ as follows. Let

$$u''_i(s) = \frac{1}{d_i} \sum_{k=1}^{N} b_{ik} z_k(s) \ , \tag{6.12}$$

where $d_i = \sum_{k=1}^{N} b_{ik}$. Then (6.10a) when $w_i(s) = 0$ yields

$$z_i(s) = g_i(s) u''_i(s) \ , \tag{6.13}$$

where

$$\begin{aligned} g_i(s) &= d_i h_i(s)(1 + d_i h_i(s))^{-1} \\ &= \frac{d_i \alpha_i a_{2i}(s + a_{4i})}{(s + a_{1i} + d_i \alpha_i a_{2i})(s + a_{4i}) + a_{2i}a_{3i}} \ . \end{aligned} \tag{6.14}$$

Note that $g_i(s), i = 1, 2, \ldots, N$ are all stable transfer function in the $\mathcal{H}_\infty$ space (see Definition D.1 in Appendix D). Define the vectors $\mathbf{z} = [z_1, z_2, \ldots, z_N]^T$ and $\mathbf{u}'' = [u''_1, u''_2, \ldots, u''_N]^T$. Then, Equations (6.12) and (6.13) can be written in matrix form as

$$\mathbf{z}(s) = G(s)\mathbf{u}''(s) \ , \tag{6.15a}$$

$$\mathbf{u}''(s) = A_b\, \mathbf{z}(s)\ . \tag{6.15b}$$

where $G(s) = \mathrm{diag}(g_1(s), g_2(s), \ldots, g_N(s))$ and $[A_b]_{ik} = b_{ik}/d_i$.

For the interconnected system defined by (6.15), Equation (6.15a) gives the transfer function of each subsystem, while (6.15b) describes the interconnection between the subsystems. The matrix A_b representing this interconnection is element-wise nonnegative, and is defined such that $\rho(A_b) \leq 1$. Compared to the system (D.2) in Appendix D, the model (6.15) satisfies all the prerequisite conditions for the application of Proposition D.2. Thus, in the following, we proceed to prove that $Co(\{g_i(j\omega) : \omega \in \mathbb{R}_+, i = 1, 2, \ldots, n\})$ does not intersect with the positive real axis.

To show this, we bound the magnitude of $g_i(j\omega)$ as follows. With the definition of all the coefficients in $g_i(j\omega)$, we have

$$\begin{aligned}
|g_i(j\omega)| &= \left| \frac{d_i\alpha_i a_{2i}(a_{4i} + j\omega)}{(a_{1i} + d_i\alpha_i a_{2i} + j\omega)(a_{4i} + j\omega) + a_{2i}a_{3i}} \right| \\
&< \left| \frac{d_i\alpha_i a_{2i}(a_{4i} + j\omega)}{(a_{1i} + d_i\alpha_i a_{2i} + j\omega)(a_{4i} + j\omega)} \right| \\
&= \left| \frac{d_i\alpha_i a_{2i}}{a_{1i} + d_i\alpha_i a_{2i} + j\omega} \right| \\
&< 1\ .
\end{aligned} \tag{6.16}$$

Therefore, the convex hull of the Nyquist plots of $g_i(s), i = 1, 2, \ldots, N$ can not intersect with the positive real axis as s grows from $j0$ to $j\infty$. By virtue of Proposition D.2, the interconnected system is stable. □

6.2.4 Characterization of the equilibrium point

The above analysis proves the stability of the system. The present subsection focuses on the objective of the control scheme, i.e. to make the frequency deviations of the different AC areas stay close to each other. For simplicity, the theoretical analysis focuses on the particular case where all AC areas have identical parameters.

Proposition 6.3. *Suppose that all AC areas have identical parameters. For any given values of $\bar{V}_1^{dc}, \bar{V}_2^{dc}, \ldots, \bar{V}_N^{dc}$ and of load demand variation, the difference between the frequency deviations of the AC areas at the equilibrium point of the (linearized) system can be made arbitrarily small by taking the controller gain sufficiently large.*

Proof. We use hereafter the notations introduced in Section 6.2.2, and drop AC area index i when referring to the parameters of the areas that have the same values.

To measure the differences between $x_1^e, x_2^e, \ldots, x_N^e$, we define $\Delta x_i^e = x_i^e - \bar{x}^e$, where $\bar{x}^e = \frac{1}{N}\sum_{i=1}^N x_i^e$. Let $\Delta\mathbf{x}^e = [\Delta x_1^e, \Delta x_2^e, \ldots, \Delta x_N^e]^T$. Let $\mathbf{q}^e = \mathbf{v}^e + \mathbf{b}$ and define $\bar{q}^e$ and $\Delta\mathbf{q}^e$ similarly. We want to bound the Euclidean norm $\|\Delta\mathbf{x}^e\|$ of $\Delta\mathbf{x}^e$.

Let $a = a_1/a_2 + a_3/a_4$. Then, (6.7) becomes

$$-\mathbf{q}^e = (\alpha L + aI_N)\mathbf{x}^e\ . \tag{6.17}$$

Premultiplying the above equation by $\mathbf{1}_N^T$ yields

$$-\mathbf{1}_N^T\mathbf{q}^e = \mathbf{1}_N^T(\alpha L + aI_N)\mathbf{x}^e = \alpha\mathbf{1}_N^T L\mathbf{x}^e + a\mathbf{1}_N^T\mathbf{x}^e \ . \tag{6.18}$$

Since $\mathbf{1}_N^T L = 0$, $\mathbf{1}_N^T\mathbf{x}^e = N\bar{x}^e$, and $\mathbf{1}_N^T\mathbf{q}^e = N\bar{q}^e$, the above equation becomes

$$-\bar{q}^e = a\bar{x}^e \ . \tag{6.19}$$

On the other hand, (6.17) can be written as

$$\begin{aligned} -(\Delta\mathbf{q}^e + \bar{q}^e\mathbf{1}_N) &= (\alpha L + aI_N)(\Delta\mathbf{x}^e + \bar{x}^e\mathbf{1}_N) \\ &= \alpha L\Delta\mathbf{x}^e + \alpha\bar{x}^e L\mathbf{1}_N + a\Delta\mathbf{x}^e + a\bar{x}^e\mathbf{1}_N \\ &= \alpha L\Delta\mathbf{x}^e + a\Delta\mathbf{x}^e + a\bar{x}^e\mathbf{1}_N \ , \end{aligned} \tag{6.20}$$

where we used the fact that $L\mathbf{1}_N = 0$. Given (6.19), the above equation yields

$$-\Delta\mathbf{q}^e = (\alpha L + aI_N)\Delta\mathbf{x}^e \ . \tag{6.21}$$

Denote by $\{\omega_1, \omega_2, \ldots, \omega_N\}$ an orthonormal set of eigenvectors of L associated to corresponding eigenvalues $\{\lambda_1 \leq \lambda_2 \leq \ldots \leq \lambda_N\}$. Because L is a Laplacian matrix, we have $\lambda_1 = 0$ associated to $\omega_1 = \frac{1}{\sqrt{N}}\,\mathbf{1}_N$, and because the grid is connected we have $\lambda_2 > 0$.

Denote by $\Delta\tilde{x}_i^e$ the components of vector $\Delta\mathbf{x}^e$ expressed in orthonormal basis $\mathcal{B} = (\omega_1, \omega_2, \ldots, \omega_N)$, and by $\Delta\tilde{q}_i^e$ the components of $\Delta\mathbf{q}^e$ expressed in this same basis. Because of the orthonormal basis $\mathcal{B}$, we have $\|\Delta\mathbf{x}^e\|^2 = \sum_i |\Delta\tilde{x}_i^e|^2$ and $\|\Delta\mathbf{q}^e\|^2 = \sum_i |\Delta\tilde{q}_i^e|^2$. Then we have from (6.21), for all $i \in \{1, 2, \ldots, N\}$,

$$|\Delta\tilde{q}_i^e| = (\alpha\lambda_i + a)|\Delta\tilde{x}_i^e| \geq (\alpha\lambda_2 + a)|\Delta\tilde{x}_i^e| \ . \tag{6.22}$$

The property is obvious for $i \geq 2$; for $i = 1$ it holds because by definition $\Delta\tilde{x}_1^e = \omega_1^T\,\Delta\mathbf{x}^e = \frac{1}{\sqrt{N}}\,\mathbf{1}_N^T\,\Delta\mathbf{x}^e = 0$, such that we get $0 \geq 0$. Therefore, (6.21) yields

$$\|\Delta\mathbf{q}^e\| = \|(\alpha L + aI_N)\Delta\mathbf{x}^e\| \geq (\alpha\lambda_2 + a)\|\Delta\mathbf{x}^e\| \ , \tag{6.23}$$

such that we have[1]

$$\|\Delta\mathbf{x}^e\| \leq \frac{1}{\alpha\lambda_2 + a}\|\Delta\mathbf{q}^e\| \leq \frac{1}{\alpha\lambda_2 + a}\|\mathbf{q}^e\| \ . \tag{6.24}$$

For a given value of $\mathbf{q}^e = \mathbf{v}^e + \mathbf{b}$, which is fixed by $\bar{V}_1^{dc}, \bar{V}_2^{dc}, \ldots, \bar{V}_N^{dc}$ and load demand variations, the right hand side of this inequality can be made arbitrarily small by taking α sufficiently large. □

Remark 6.2. *Proposition 6.3 gives an upper bound on the differences between $x_1, x_2, \ldots, x_n$. However, such differences cannot be eliminated as long as $\alpha_1 = \alpha_2 = \ldots = \alpha_N = \alpha$, even for the case of identical subsystems. In fact, the differences between $x_1, x_2, \ldots, x_n$ (and thus $\Delta f_1, \Delta f_2, \ldots, \Delta f_N$) in steady state is necessary for the DC-voltage-based control scheme to work, i.e. to share primary reserves between the AC areas. To see this, refer to Equation* (6.2c)*, it can be noted that P_{ij} results from the difference between V_i and V_j. Thus, if $\Delta f_i = \Delta f_j$, then $\Delta V_i = \alpha\Delta f_i = \alpha\Delta f_j = \Delta V_j$, which means that P_{ij} will remain the same as its value at the*

[1]The last inequality directly follows by writing $\Delta\mathbf{q}^e = (I_N - \omega_1\omega_1^T)\mathbf{q}^e$: when expressed in orthonormal basis $\mathcal{B}$, $\Delta\mathbf{q}^e$ and $\mathbf{q}^e$ differ only in the first component, which equals 0 for $\Delta\mathbf{q}^e$.

reference operating point, and thus area i and j will not share their primary reserves [2]*. To conclude, the presence of the differences between $x_1, x_2, \ldots, x_n$ in steady state is an inherent and well-predicted consequence of the control scheme.*

6.3 Simulations

The effectiveness of the proposed control scheme is illustrated hereafter in the context of the five-area benchmark system described in Chapter 4. The simulation conditions are also the same as in Section 5.3.

Figure 6.1 depicts the evolution of the frequencies when $\alpha = 2 \times 10^3$. For comparison, it also shows the evolution of f_2 when $\alpha = 0$ (i.e. $V_1^{dc}, V_2^{dc}, \ldots, V_5^{dc}$ are kept constant). These simulations show that without the controller ($\alpha = 0$), the frequency of area 2 undergoes a deviation with transient maximum of 0.196Hz and stabilizes at 49.927Hz. With the controller defined by (6.1), the maximum transient deviation of f_2 drops to 0.055Hz, and the frequencies of the five areas exhibit the same variation pattern and finally settle within a band between 49.976Hz and 49.988Hz. The curves representing the evolution of the control variables, $V_1^{dc}, V_2^{dc}, \ldots, V_5^{dc}$, are shown in Figure 6.2. We observe that the variations in V_i^{dc} are proportional to the frequency deviation of the corresponding area, and that these variations remain smaller than the range of initial values $\bar{V}_i^{dc}$, which indicates that such variations do not result in excessively high or low voltages within the DC grid. Figure 6.3 shows the evolution of the power injections from the AC areas into the DC grid, $P_1^{dc}, P_2^{dc}, \ldots, P_5^{dc}$, expressed in MW. Their variations remain within 10% of the original values, which is moderately small.

The above results show that our control scheme leads to a significant improvement in both the steady-state frequency deviations (from 0.073Hz to 0.024Hz) and the maximum transient deviations (from 0.196Hz to 0.055Hz) of area 2. However, the frequency deviations of the different AC areas do not converge to each other and remain within a band, whose width is 0.012Hz.

Figures 6.4-6.6 show the results when α is doubled to 4×10^3. We observe that the width of the band of the frequencies in steady state is reduced to 0.007Hz. This indicates that a property similar to Proposition 6.3 seems to still hold when AC areas have different parameter values.

6.4 Partial application of the DC-voltage-based control scheme

In the previous sections of the current chapter, we assumed that all the HVDC converters are implementing the DC-voltage-based control scheme. However, this assumption can be relaxed without jeopardizing the stability of the system. In fact, an AC area can possibly choose not to share its primary reserves with other areas, but simply track its scheduled power injection. Such a choice may result from failure to reach an agreement between the areas on the primary frequency control practice.

In the current section, we investigate the stability properties of the interconnected system in this case. We first give the expression of the unique equilibrium point. Then we prove stability.

[2] An exception is the case where α differs from one AC area to another, Δf_i and Δf_j can accidentally be equal to each other.

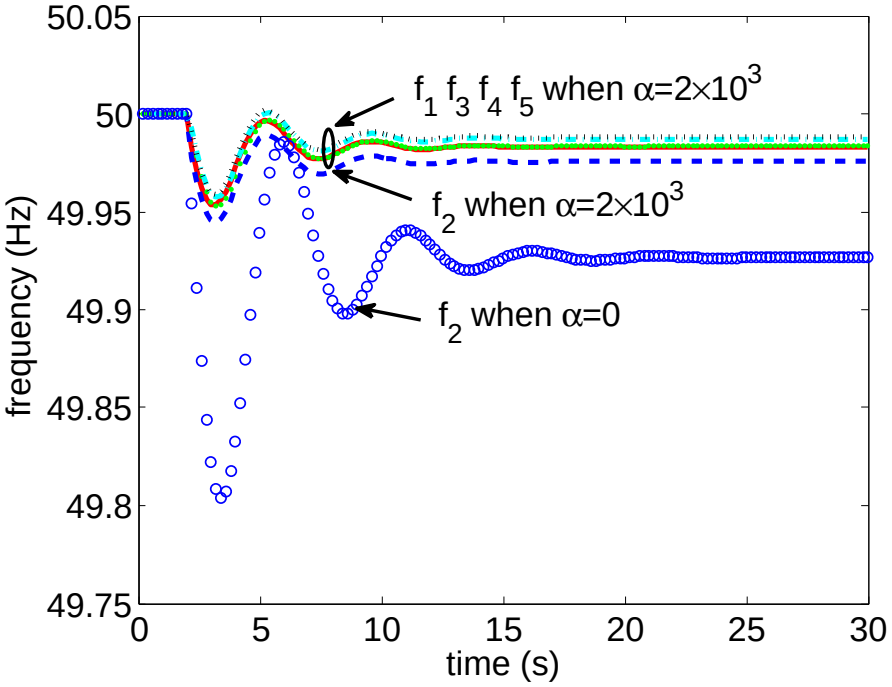

Figure 6.1: Frequencies of the five AC areas under the DC-voltage-based control scheme with $\alpha = 2 \times 10^3$. f_2 when $\alpha = 0$ is also shown.

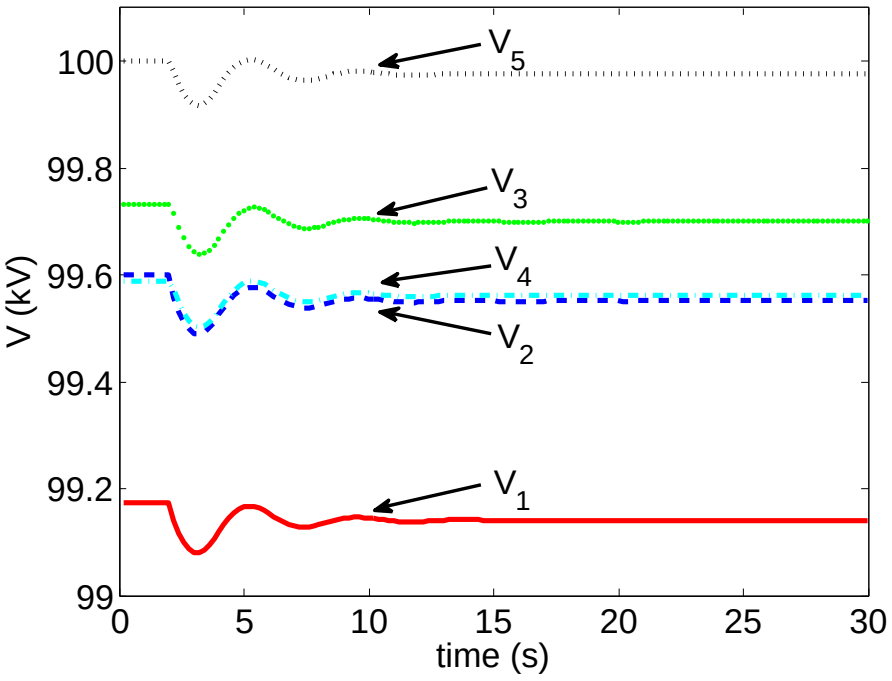

Figure 6.2: DC-side voltages of the converters under the DC-voltage-based control scheme with $\alpha = 2 \times 10^3$.

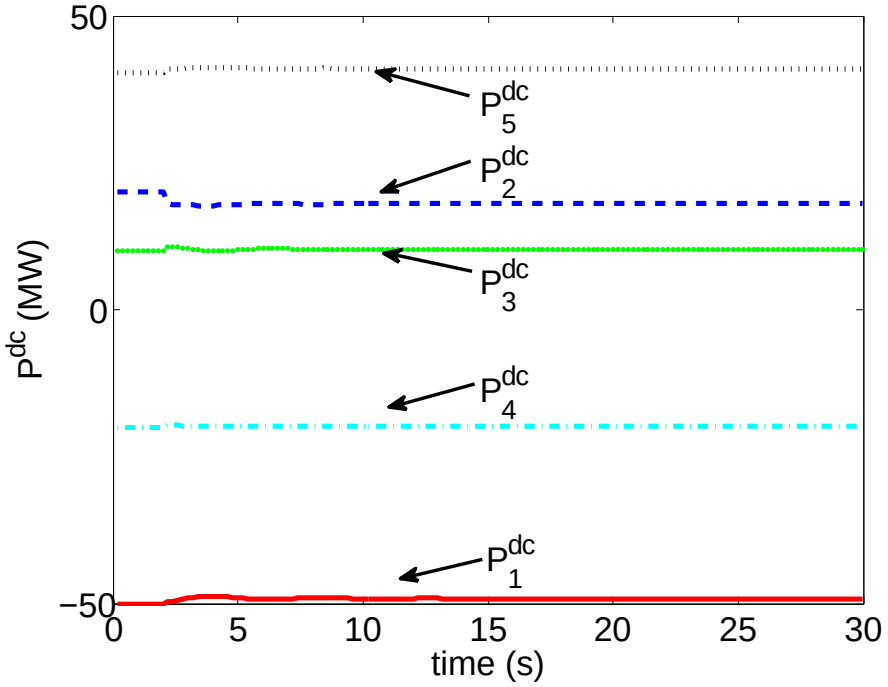

Figure 6.3: Power injections from the five AC areas into the DC grid under the DC-voltage-based control scheme with $\alpha = 2 \times 10^3$.

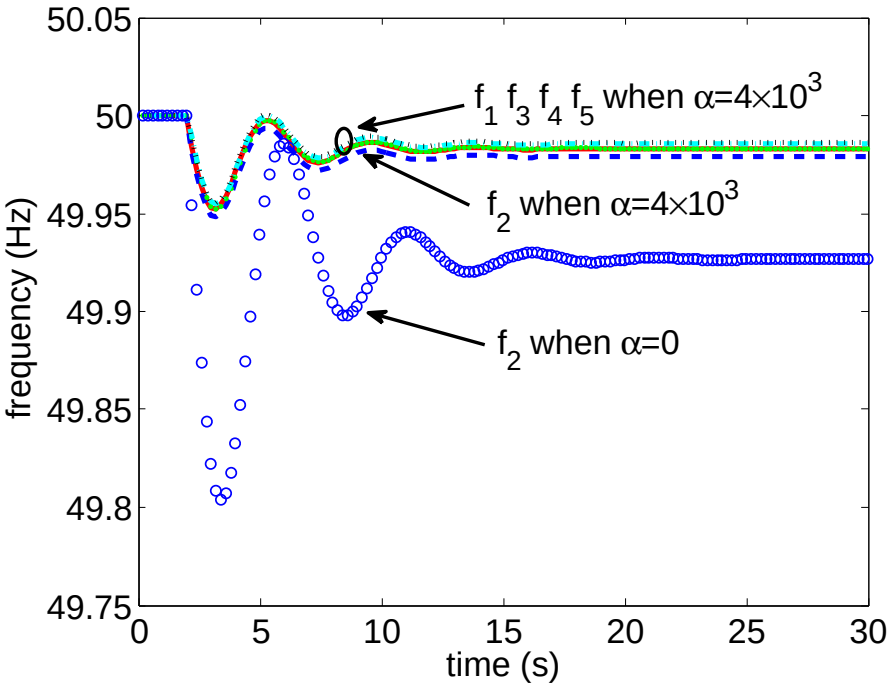

Figure 6.4: Frequencies of the five AC areas under the DC-voltage-based control scheme with $\alpha = 4 \times 10^3$. f_2 when $\alpha = 0$ is also shown.

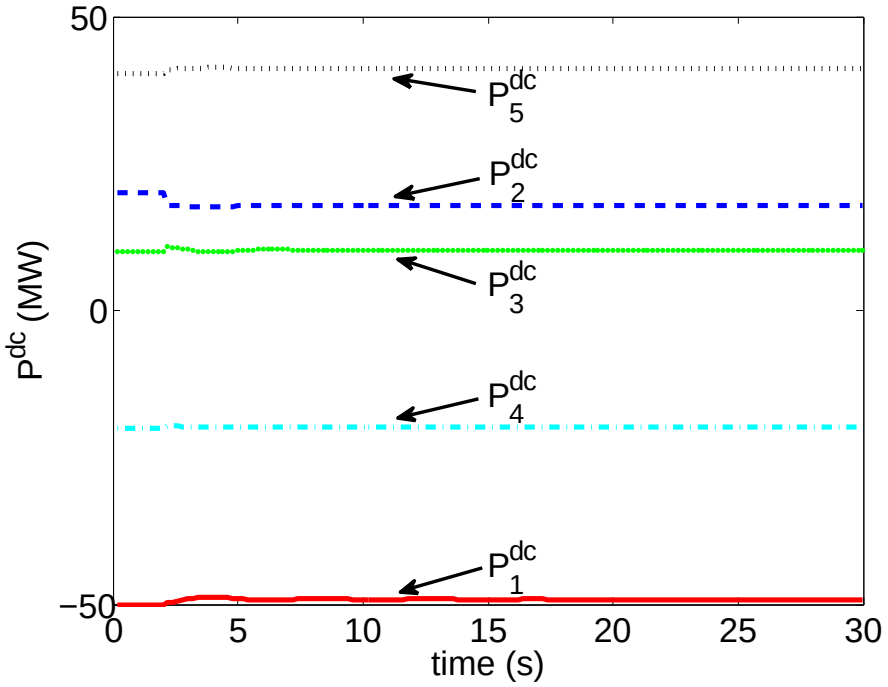

Figure 6.5: Power injections from the five AC areas into the DC grid under the DC-voltage-based control scheme with $\alpha = 4 \times 10^3$.

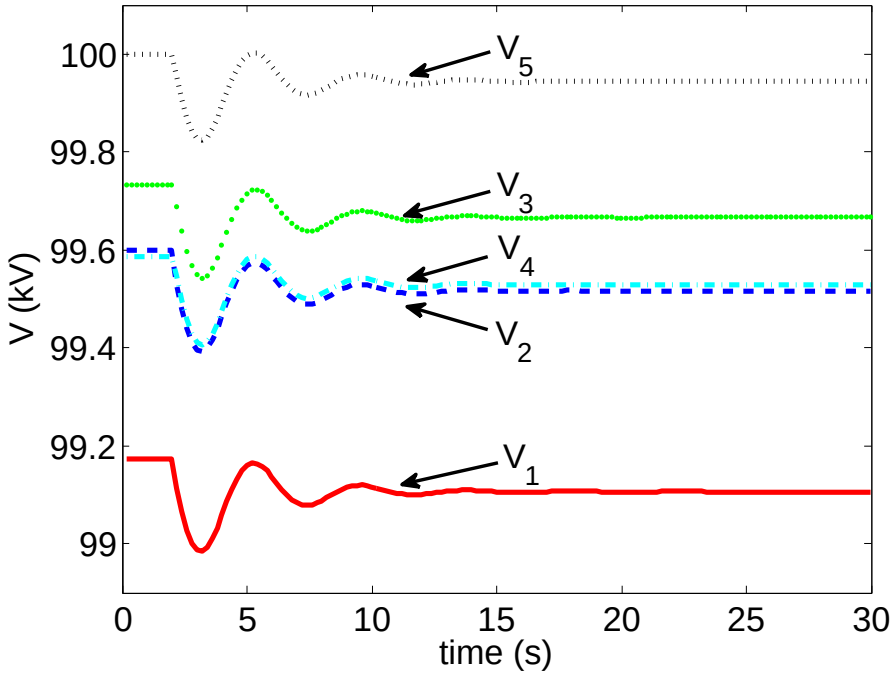

Figure 6.6: DC-side voltages of the converters under the DC-voltage-based control scheme with $\alpha = 4 \times 10^3$.

Finally, we discuss the effectiveness of the control scheme for the areas applying it.

6.4.1 Equilibrium point

Denote the index set of the converters applying the DC-voltage-based control scheme (tracking the scheduled power injection, resp.) by $\mathbb{V}$ ($\mathbb{P}$, resp.). From this definition, we have for all $i \in \mathbb{V}$

$$V_i^{dc}(t) = \alpha_i f_i(t) \,, \tag{6.25}$$

and for all $i \in \mathbb{P}$

$$P_i^{dc}(t) = \bar{P}_i^{dc} \,. \tag{6.26}$$

Proposition 6.4. *Consider that the system, initially operating at the reference operating point, is suddenly subjected to a step change in the load demand of one of its AC areas. The (linearized) HVDC system defined by* (6.2a)-(6.2c) *for all* $i \in \{1, 2, \ldots, N\}$, (6.25) *for all* $i \in \mathbb{V}$, *and* (6.26) *for all* $i \in \mathbb{P}$ *has a unique equilibrium point.*

Proof. We use the same notations introduced in the proof of Proposition 6.1. Let $\mathbf{x}_{\mathbb{V}}$ (resp. $\mathbf{x}_{\mathbb{P}}$) be the vector containing x_i for all $i \in \mathbb{V}$ (resp. $i \in \mathbb{P}$). Other symbols with subscript $\mathbb{P}$ or $\mathbb{V}$ are defined in a similar manner. Denote the value of $u_i(t)$ as u_i^o for all $i \in \mathbb{P}$. Then, Equations (6.25) and (6.26) yield

$$\mathbf{z}_{\mathbb{V}}^e = A_{\alpha,\mathbb{V}} \mathbf{x}_{\mathbb{V}}^e \,, \tag{6.27}$$

$$\mathbf{u}_{\mathbb{P}}^e = \mathbf{u}_{\mathbb{P}}^o = 0 \,. \tag{6.28}$$

For all $i \in \{1, 2, \ldots, N\}$, (6.3a) and (6.3b) still hold, which yields

$$\mathbf{x}_{\mathbb{V}}^e = -\left(A_{1,\mathbb{V}} A_{2,\mathbb{V}}^{-1} + A_{3,\mathbb{V}} A_{4,\mathbb{V}}^{-1}\right)^{-1} (\mathbf{v}_{\mathbb{V}}^e + \mathbf{u}_{\mathbb{V}}^e) \,, \tag{6.29}$$

$$\mathbf{x}_{\mathbb{P}}^e = -\left(A_{1,\mathbb{P}} A_{2,\mathbb{P}}^{-1} + A_{3,\mathbb{P}} A_{4,\mathbb{P}}^{-1}\right)^{-1} (\mathbf{v}_{\mathbb{P}}^e + \mathbf{u}_{\mathbb{P}}^o) \,, \tag{6.30}$$

$$\mathbf{y}_{\mathbb{V}}^e = -A_{3,\mathbb{V}} A_{4,\mathbb{V}}^{-1} \mathbf{x}_{\mathbb{V}}^e \,, \tag{6.31}$$

$$\mathbf{y}_{\mathbb{P}}^e = -A_{3,\mathbb{P}} A_{4,\mathbb{P}}^{-1} \mathbf{x}_{\mathbb{P}}^e \,. \tag{6.32}$$

In the sequel, we proceed to find $x_{\mathbb{V}}^e$ expressed in external inputs ($\mathbf{v}_{\mathbb{V}}^e$ and $\mathbf{u}_{\mathbb{P}}^o$) and system parameters. Equation (6.3d) can be written in matrix form as

$$\mathbf{u}^e = L\mathbf{z}^e + \mathbf{b}^e \,, \tag{6.33}$$

Reordering the elements in $\mathbf{u}^e$ and $\mathbf{z}^e$ yields

$$\begin{bmatrix} \mathbf{u}_{\mathbb{V}}^e \\ \mathbf{u}_{\mathbb{P}}^o \end{bmatrix} = L' \begin{bmatrix} \mathbf{z}_{\mathbb{V}}^e \\ \mathbf{z}_{\mathbb{P}}^e \end{bmatrix} = \begin{bmatrix} L_1 & L_2 \\ L_2^T & L_3 \end{bmatrix} \begin{bmatrix} A_{\alpha,\mathbb{V}} \mathbf{x}_{\mathbb{V}}^e \\ \mathbf{z}_{\mathbb{P}}^e \end{bmatrix} + \begin{bmatrix} \mathbf{b}_{\mathbb{V}} \\ \mathbf{b}_{\mathbb{P}} \end{bmatrix} \,, \tag{6.34}$$

where L_1, L_2, and L_3 are submatrices of L' of adequate dimensions. We thus find a relation between $\mathbf{z}_{\mathbb{P}}$ and $\mathbf{x}_{\mathbb{V}}$ as

$$\mathbf{u}_{\mathbb{P}}^o = L_2^T A_{\alpha,\mathbb{V}} \mathbf{x}_{\mathbb{V}}^e + L_3 \mathbf{z}_{\mathbb{P}}^e + \mathbf{b}_{\mathbb{P}} \,. \tag{6.35}$$

In fact, L_3 is invertible. To see this, recall the definition of L and note that the DC grid can not split into several isolated parts. Thus, L is the Laplacian matrix associated to a connected

communication graph, and so is L'. Consequently, the trace of L_3 is necessarily larger than the sum of all its off-diagonal entries, which means that we can view L_3, a principal minor of L', as the sum of a Laplacian matrix and a positive semidefinite diagonal matrix. Thus, L_3 is invertible. We then have

$$\mathbf{z}^e_{\mathbb{P}} = -L_3^{-1}L_2^T A_{\alpha,\mathbb{V}}\mathbf{x}^e_{\mathbb{V}} + L_3^{-1}\mathbf{u}^o_{\mathbb{P}} - L_3^{-1}\mathbf{b}_{\mathbb{P}} \ . \tag{6.36}$$

Replacing $\mathbf{z}^e_{\mathbb{P}}$ in (6.34) by the above equation yields

$$\mathbf{u}^e_{\mathbb{V}} = (L_1 - L_2L_3^{-1}L_2^T)A_{\alpha,\mathbb{V}}\mathbf{x}^e_{\mathbb{V}} + L_2L_3^{-1}\mathbf{u}^o_{\mathbb{P}} - L_2L_3^{-1}\mathbf{b}_{\mathbb{P}} + \mathbf{b}_{\mathbb{V}} \ . \tag{6.37}$$

Given (6.29), we obtain

$$\begin{aligned}&(L_1A_{\alpha,\mathbb{V}} - L_2L_3^{-1}L_2^TA_{\alpha,\mathbb{V}} + A_{1,\mathbb{V}}A_{2,\mathbb{V}}^{-1} + A_{3,\mathbb{V}}A_{4,\mathbb{V}}^{-1})\mathbf{x}^e_{\mathbb{V}}\\ =& -(\mathbf{v}^e_{\mathbb{V}} + L_2L_3^{-1}\mathbf{u}^o_{\mathbb{P}} - L_2L_3^{-1}\mathbf{b}_{\mathbb{P}} + \mathbf{b}_{\mathbb{V}}) \ .\end{aligned} \tag{6.38}$$

We now show that $(L_1A_{\alpha,\mathbb{V}} - L_2L_3^{-1}L_2^TA_{\alpha,\mathbb{V}} + A_{1,\mathbb{V}}A_{2,\mathbb{V}}^{-1} + A_{3,\mathbb{V}}A_{4,\mathbb{V}}^{-1})$ is also invertible. By virtue of Proposition B.3 in Appendix B, we see that $(L_1 - L_2L_3^{-1}L_2^T)$ is also a Laplacian and is thus positive semidefinite. On the other hand, $A_{\alpha,\mathbb{V}}$ is a positive definite diagonal matrix. Thus, $(L_1A_{\alpha,\mathbb{V}} - L_2L_3^{-1}L_2^TA_{\alpha,\mathbb{V}})$ has no negative eigenvalue. In addition, $(A_{1,\mathbb{V}}A_{2,\mathbb{V}}^{-1} + A_{3,\mathbb{V}}A_{4,\mathbb{V}}^{-1})$ is a positive definite diagonal matrix. Therefore, $(L_1A_{\alpha,\mathbb{V}} - L_2L_3^{-1}L_2^TA_{\alpha,\mathbb{V}} + A_{1,\mathbb{V}}A_{2,\mathbb{V}}^{-1} + A_{3,\mathbb{V}}A_{4,\mathbb{V}}^{-1})$ is invertible.

We thus have

$$\begin{aligned}\mathbf{x}^e_{\mathbb{V}} =& -(L_1A_{\alpha,\mathbb{V}} - L_2L_3^{-1}L_2^TA_{\alpha,\mathbb{V}} + A_{1,\mathbb{V}}A_{2,\mathbb{V}}^{-1} + A_{3,\mathbb{V}}A_{4,\mathbb{V}}^{-1})^{-1}\\ &(\mathbf{v}^e_{\mathbb{V}} + L_2L_3^{-1}\mathbf{u}^o_{\mathbb{P}} - L_2L_3^{-1}\mathbf{b}_{\mathbb{P}} + \mathbf{b}_{\mathbb{V}}) \ .\end{aligned} \tag{6.39}$$

Thus, the system has a unique equilibrium point described by (6.28), (6.30), (6.32), (6.36) for the subsystems in $\mathbb{P}$ and (6.27), (6.31), (6.37), (6.39) for the subsystems in $\mathbb{V}$. □

Remark 6.3. *The case when some of the HVDC converters reach their limits on P_i^{dc} can be studied in the same way. The equilibrium point given above remains the same. The only difference is that $u_i(t) \neq 0$ if converter i reaches its limits on P_i^{dc}.*

6.4.2 Stability

Proposition 6.5. *The closed-loop system defined by* (6.2a)-(6.2c) *for all $i \in \{1, 2, \ldots, N\}$,* (6.25) *for all $i \in \mathbb{V}$, and* (6.26) *for all $i \in \mathbb{P}$ is stable.*

Proof. We describe the system with the notations introduced in the proof of Proposition 6.2. For all $i \in \{1, 2, \ldots, N\}$,

$$\frac{dx_i}{dt} = -a_{1i}x_i + a_{2i}y_i - a_{2i}u_i - a_{2i}v_i \ , \tag{6.40}$$

$$\frac{dy_i}{dt} = -a_{3i}x_i - a_{4i}y_i \ , \tag{6.41}$$

$$u_i = \sum_{k=1}^{N} b_{ik}(z_i - z_k) + b_i \ . \tag{6.42}$$

For all $i \in \mathbb{V}$,

$$z_i = \alpha_i x_i \ , \tag{6.43}$$

and for all $i \in \mathbb{P}$,

$$u_i = 0 \ . \tag{6.44}$$

By appropriate arrangement, we obtain for the areas in $\mathbb{P}$,

$$\frac{dx_i}{dt} = -a_{1i}x_i + a_{2i}y_i - a_{2i}v_i \ , \tag{6.45}$$

$$\frac{dy_i}{dt} = -a_{3i}x_i - a_{4i}y_i \ . \tag{6.46}$$

Each subsystem in $\mathbb{P}$ is isolated from all the other subsystems. Thus, the stability is determined by individual subsystems, which are all stable themselves.

As for the subsystems in $\mathbb{V}$, we obtain by following the similar procedure as in the proof for Proposition 6.4

$$\mathbf{u}_{\mathbb{V}} = (L_1 - L_2 L_3^{-1} L_2^T) A_{\alpha,\mathbb{V}} \mathbf{x}_{\mathbb{V}} - L_2 L_3^{-1} \mathbf{b}_{\mathbb{P}} + \mathbf{b}_{\mathbb{V}} \ . \tag{6.47}$$

By virtue of Proposition B.3 in Appendix B, we see that $(L_1 - L_2 L_3^{-1} L_2^T)$ is also a Laplacian associated with a connected undirected graph. Thus, by following the same procedure as in the proof of Proposition 6.2, we can prove stability for the interconnected system composed of AC areas in $\mathbb{V}$. □

Remark 6.4. *For the special case where $\#\mathbb{V} = 1$, only one AC converter (indexed by k) applies the DC-voltage-based control scheme, while all the other converters keep tracking their scheduled power injections. In this case, the matrix $L_1 - L_2 L_3^{-1} L_2^T$ is a scalar, and it is equal to zero (See Remark B.1 in Appendix B). Thus, by virtue of* (6.47)*, u_k is decoupled from x_k, and u_k is always equal to 0 if we neglect the second-order perturbation terms $b_{\mathbb{P}}$ and $b_{\mathbb{V}}$. Practically, this means that when converter k changes V_k^{dc} by ΔV_k^{dc} in response to a frequency deviation in area k, all other converters will try to keep their $P_i^{dc}, i \neq k$ unchanged by modifying their $V_i^{dc}, i \neq k$ by the same amplitude (i.e. equal to ΔV_k^{dc}), which results in an unchanged P_k^{dc} (i.e. the objective of the control scheme is not achieved) as well as an identical variation in $V_1^{dc}, V_1^{dc}, \ldots, V_N^{dc}$. This common variation in $V_1^{dc}, V_1^{dc}, \ldots, V_N^{dc}$ is not desirable for the sake of the good operation of the HVDC system as the DC voltages of the converters may reach their limits (See Section 6.1.3). Indeed, as stated in Section 4.1.2, when $N-1$ areas track their scheduled power injections, the last area must play the role of a slack bus to keep the power balance within the DC grid.*

6.4.3 Effectiveness of the control scheme

As found in the proof of Proposition 6.5, when $\#\mathbb{V} \geq 2$, the AC areas in $\mathbb{V}$ constitute an interconnected system that is qualitatively the same as the system composed of all the AC areas when $\#\mathbb{V} = 0$. Thus, we have the following proposition on the effectiveness of the control based when partially applied.

Proposition 6.6. *Consider the closed-loop system defined by* (6.2a)-(6.2c) *for all* $i \in \{1, 2, \ldots, N\}$, (6.25) *for all* $i \in \mathbb{V}$, *and* (6.26) *for all* $i \in \mathbb{P}$, *and suppose that all AC areas in* $\mathbb{V}$ *have identical parameters. For any given values of* $\bar{V}_1^{dc}, \bar{V}_2^{dc}, \ldots, \bar{V}_N^{dc}$ *and of load demand variation, the difference between the frequency deviations of the AC areas in* $\mathbb{V}$ *at the equilibrium point of the (linearized) system can be made arbitrarily small by taking the controller gain sufficiently large.*

Proof. We drop AC area index i when referring to the parameters of the areas in $\mathbb{V}$ that have the same values. Let $a = a_1/a_2 + a_3/a_4$ and $\mathbf{q}_{\mathbb{V}}^e = \mathbf{v}_{\mathbb{V}}^e - L_2 L_3^{-1} \mathbf{b}_{\mathbb{P}} + \mathbf{b}_{\mathbb{V}}$. Then, Equation (6.39) on the relation between $\mathbf{x}_{\mathbb{V}}^e$ and $\mathbf{q}_{\mathbb{V}}^e$ can be rewritten as

$$-\mathbf{q}_{\mathbb{V}}^e = (\alpha(L_1 + L_2 L_3^{-1} L_2^T) + a I_{\#\mathbb{V}}) \mathbf{x}_{\mathbb{V}}^e \, . \tag{6.48}$$

As proved in Proposition 6.4, $(L_1 + L_2 L_3^{-1} L_2^T)$ is also a Laplacian. Thus, the above equation is qualitatively the same as (6.17). By following the same procedure as in the proof of Proposition 6.3, we can prove that the difference between the components of $\mathbf{x}_{\mathbb{V}}$ at the equilibrium point of the (linearized) system can be made arbitrarily small by taking the controller gain sufficiently large. □

6.5 Practical implementation

The reference operating point is obtained when all the converters except one track their scheduled power injections, while the last converter keeps the power balance within the DC grid. How to shift from this working mode to the DC-voltage-based control scheme must be addressed.

In this section, we first revisit of the role of the DC-voltage-regulating converter in the context of the DC-voltage-based control scheme. Then we discuss the practical implementation of the control scheme.

6.5.1 Revisiting of the role of the DC-voltage-regulating converter in the context of the DC-voltage-based control scheme

In this subsection, we study the stability properties of the HVDC system when the DC-voltage-based control scheme is partially applied to some converters while there exists a converter that keeps the power balance within the DC grid by regulating the DC-side voltage at V_{ref}^{dc}.

Stability analysis of Section 6.4 shows that the DC-voltage-based control scheme can be partially applied to some but not all of the converters, without jeopardizing the stability of the interconnected system. Those converters applying the control scheme constitute an interconnected system that is qualitatively the same as the case when all the converters are applying the control scheme, with the exception that in this case, the Laplacian is of reduced dimension and is equal to $L_1 - L_2 L_3^{-1} L_2^T$.

Without loss of generality, we suppose in this subsection that converters $1, 2, \ldots, \#\mathbb{V}$ apply the control scheme, and that converter N regulates V_N^{dc} at V_{ref}^{dc}. In the following, we study the interconnected system composed of areas $1, 2, \ldots, \#\mathbb{V}$ and N. The Laplacian of this system is denoted as $\tilde{L}$.

Equilibrium point

Similar to (6.34), we obtain

$$\begin{bmatrix} \mathbf{u}^e_{\mathbb{V}} \\ u^e_N \end{bmatrix} = \tilde{L} \begin{bmatrix} \mathbf{z}^e_{\mathbb{V}} \\ z^e_N \end{bmatrix} = \begin{bmatrix} \tilde{L}_1 & \tilde{L}_2 \\ \tilde{L}_2^T & \tilde{L}_3 \end{bmatrix} \begin{bmatrix} A_{\alpha,\mathbb{V}} \mathbf{x}^e_{\mathbb{V}} \\ 0 \end{bmatrix} + \begin{bmatrix} \mathbf{b}_{\mathbb{V}} \\ b_N \end{bmatrix} , \tag{6.49}$$

where $\tilde{L}_1$, $\tilde{L}_2$, and $\tilde{L}_3$ are submatrices of $\tilde{L}$ of adequate dimensions. Given (6.29), we obtain

$$-(\tilde{L}_1 \mathbf{A}_{\alpha,\mathbb{V}} + A_{1,\mathbb{V}} A^{-1}_{2,\mathbb{V}} + A_{3,\mathbb{V}} A^{-1}_{4,\mathbb{V}}) \mathbf{x}^e_{\mathbb{V}} = \mathbf{v}^e_{\mathbb{V}} + \mathbf{b}_{\mathbb{V}} . \tag{6.50}$$

Since $(\tilde{L}_1 \mathbf{A}_{\alpha,\mathbb{V}} + A_{1,\mathbb{V}} A^{-1}_{2,\mathbb{V}} + A_{3,\mathbb{V}} A^{-1}_{4,\mathbb{V}})$ is invertible, we obtain

$$\mathbf{x}^e_{\mathbb{V}} = -(\tilde{L}_1 \mathbf{A}_{\alpha,\mathbb{V}} + A_{1,\mathbb{V}} A^{-1}_{2,\mathbb{V}} + A_{3,\mathbb{V}} A^{-1}_{4,\mathbb{V}})^{-1} (\mathbf{v}^e_{\mathbb{V}} + \mathbf{b}_{\mathbb{V}}) . \tag{6.51}$$

As for subsystem N, we have

$$u^e_N = \tilde{L}_2^T A_{\alpha,\mathbb{V}} \mathbf{x}^e_{\mathbb{V}} + b_N . \tag{6.52}$$

At the equilibrium point, x^e_N must satisfy

$$x^e_N = -(a_{1N} a^{-1}_{2N} + a_{3N} a^{-1}_{4N})^{-1} (v^e_N + u^e_N) . \tag{6.53}$$

Thus,

$$x^e_N = -(a_{1N} a^{-1}_{2N} + a_{3N} a^{-1}_{4N})^{-1} (v^e_N + b_N + L_2^T A_{\alpha,\mathbb{V}} \mathbf{x}^e_{\mathbb{V}}) . \tag{6.54}$$

Stability

In fact, this case can be assimilated into the general case studied in Section 6.2 with $\alpha_N = 0$. Referring to Proposition 6.2, we see that in this case, the transfer function $g_N(s)$ is degenerated to 0. According to Proposition 6.2, the interconnected system is still stable.

Closeness between the components of $x^e_{\mathbb{V}}$

To study the relationship between the components of $x^e_{\mathbb{V}}$, we assume that subsystems in $\mathbb{V}$ have identical parameters. In order to use the results of Proposition 6.3, we make an additional assumption that

$$b_{1N} = b_{2N} = \ldots = b_{\#\mathbb{V},N} = b_{*N} . \tag{6.55}$$

Similar to (6.17), we obtain

$$-\mathbf{q}^e_{\mathbb{V}} = (\alpha \tilde{L}_1 + a I_{\#\mathbb{V}}) \mathbf{x}^e_{\mathbb{V}} . \tag{6.56}$$

Here, $\tilde{L}_1$ is not a Laplacian. However, given the definition of L (See Equation (6.5)), we can decompose $\tilde{L}_1$ as

$$\tilde{L}_1 = \tilde{L}^*_1 + \mathrm{diag}(b_{1N}, b_{2N}, \ldots, b_{\#\mathbb{V},N}) , \tag{6.57}$$

where $\tilde{L}^*_1$ is a Laplacian. Under the assumption (6.55), Equation (6.56) becomes

$$-\mathbf{q}^e_{\mathbb{V}} = (\alpha \tilde{L}^*_1 + \alpha \cdot \mathrm{diag}(b_{1N}, b_{2N}, \ldots, b_{\#\mathbb{V},N}) + a I_{\#\mathbb{V}}) \mathbf{x}^e_{\mathbb{V}}$$

$$
\begin{aligned}
&= (\alpha \tilde{L}_1^* + \alpha b_{*N} I_{\#\mathbb{V}} + a I_{\#\mathbb{V}}) \mathbf{x}_{\mathbb{V}}^e \\
&= (\alpha \tilde{L}_1^* + (\alpha b_{*N} + a) I_{\#\mathbb{V}}) \mathbf{x}_{\mathbb{V}}^e \, .
\end{aligned} \tag{6.58}
$$

By following the same procedure as in the proof of Proposition 6.3, we can prove that

$$
\|\Delta \mathbf{x}_{\mathbb{V}}^e\| \leq \frac{1}{\alpha \lambda_2(\tilde{L}_1^*) + \alpha b_{*N} + a} \|\mathbf{q}_{\mathbb{V}}^e\| \, , \tag{6.59}
$$

where $\lambda_2(\tilde{L}_1^*)$ denotes the smallest nonzero eigenvalue of $\tilde{L}_1^*$. This means that the DC-voltage-based control scheme is still effective among the AC areas in $\mathbb{V}$.

Interpretation of x_N^e

Equation (6.54) shows that x_N^e is composed of two parts. Let

$$
x_N^{ea} = -(a_{1N} a_{2N}^{-1} + a_{3N} a_{4N}^{-1})^{-1} (v_N^e + b_N) \, , \tag{6.60}
$$

$$
x_N^{eb} = -(a_{1N} a_{2N}^{-1} + a_{3N} a_{4N}^{-1})^{-1} \tilde{L}_2^T A_{\alpha,\mathbb{V}} \mathbf{x}_{\mathbb{V}}^e \, . \tag{6.61}
$$

It can be seen that the first part, x_N^{ea}, is due to the presence of a power imbalance originating from its own area, while the second part, x_N^{eb}, reflects the influence of frequency deviations of other areas. We observe that area N will react to an power imbalance from an area in $\mathbb{V}$, while a power imbalance from N will not be addressed by other areas. In this sense, the sharing of primary reserves is nonreciprocal.

In the following, we study to what extent the primary reserves of area N are shared. In particular, we investigate the relative size between x_N^{eb} and $\mathbf{x}_{\mathbb{V}}^e$.

Given the definition of L (See Equation (6.5)), Equation (6.61) can be rewritten as

$$
\begin{aligned}
x_N^{eb} &= -(a_{1N} a_{2N}^{-1} + a_{3N} a_{4N}^{-1})^{-1} \tilde{L}_2^T A_{\alpha,\mathbb{V}} \mathbf{x}_{\mathbb{V}}^e \\
&= (a_{1N} a_{2N}^{-1} + a_{3N} a_{4N}^{-1})^{-1} \begin{bmatrix} b_{1N} & b_{2N} & \cdots & b_{\#\mathbb{V},N} \end{bmatrix} A_{\alpha,\mathbb{V}} \mathbf{x}_{\mathbb{V}}^e \\
&= \frac{1}{a_{1N} a_{2N}^{-1} + a_{3N} a_{4N}^{-1}} \sum_{i=1}^{\#\mathbb{V}} b_{iN} \alpha_i x_i^e \, .
\end{aligned} \tag{6.62}
$$

Consider a power imbalance originates from area 1. When $\#\mathbb{V} > 1$, areas $2, 3, \ldots, \#\mathbb{V}$ offer their primary reserves, which implies that x_N^{eb} is necessarily larger than the case when $\#\mathbb{V} = 1$. Thus,

$$
|x_N^{eb}| \leq \frac{b_{1N} \alpha_1}{a_{1N} a_{2N}^{-1} + a_{3N} a_{4N}^{-1}} |x_1^e| \, . \tag{6.63}
$$

The above equation shows that the relative size of x_N^{eb} to x_1^e is determined by a factor that depends on the parameters of area N, the DC network parameter, and the control gain of area 1.

6.5.2 Progress implementation of the DC-voltage-based control scheme

The different working modes of HVDC converters are summarized in Table 6.5.2.

Table 6.1: Working mode combination of HVDC converters

No.	$\#\mathbb{P}$	$\#\mathbb{V}$	$\exists m : V_m^{dc} = V_{ref}^{dc}$	Feasibility	See also
1	$N-1$	0	Yes	Feasible	Section 4.1.2
2	$N-1$	1	No	Infeasible	Remark 6.4
3	$\leq N-2$	≥ 1	Yes	Feasible	Section 6.4
4	$\leq N-2$	≥ 2	No	Feasible	Section 6.5.1

Table 6.5.2 shows that between the mode where the reference operating point is obtained (mode 1) and the full implementation of the control scheme by all converters (mode 4), only mode 2 is to be avoided. Therefore, from an initial condition at mode 1, any converter except the DC-voltage-regulating one can first apply the control scheme. Then all the other converters (including the DC-voltage-regulating one) may choose to apply it at will.

Chapter 7

Coordination on the level of secondary frequency control

The two control schemes proposed in the previous chapters make the AC areas collectively react to power imbalances within the system, but as stated in Propositions 5.1 and 6.1, the control schemes make neither the frequencies of the AC areas nor the power exchanges between the AC areas return to their nominal or scheduled values. To restore the frequencies and the power exchanges, every AC area must resort to secondary frequency control, which acts on the setting for the mechanical power of the aggregated generator.

To discuss the long-term dynamics of the AC areas connected by an MT-HVDC system under the two proposed control schemes, we present in the present chapter one solution for the AC areas to implement secondary frequency control in line with the recommendations of the UCTE. Section 7.1 describes the secondary frequency controller, which is inspired by the practice of the UCTE for secondary frequency control in a synchronous area. Section 7.2 analyzes the stability of the closed-loop system under this control scheme for secondary frequency control combined with the DC-voltage-based control scheme for primary frequency control. Section 7.3 presents simulation results.

7.1 Secondary frequency control scheme

As stated in Chapter 2, secondary frequency control has two objectives: (i) to restore the frequencies of all the AC areas back to their nominal values; (ii) to restore the power exchanged between control blocks (the AC areas in the context of our study) back to their scheduled values. These objectives can be achieved if a power imbalance originating in one area is fully compensated by a change in the setting for the mechanical power of the aggregated generator.

Compared to a synchronous area composed of several control areas, a multi-terminal HVDC system under the control schemes proposed in Chapters 5 and 6 behaves in a similar manner in that each AC area reacts to power imbalances originating in AC areas by sharing its primary reserves. Thus, the principle of secondary frequency control of a synchronous area elaborated in Section 2.3.2 can be used to the multi-terminal HVDC system.

In particular, we define the network power frequency characteristic for AC area i as

$$\lambda_i^{\mathrm{NPFC}} = \frac{-\Delta P_i^{dc*}}{\Delta f_i}\,, \tag{7.1}$$

where ΔP_i^{dc*} is the change of the power injection from AC area i into the DC grid with respect to its scheduled value following a power imbalance originating *outside area* i, and Δf_i the frequency deviation of area i from its nominal value. As the frequency differs one AC area from another, the frequency of the AC area in question is used in the above definition. This is in contrast to the definition in (2.7) in Section 2.3.2, where there is only one unique frequency for the entire synchronous area. The network power frequency characteristic can be used to assess the area control error, which is defined as

$$E_i = \Delta P_i^{dc} + \lambda_i^{\mathrm{NPFC}} \Delta f_i\,, \tag{7.2}$$

where ΔP_i^{dc} is the *actual* change of the power injection from AC area i into the DC grid with respect to its scheduled value, irrespective of the location of the power imbalance.

To realize secondary frequency control, each AC area uses an integral controller that adjusts the power settings for the generators within that area. The output of the secondary frequency controller for area i is given as

$$P_{mi}^o = \bar{P}_{mi}^o - \gamma_i \int E_i dt\,, \tag{7.3}$$

where $\bar{P}_{mi}^o$ is the value of P_{mi}^o at the reference operating point defined in Section 4.2, and $\gamma_i > 0$ the secondary frequency controller gain of area i. The value of γ_i should be chosen small enough so that P_{mi}^o can be considered constant on the time scale of primary frequency control.

7.2 Theoretical study

In the present section, we study the effects of secondary frequency control scheme on stability. For simplicity, we consider the DC-voltage-based control scheme. Similar results can be obtained for the power-injection-based control scheme. First, the linearized closed-system model is given, which is largely borrowed from Section 6.2. Second, a time-scale decomposition is carried out to obtain two reduced-order subsystems describing the slow and the fast dynamics, corresponding respectively to the secondary frequency control scheme proposed in the current chapter and the DC-voltage-based control scheme for primary frequency control. Finally, stability properties of the two subsystems are studied separately.

7.2.1 Linearized closed-loop system

The linearized closed-loop system is the same as the one studied in Section 6.2, except that the secondary frequency control scheme (7.3) is also included. For this section to be self-included, we rewrite all the equations as follows where we continue to use the notations introduced in Chapter 6

$$2\pi J_i \frac{df_i}{dt} = \frac{P_{mi} - P_{li}^o - P_i^{dc}}{2\pi f_{nom,i}} - 2\pi D_i (f_i - f_{nom,i})\,, \tag{7.4a}$$

$$T_{smi}\frac{dP_{mi}}{dt} = P^o_{mi} - P_{mi} - \frac{P_{Ni}}{\sigma_i}\frac{f_i - f_{nom,i}}{f_{nom,i}} \ , \tag{7.4b}$$

$$P^{dc}_i = \sum_{j=1}^{N} \frac{V^{dc}_{ref}(V^{dc}_i - V^{dc}_j)}{R_{ij}} \ , \tag{7.4c}$$

$$V^{dc}_i = \bar{V}^{dc}_i + \alpha_i \Delta f_i \ , \tag{7.4d}$$

$$\frac{dP^o_{mi}}{dt} = -\gamma_i(\Delta P^{dc}_i + \lambda^{\text{NPFC}}_i \Delta f_i) \ . \tag{7.4e}$$

We introduce the following variables: $x_i = \Delta f_i$, $y_i = P_{mi} - \bar{P}_{mi}$, $z_i = V^{dc}_i - \bar{V}^{dc}_i$, $u_i = P^{dc}_i - \bar{P}^{dc}_i$, $v_i = P^o_{li} - \bar{P}^o_{li}$, and $w_i = P^o_{mi} - \bar{P}^o_{mi}$. With these notations and taking into account the equations describing the reference operating point (4.6)-(4.10), Equation (7.4) becomes

$$\frac{dx_i}{dt} = -a_{1i}x_i + a_{2i}y_i - a_{2i}u_i - a_{2i}v_i \ , \tag{7.5a}$$

$$\frac{dy_i}{dt} = -a_{3i}x_i - a_{4i}y_i + a_{4i}w_i \ , \tag{7.5b}$$

$$z_i = \alpha_i x_i \ , \tag{7.5c}$$

$$u_i = \sum_{j=1}^{N} b_{ij}(z_i - z_j) + b_i \ , \tag{7.5d}$$

$$\frac{dw_i}{dt} = -\gamma_i a_{5i}x_i - \gamma_i u_i \ , \tag{7.5e}$$

where $a_{1i} = D_i/J_i$, $a_{2i} = 1/(4\pi^2 f_{nom,i}J_i)$, $a_{3i} = P_{nom,i}/(T_{smi}\sigma_i f_{nom,i})$, $a_{4i} = 1/T_{smi}$, $a_{5i} = \lambda^{\text{NPFC}}_i$, $b_i = \sum_j (V^{dc}_{ref} - \bar{V}^{dc}_i)(\bar{V}^{dc}_i - \bar{V}^{dc}_j)/R_{ij}$, and $b_{ij} = V^{dc}_{ref}/R_{ij}$. Note that a_{1i}, a_{2i}, a_{3i}, a_{4i}, and b_{ij} are all positive constants.

Define the vectors $\mathbf{x} = [x_1, x_2, \ldots, x_N]^T$, $\mathbf{y} = [y_1, y_2, \ldots, y_N]^T$, $\mathbf{u} = [u_1, u_2, \ldots, u_N]^T$, $\mathbf{v} = [v_1, v_2, \ldots, v_N]^T$, $\mathbf{w} = [w_1, w_2, \ldots, w_N]^T$, $\mathbf{b} = [b_1, b_2, \ldots, b_N]^T$ and the matrices $A_i = \text{diag}(a_{i1}, a_{i2}, \ldots, a_{iN})$, $i = 1, 2, 3, 4, 5$, $A_\alpha = \text{diag}(\alpha_1, \alpha_2, \ldots, \alpha_N)$, $A_\gamma = \text{diag}(\gamma_1, \gamma_2, \ldots, \gamma_N)$, and L

$$[L]_{ij} = \begin{cases} -b_{ij} & \text{for } i \neq j \ , \\ \sum_{j\neq i} b_{ij} & \text{for } i = j \ . \end{cases} \tag{7.6}$$

Then, (7.5) gives rise to the following model in matrix form

$$\frac{d\mathbf{x}}{dt} = -A_1\mathbf{x} + A_2\mathbf{y} - A_2LA_\alpha\mathbf{x} - A_2\mathbf{b} - A_2\mathbf{v} \ , \tag{7.7a}$$

$$\frac{d\mathbf{y}}{dt} = -A_3\mathbf{x} - A_4\mathbf{y} + A_4\mathbf{w} \ , \tag{7.7b}$$

$$\frac{d\mathbf{w}}{dt} = -A_\gamma(A_5 + LA_\alpha)\mathbf{x} - A_\gamma A_2\mathbf{b} \ . \tag{7.7c}$$

7.2.2 Time-scale decomposition

The model described by (7.7) is a $3N$-order system. We can of course analyze its stability by investigating all its $3N$ eigenvalues. However, since the values of γ_i are chosen small enough

so that $\mathbf{w}$ can be considered constant on the time scale of primary frequency control, we can consider the fast and the slow dynamics separately in order to facilitate study and to gain a further insight on the entire system. In the following, we carry out a time-scale decomposition (See Appendix E) on the system (7.7) to obtain two reduced-order subsystems, with the slow one describing the dynamics of $\mathbf{w}$ and the fast one that of $\mathbf{x}$ and $\mathbf{y}$.

We denote by $\mathbf{w}_s$, $\mathbf{x}_s$, $\mathbf{y}_s$ the slow components and by $\mathbf{w}_f$, $\mathbf{x}_f$, $\mathbf{y}_f$ the fast components of the state variable such that

$$\mathbf{w} = \mathbf{w}_s + \mathbf{w}_f \ , \tag{7.8a}$$
$$\mathbf{x} = \mathbf{x}_s + \mathbf{x}_f \ , \tag{7.8b}$$
$$\mathbf{y} = \mathbf{y}_s + \mathbf{y}_f \ . \tag{7.8c}$$

Slow dynamics

For the linear system (7.7), its slow manifold is such that the fast dynamics are not excited, so that $\mathbf{w} = \mathbf{w}_s, \mathbf{x} = \mathbf{x}_s, \mathbf{y} = \mathbf{y}_s$.

A quasi-steady-state approximation of the slow subsystem can be obtained by when the fast subsystem is at its equilibrium, i.e.

$$0 = -A_1\mathbf{x}_s + A_2\mathbf{y}_s - A_2LA_\alpha\mathbf{x}_s - A_2\mathbf{b} - A_2\mathbf{v} \ , \tag{7.9a}$$
$$0 = -A_3\mathbf{x}_s - A_4\mathbf{y}_s + A_4\mathbf{w}_s \ , \tag{7.9b}$$
$$\frac{d\mathbf{w}_s}{dt} = -A_\gamma(A_5 + LA_\alpha)\mathbf{x}_s - A_\gamma A_2\mathbf{b} \ . \tag{7.9c}$$

For a given $\mathbf{w}_s$, (7.9a) and (7.9b) are the equilibrium condition for $\mathbf{x}$ and $\mathbf{y}$, from which we obtain for a fixed value $\mathbf{v} = \mathbf{v}^e$

$$\mathbf{x}_s = (LA_\alpha + A_1A_2^{-1} + A_3A_4^{-1})^{-1}(\mathbf{w}_s - \mathbf{v}^e - \mathbf{b}) \ , \tag{7.10a}$$
$$\mathbf{y}_s = -A_3A_4^{-1}\mathbf{h}_{10} + \mathbf{w}_s \ , \tag{7.10b}$$

where we used the fact that $(LA_\alpha + A_1A_2^{-1} + A_3A_4^{-1})$ is invertible. It is noted that when the secondary control scheme is not implemented, i.e. $\mathbf{w} = 0$, Equation (7.10) is exactly the same as (6.8a) and (6.8b) in Section 6.2.2.

We now study the stability properties of the slow subsystem. Replacing $\mathbf{x}_s$ in (7.9c) by (7.10a) yields

$$\begin{aligned}\frac{d\mathbf{w}_s}{dt} &= -A_\gamma(A_5 + LA_\alpha)\mathbf{x}_s - A_\gamma A_2\mathbf{b} \\ &= A_{\text{slow}}(\mathbf{w}_s - \mathbf{v}^e - \mathbf{b}) - A_\gamma A_2\mathbf{b} \\ &= A_{\text{slow}}\mathbf{w}_s - A_{\text{slow}}\mathbf{v}^e - (A_{\text{slow}} + A_\gamma A_2)\mathbf{b} \ ,\end{aligned} \tag{7.11}$$

where $A_{\text{slow}} = -A_\gamma(A_5 + LA_\alpha)(LA_\alpha + A_1A_2^{-1} + A_3A_4^{-1})^{-1}$.

It is difficult, if not impossible, to prove Hurwitz stability of the matrix A_{slow} for the general case. For a given system, stability of the slow subsystem can be checked by numerically calculating the eigenvalues of A_{slow}.

Fast dynamics

In order to approximate the fast dynamics, we assume that $\mathbf{w}$ is predominantly slow, i.e. $\mathbf{w} \approx \mathbf{w}_s$. Thus, the state variables of the fast subsystem are the fast components $\mathbf{x}_f$, $\mathbf{y}_f$ introduced in (7.8b), (7.8c). The equilibrium point of the fast manifold is at the slow manifold, i.e. $\mathbf{x}_f = \mathbf{y}_f = 0$.

Linearizing (7.9a) around a point $(\mathbf{w}_s, \mathbf{x}_s, \mathbf{y}_s)$ on the slow manifold yields

$$\frac{d}{dt}\begin{bmatrix}\Delta\mathbf{x}_f \\ \Delta\mathbf{y}_f\end{bmatrix} = \begin{bmatrix}-A_1 - A_2 L A_\alpha & A_2 \\ -A_3 & -A_4\end{bmatrix}\begin{bmatrix}\Delta\mathbf{x}_f \\ \Delta\mathbf{y}_f\end{bmatrix}, \tag{7.12}$$

which is the same as the system studied in Proposition 6.1 in Section 6.2, where exponential stability is proved using a frequency-domain approach. Thus, the fast subsystem is stable.

7.3 Simulation results

To illustrate the impact of secondary frequency control, we run simulations under the same conditions as in Section 5.3. Figures 7.1 and 7.2 depict the evolution of the frequencies and the power setting P_m^o of the five AC areas when the secondary frequency control scheme is implemented in combination with the DC-voltage-based control scheme, and Figures 7.3 and 7.4 show the evolution of ΔV^{dc} and ΔP^{dc}, which are the deviations of V^{dc} and P^{dc} with respect to their nominal or scheduled values. As secondary frequency control has a time scale of a few minutes, we extend the observation window to ten minutes. The controller gains are chosen as $\alpha_1 = \alpha_2 = \ldots = \alpha_5 = 2 \times 10^3$ and $\gamma_1 = \gamma_2 = \ldots = \gamma_5 = 2$.

The behavior during the first few seconds in Figure 7.1 is essentially equal to Figure 6.1 in the previous chapter. This means that the primary frequency control dominates, unperturbed by secondary frequency control. The latter also performs as expected: only the power setting for the disturbed area 2, P_{m2}^o, is changed significantly, and the frequencies converge back to their nominal values in the long term. The evolution of P_i^{dc} indicates that the power injections into the DC grid are also restored to their scheduled values. Also, the DC-side voltages of the converters V_i^{dc} return to their initial values.

The above results show that our secondary frequency control scheme achieves its two objectives: to restore the frequencies and the power exchanges to their nominal or scheduled values. In addition, the secondary control scheme acts within minutes, so the variations of P_m^o are well decoupled from the DC-voltage-based control scheme for primary frequency control.

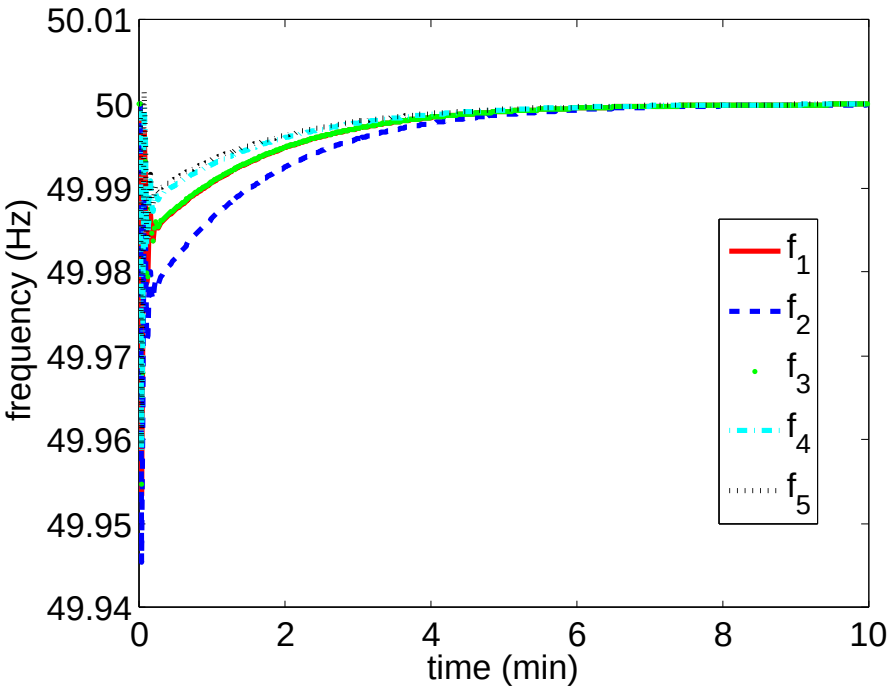

Figure 7.1: Frequencies of the five AC areas under the DC-voltage-based control scheme and the secondary frequency control scheme.

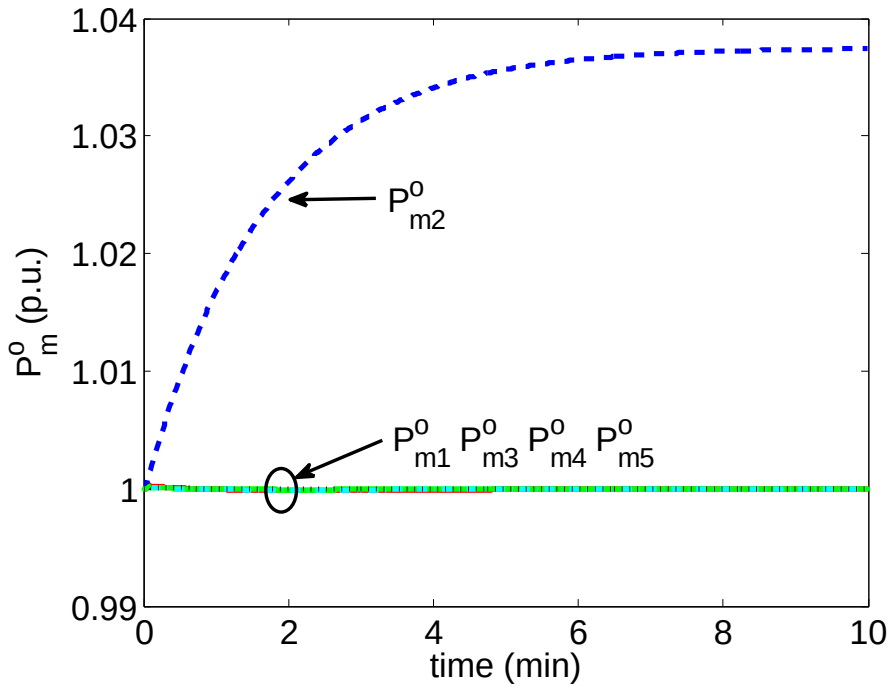

Figure 7.2: P_m^o of the five AC areas under the DC-voltage-based control scheme and the secondary frequency control scheme.

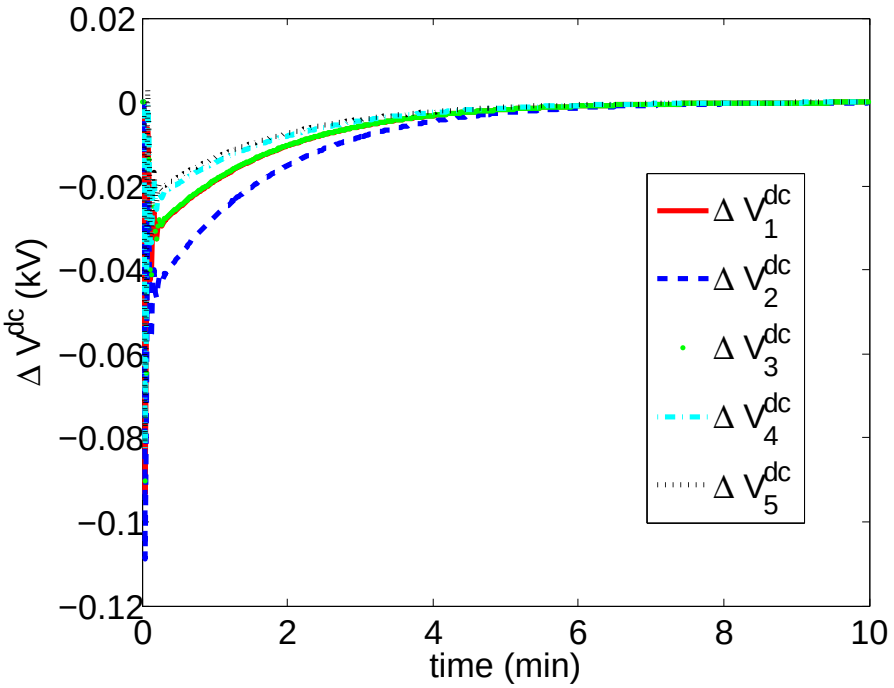

Figure 7.3: ΔV^{dc} of the five AC areas under the DC-voltage-based control scheme and the secondary frequency control scheme.

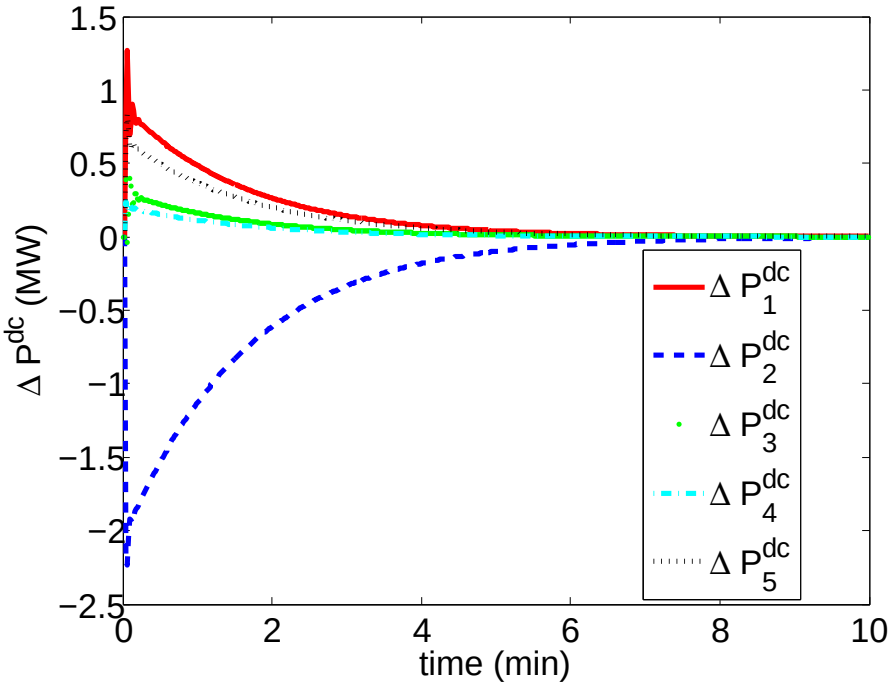

Figure 7.4: ΔP^{dc} of the five AC areas under the DC-voltage-based control scheme and the secondary frequency control scheme.

Chapter 8

Conclusions

8.1 Summary of contributions

In the present dissertation, we proposed three control schemes for frequency control in a power system composed of several non-synchronous AC areas connected by a multi-terminal HVDC grid.

The first control scheme, called power-injection-based control scheme, is distributed by nature. Based on remote measurements of the other areas' frequencies, this control scheme modifies the power injections from the different AC areas into the DC grid so as to make the system collectively react to load imbalances. This collective reaction allows each individual AC area to downscale its primary reserves. The scheme is inspired by algorithms for the consensus problem extensively studied by the control theory community. As remote measurements are used, the effects of time-delays on the control scheme's effectiveness are investigated. A stability analysis of the closed-loop system shows that with some assumptions, as long as the time-delays are within an acceptable limit, the system converges to an equilibrium point at which the AC areas' frequency deviations are equal to each other. A Nyquist criterion is obtained to determine whether the time-delays would destabilize the system. Simulations on a benchmark system with five non-identical AC areas show that in the absence of time-delays, the frequency deviations of all the areas rapidly converge to each other following a step change in the load demand. In the presence of time-delays, we found that for delays above a threshold value, the control scheme may cause undamped frequency oscillations, and that these undamped frequency oscillations are more likely to appear when using high values of the controller gains. The simulations highlight that power-injection-based control scheme can make good use of the fast power-tracking capability of HVDC converters to coordinate primary frequency control efforts among non-synchronous AC areas.

To avoid the problem of time-delays associated with the power-injection-based control scheme, a second control scheme is introduced. It has the same objective with the first one, but acts on the DC voltages of the HVDC converters, hence its name DC-voltage-based control scheme. In particular, it modifies the DC voltage of each converter based on the frequency deviation of the AC area it is connected to. This decentralized nature frees it from the problems related to the dependence on remote information. A theoretical study shows that the interconnected system is stable and converges to an equilibrium at which, for bounded load perturbations, the

difference between the frequency deviations induced in all the areas can be made arbitrarily small by choosing a sufficiently large control gain. Simulation results on the same benchmark system showed that by using local information only, the control scheme allows to significantly reduce the impact of a power imbalance by distributing the associated frequency deviation over all areas.

The last control scheme aims at restoring the frequencies and the power exchanges to their nominal or scheduled values in the aftermath of a power imbalance. It can be combined with the other two control schemes. To study its stability properties, a timescale decomposition is carried out on the closed-loop system under this control scheme combined with the DC-voltage-based control scheme. The two reduced-order subsystems thus obtained describing the slow and the fast dynamics respectively are both shown to be stable, which implies the stability of the entire system. Simulation results on the benchmark system confirm the good performance of the control scheme.

8.2 Perspectives for further works

The two control schemes for primary frequency control can be improved along several lines.

First, it would be interesting to study the effects of the gain of each subcontroller, so as to find a systematic way to choose them. Indeed, these gains influence the degree of participation of every area in the primary frequency control scheme, and, by better understanding their influence, one should be able to choose them so as to take into account the technical and economic characteristics of each area. For example, the relative size of one area with respect to others can be considered, so that in response to a major power imbalance in a larger area, a smaller area with less primary reserves can choose to stop sharing its own reserve if it judges that a further sharing of its reserve would jeopardize its own stability. In this way, the HVDC system would still play the role of "firewall" that prevents cascading outages across AC areas. These gains could probably also be tuned dynamically in the time frame of the secondary frequency control scheme, so as to reflect the change of the operating point and reduce the likelihood of congestions in the DC lines following a disturbance.

Second, while the control schemes for primary frequency control call for primary reserves simultaneously from all areas of the system in the aftermath of a power imbalance in an area, it would also be worth investigating whether it could be adapted to the case where the primary reserves of different AC areas are solicited in a sequential way, so that the reserves from remote areas are deployed only when local reserves have been depleted.

Third, the theoretical study could be extended by relaxing some of the assumptions done for establishing the proofs.

Fourth, it would be interesting to test these control schemes on more sophisticated power system benchmarks such as those that would not neglect for example voltage regulation in the AC areas.

Finally, using a multi-terminal HVDC grid for sharing primary reserves between the AC areas may have an adverse effect. Indeed, the areas may become more vulnerable with respect to contingencies resulting in a disconnection from the HVDC link, because such contingencies may create a dangerous power imbalance in an area while at the same time reducing the primary

reserves that the area has access to. This is certainly an issue to be considered when relying on an HVDC system for offering such a type of ancillary service.

The control schemes proposed in the dissertation give an example of using HVDC systems to provide ancillary services to power system. We expect that as an active research area, the potentials of HVDC systems to improve power system stability will be further investigated and better exploited.

Appendix A

Basic notations and definitions

The sequence of integers from 1 to $N > 1$ is summarized as $1, 2, \ldots, N$. Similarly, the sequence of elements from a_1 to a_N is summarized as $a_1, a_2, \ldots, a_N$. $a \in A$ ($a \notin A$, resp.) means that element a belongs to (does not belong to, resp.) set A. $\#A$ denotes the cardinality of set A. $A \subseteq B$ ($A \subset B$, resp.) means that set A is a subset (proper subset, resp.) of set B. Given two sets A and B, $A \times B$ denotes their Cartesian product, and $A \cup B$ ($A \cap B$, resp.) their union (intersection, resp.).

The set of all real numbers (positive real numbers, resp.) is denoted as $\mathbb{R}$ ($\mathbb{R}_+$, resp.). The set of all complex numbers is denoted as $\mathbb{C}$. The imaginary unit is denoted as $j = \sqrt{-1}$. The magnitude and the argument of a number $a \in \mathbb{C}$ are denoted as $|a|$ and $\arg(a)$, respectively. The set of all vectors containing n real numbers (complex numbers, resp.) is denoted as $\mathbb{R}^n$ ($\mathbb{C}^n$, resp.). The set of all real matrices (complex matrices, resp.) of n rows and m columns is denoted as $\mathbb{R}^{n\times m}$ ($\mathbb{C}^{n\times m}$, resp.). Let $\mathbf{1}_N$ denote the column vector of length N with all components equal to 1. Let I_N denoted the $N \times N$ identity matrix. For matrix $A \in \mathbb{R}^{n\times m}$, A^T denotes the transpose of A. $\mathrm{diag}(a_1, a_2, \ldots, a_N)$ denotes the diagonal matrix whose diagonal elements are $a_1, a_2, \ldots, a_N$. The element in the ith row and kth column of matrix A is denoted as $[A]_{ik}$. The norm of a vector $\mathbf{x} = [x_1, x_2, \ldots, x_N]^T \in \mathbb{R}^N$ is denoted as $\|\mathbf{x}\|$ with

$$\|\mathbf{x}\| = \sqrt{x_1^2 + x_2^2 + \ldots + x_N^2}\,. \tag{A.1}$$

The norm of a vector $\mathbf{z} = [z_1, z_2, \ldots, z_N]^T \in \mathbb{C}^N$ is denoted as $\|\mathbf{z}\|$ with

$$\|\mathbf{z}\| = \sqrt{|z_1|^2 + |z_2|^2 + \ldots + |z_N|^2}\,. \tag{A.2}$$

For matrix $A \in \mathbb{R}^{n\times n}$, $\det(A)$ denotes the determinant of A. Denote the eigenvalues of matrix $A \in \mathbb{C}^{n\times n}$ by $\lambda_1, \lambda_2, \ldots, \lambda_n$, then the spectral radius of A is denoted as $\rho(A)$, i.e.

$$\rho(A) = \max_{i=1,2,\ldots,n} |\lambda_i|\,. \tag{A.3}$$

The maximum singular value of a matrix $Q \in \mathbb{C}^{n\times m}$ is denoted as $\bar{\sigma}(Q)$, which can be calculated as

$$\bar{\sigma}(Q) = \max_{\|u\|=1} \|Qu\|\,, \tag{A.4}$$

with $u \in \mathbb{C}^m$. Given $A \in \mathbb{C}^{n\times m}$ and $B \in \mathbb{C}^{p\times q}$, $A \otimes B$ is their Kronecker product, i.e.

$$A \otimes B = \begin{bmatrix} [A]_{1,1}B & \cdots & [A]_{1,m}B \\ \vdots & \ddots & \vdots \\ [A]_{n,1}B & \cdots & [A]_{n,m}B \end{bmatrix} \in \mathbb{C}^{np\times mq} . \tag{A.5}$$

A set in Euclidean space $\mathbb{R}^n$ is convex set if it contains all the line segments connecting any pair of its points. The convex hull of a set of points A in n dimensions is denoted as $Co(A)$, which is the intersection of all convex sets containing A.

For a differentiable function $f(x) : \mathbb{R} \to \mathbb{R}$, df/dx denotes the derivative of f w.r.p to x. For a differentiable function $f(x_1, x_2, \ldots, x_N) : \mathbb{R}^N \to \mathbb{R}$, $\partial f/\partial x_i$ denotes the partial derivative of f w.r.p to x_i.

Appendix B

Graph theory

In Chapters 5 and 6, some notions in graph theory, e.g. the Laplacian, are invoked. This appendix gives the fundamentals of graph theory, where those notions are formally defined and interesting results can be used in studying the properties of the control schemes for primary frequency control. The materials in this appendix can be found in any textbook on graph theory, e.g. [86].

Definition B.1. *A* directed graph *(or* digraph*)* $\mathcal{G}(\mathcal{V}, \mathcal{E})$ *is composed of a finite set* $\mathcal{V}$ *of nodes and a set* $\mathcal{E} \subseteq \mathcal{V} \times \mathcal{V}$ *of edges.*

The nodes are indexed by positive integers so that $\mathcal{V} = \{1, 2, \ldots, N\}$. An edge is denoted by e_{ik}, with $i, k \in \mathcal{V}$. We assume that $\mathcal{G}$ contains no *self-loops*, i.e. $e_{ii} \notin \mathcal{E}, \forall i \in \mathcal{V}$.

Definition B.2. *A* undirected graph *(or* graph*)* $\mathcal{G}(\mathcal{V}, \mathcal{E})$ *is a digraph for which* $e_{ik} \in \mathcal{E}$ *whenever* $e_{ki} \in \mathcal{E}$*.*

Definition B.3. *A* weighted digraph $\mathcal{G}(\mathcal{V}, \mathcal{E}, \mathcal{A})$ *is a digraph associated with a set* $\mathcal{A}$*, which assigns a positive weight* a_{ik} *to each edge* $e_{ik} \in \mathcal{E}$*. By convention,* $a_{ik} = 0$ *if* $e_{ik} \notin \mathcal{E}$*.*

Definition B.4. *A* weighted graph $\mathcal{G}(\mathcal{V}, \mathcal{E}, \mathcal{A})$ *is a weighted digraph for which* $a_{ik} = a_{ki}, \forall e_{ki} \in \mathcal{E}$*.*

A way of representing a graph by a matrix is to define the *adjacency matrix* $A \in \mathbb{R}^{N \times N}$, which contains a_{ik} in row i and column k.

Definition B.5. *The* in-degree *of node* i *is* $d_i^{(i)} = \sum_{k=1}^{N} a_{ki}$*. The* out-degree *of node* i *is* $d_i^{(o)} = \sum_{k=1}^{N} a_{ik}$*. A digraph is* balanced *if* $d_i^{(i)} = d_i^{(o)}, \forall i \in \mathcal{V}$*.*

In particular, undirected graphs are balanced. The in- and out-degrees of nodes $1, 2, \ldots, N$ can be assembled in diagonal matrices $D^{(i)}$ and $D^{(o)}$. For a balanced graph, it is simply denoted by D.

Definition B.6. *The in-Laplacian of a digraph* $\mathcal{G}$ *is* $L^{(i)} = D^{(i)} - A$*. The out-Laplacian of a digraph* $\mathcal{G}$ *is* $L^{(o)} = D^{(o)} - A$*. For a balanced graph, the Laplacian* $L = L^{(i)} = L^{(o)}$*.*

For a general graph, $\mathbf{1}_N^T L^{(i)} = 0$ and $L^{(o)} \mathbf{1}_N = 0$. For an undirected graph, L is symmetric.

Definition B.7. *A* directed path *of length l between node i and k is a sequence of nodes $v_0, v_1, \ldots, v_l$ such that $v_0 = i$, $v_l = k$, and $e_{m,m+1} \in \mathcal{E}$, for $m = 1, 2, \ldots, l-1$.*

Definition B.8. *An* undirected path *of length l between node i and k is a sequence of nodes $v_0, v_1, \ldots, v_l$ such that $v_0 = i$, $v_l = k$, and $e_{m,m+1} \in \mathcal{E}$ or $e_{m+1,m} \in \mathcal{E}$ for $m = 1, 2, \ldots, l-1$.*

Definition B.9. *A digraph $\mathcal{G}$ is* strongly connected *if there exists a directed path from every node to every other node. A digraph $\mathcal{G}$ is* weakly connected *if there is an undirected path between any two of its nodes.*

For an undirected graph, the notions of strongly-connected and weakly-connected are equivalent and are simply termed *connected*. Thus, an undirected graph is *connected* if there exists an undirected path between any two of its nodes.

Proposition B.1. *The out-Laplacian $L^{(o)}$ has the following properties: All the eigenvalues of $L^{(o)}$ have nonnegative real parts; If $\mathcal{G}$ is strongly connected, then 0 is a simple eigenvalue of $L^{(o)}$. $L^{(o)}$ is positive-semidefinite if and only if $\mathcal{G}$ is balanced. These properties also apply to the transposed in-Laplacian $(L^{(i)})^T$.*

Proposition B.2. *The Laplacian L of a balanced connected graph $\mathcal{G}$ is such that all the eigenvalues are real numbers. Denote the eigenvalues such that $\lambda_1 \leq \lambda_2 \leq \ldots, \leq \lambda_N$. Then, $\lambda_1 = 0$ and $\lambda_2 > 0$. In addition, the second smallest eigenvalue is called the* algebraic connectivity *of the graph.*

Proposition B.3. *Consider that an $n \times n$ Laplacian L associated with a balanced connected graph is partitioned as*

$$L = \begin{bmatrix} L_1 & L_2 \\ L_2^T & L_3 \end{bmatrix} \tag{B.1}$$

where L_1, L_2, and L_3 are submatrices of L of dimension $p \times p$, $p \times q$, and $q \times q$, respectively. Then, the matrix $L_r = L_1 - L_2 L_3^{-1} L_2^T$ is also a Laplacian associated with a balanced connected graph, i.e.

- *L_r is positive-semidefinite;*
- *$L_r \mathbf{1}_p = 0$.*

Proof. The proof is divided into three parts: We prove respectively that (i) L_r is symmetric, (ii) $\mathbf{x}^T L_r \mathbf{x} \geq 0$ for any nonzero column vector $\mathbf{x}$ of length p, and (iii) $L_r \mathbf{1}_p = 0$.

(i) From the partition of L, we see that both L_1 and L_3 are symmetric. Thus,

$$\begin{aligned} L_r^T &= (L_1 - L_2 L_3^{-1} L_2^T)^T \\ &= L_1^T - L_2 (L_3^{-1})^T L_2^T \\ &= L_1 - L_2 (L_3^T)^{-1} L_2^T \\ &= L_1 - L_2 L_3^{-1} L_2^T \\ &= L_r \, . \end{aligned} \tag{B.2}$$

(ii) Since L is positive semidefinite, we have

$$x^T L x \geq 0 \tag{B.3}$$

where $\mathbf{x}$ is an arbitrary nonzero vector of length n. Thus, the above equation also holds for any $\mathbf{x} = [\mathbf{x}_1, \mathbf{x}_2]^T$ such that

$$\mathbf{x}_2 = -L_3^{-1} L_2^T \mathbf{x}_1 \,, \tag{B.4}$$

for which (B.3) becomes

$$\begin{aligned}
&\begin{bmatrix} \mathbf{x}_1 \\ \mathbf{x}_2 \end{bmatrix}^T \begin{bmatrix} L_1 & L_2 \\ L_2^T & L_3 \end{bmatrix} \begin{bmatrix} \mathbf{x}_1 \\ \mathbf{x}_2 \end{bmatrix} \\
&= \mathbf{x}_1^T L_1 \mathbf{x}_1 + \mathbf{x}_1^T L_2 \mathbf{x}_2 + \mathbf{x}_2^T L_2^T \mathbf{x}_1 + \mathbf{x}_2^T L_3 \mathbf{x}_2 \\
&= \mathbf{x}_1^T L_1 \mathbf{x}_1 + \mathbf{x}_1^T L_2 (-L_3^{-1} L_2^T \mathbf{x}_1) + \mathbf{x}_2^T (L_2^T \mathbf{x}_1 + L_3 \mathbf{x}_2) \\
&= \mathbf{x}_1^T (L_1 - L_2 L_3^{-1} L_2^T) \mathbf{x}_1 + 0 \\
&\geq 0 \,.
\end{aligned}$$

(iii) From Proposition B.2, we have

$$L \mathbf{1}_n = \begin{bmatrix} L_1 & L_2 \\ L_2^T & L_3 \end{bmatrix} \begin{bmatrix} \mathbf{1}_p \\ \mathbf{1}_q \end{bmatrix} = \begin{bmatrix} 0 \\ 0 \end{bmatrix} \tag{B.5}$$

which yields

$$L_1 \mathbf{1}_p + L_2 \mathbf{1}_q = 0 \,, \tag{B.6a}$$

$$L_2^T \mathbf{1}_p + L_3 \mathbf{1}_q = 0 \,. \tag{B.6b}$$

Thus, we have

$$\begin{aligned}
&(L_1 - L_2 L_3^{-1} L_2^T) \mathbf{1}_p \\
&= L_1 \mathbf{1}_p - L_2 L_3^{-1} L_2^T \mathbf{1}_p \\
&= -L_2 \mathbf{1}_q - L_2 L_3^{-1} (-L_3 \mathbf{1}_q) \\
&= -L_2 (\mathbf{1}_q + L_3^{-1} L_3 \mathbf{1}_q) \\
&= 0 \,.
\end{aligned} \tag{B.7}$$

This concludes the proof. □

Remark B.1. *For the trivial case where $p = 1$, L_r is a scalar. Since $L_r \mathbf{1}_p = 0$, we must have $L_r = 0$.*

Appendix C

Consensus problem

The consensus problem deals with coordination within a multi-agent system. It is an active research domain with many applications, among which the unmanned aerial vehicles (UAVs). Given the resemblance between (i) a multi-terminal HVDC power system under the control schemes givens in Chapters 5 and 6 and (ii) a multi-agent system seeking for consensus among agents, we give in the current appendix a brief description of the simplest form of the consensus problem. The following materials can be found in most of the literature in this area, e.g. [33].

C.1 Problem definition and consensus protocol

An *multi-agent system* is defined as a system composed of multiple intelligent agents. By *intelligent agent* (or simply *agent*) we mean an autonomous entity that is capable of observing the environment (thus including other agents) and taking actions in order to achieve a certain objective. The notion of multi-agent systems is an abstraction of real-world systems. In the case of a set of UAVs, each vehicle can be considered as an agent, which adjusts its own position based on the observation on other vehicle, in order to attain a goal, for example a common altitude.

Consider a multi-agent system composed of N agents, each has the following dynamics

$$\frac{dx_i(t)}{dt} = u_i(t) \ , \tag{C.1}$$

where $x_i \in \mathbb{R}$ is the state of agent i and $u_i \in \mathbb{R}$ its action. Assume that agent i has access to the states of some of the others agents. The objective of all agents is to achieve *consensus*[1] asymptotically, i.e.

$$x_1 = x_2 = \ldots = x_N \ . \tag{C.2}$$

The above problem can be solved by the following controller for agent $i, \forall i \in \{1, 2, \ldots, N\}$, usually referred to as a *consensus protocol*:

$$u_i(t) = \alpha \sum_{k=1}^{N} a_{ki}(x_k(t) - x_i(t)) \ , \tag{C.3}$$

[1] With respect to a vector space, the term *synchronization* can also be used.

where $\alpha > 0$ is a gain and a_{ki} is a weight determined by the communication link between agent i and k. In particular, if agent i has access to information on agent k, $a_{ki} > 0$; otherwise, $a_{ki} = 0$.

C.2 Stability properties

To study the stability properties of the multi-agent system (C.1) under the consensus protocol (C.3), we write the closed-loop system in matrix form. Let $\mathbf{x} = [x_1, x_2, \ldots, x_N]^T$ and $\mathbf{u} = [u_1, u_2, \ldots, u_N]^T$. Then, (C.1) and (C.3) yield

$$\frac{d\mathbf{x}(t)}{dt} = -\alpha L\mathbf{x}(t) \ , \tag{C.4}$$

where

$$[L]_{ik} = \begin{cases} -a_{ik} & \text{for } i \neq k \ , \\ \sum_{k \neq i} a_{ik} & \text{for } i = k \ . \end{cases} \tag{C.5}$$

The introduction of matrix L allows us to represent the interaction between the agents by means of a weighted digraph, called *communication graph*. In this graph, each agent is represented by a node, and the interaction between two agents is represented by an edge between the two nodes. The edge from node k to node i is associated with the weight a_{ki}. Referring to Appendix B, it can be seen that L is the transposed in-Laplacian of this communication graph.

Since $\mathbf{1}_N$ is a left eigenvector associated with a zero eigenvalue of an in-Laplacian, the consensus condition described by (C.2) is an equilibrium point for system (C.4). In addition, in order that all the agents achieve consensus, it is necessary that all the eigenvectors of L lie in the eigenspace spanned by $\mathbf{1}_N$. This is true when the communication graph is strongly connected. The convergence properties of the closed-system towards consensus is determined by the eigenvalues of L. Thus, the stability of the interconnected system can be determined by investigating the semi-positiveness of L using the results in graph theory. As to the convergence speed, much information can be obtained from the second smallest eigenvalue of L which determines the worst case speed of convergence.

For a practical system, the dynamics of each agent may be much more complicated and potentially nonlinear, and they may differ from one agent to another. In addition, the communication graph may also be time-varying. All these general cases are the subject of the intensive research, and the results can be found in [33, 30, 87, 29].

Appendix D

A frequency-domain stability criterion for interconnected systems

In the present appendix, we presents a frequency-domain approach introduced in [85]. The result in this appendix is used in Section 6.2 to prove stability of the DC-voltage-based control scheme for primary frequency control. We first give a proposition on stable system, which is borrowed from in [88]. Then, we give the stability criterion.

D.1 $\mathcal{H}_\infty$ space and stable transfer functions

Definition D.1. *The $\mathcal{H}_\infty$ space is the class of systems if its transfer function $\mathbf{G}(s)$ satisfies*

- *$\mathbf{G}(s)$ is analytic in the open-right-half plane,*
- *The supremum of $\mathbf{G}(s)$ is finite, i.e.*

$$\|\mathbf{G}(s)\|_\infty = \sup_{\alpha>0} \left\{ \sup_{\omega} \bar{\sigma}(\mathbf{G}(\alpha + j\omega)) \right\} < \infty \,, \tag{D.1}$$

With the above definition, we denote $\mathcal{C}_0$ is the class of functions continuous in $j\mathbb{R} \cup \{\infty\}$, and $\mathcal{A}_0 = \mathcal{H}_\infty \cap \mathcal{C}_0$.

Proposition D.1. *A transfer function matrix $\mathbf{G}$ defines a stable system if and only if $\mathbf{G} \in \mathcal{H}_\infty$.*

D.2 Stability criterion

Consider an interconnected system defined by

$$\mathbf{y}(s) = \mathbf{G}(s)\mathbf{u}(s) \,, \tag{D.2a}$$

$$\mathbf{u}(s) = A\mathbf{y}(s) \,, \tag{D.2b}$$

where $\mathbf{G}(s) = \mathrm{diag}(g_1(s), g_2(s), \ldots, g_n(s))$ and $A = A^T \in \mathbb{R}^{n\times n}$. It can be seen that in this interconnected system, $g_i(s)$ represents the dynamics of the subsystem i, while matrix A describes the interconnections between the subsystems. The system is shown in Figure D.1.

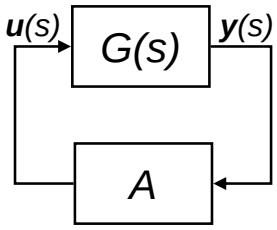

Figure D.1: An interconnected system

Proposition D.2. *The system defined by Equation* (D.2)*, where* $\rho(A) \leq 1$ *and* $g_i(s) \in \mathcal{A}_0$*, for* $i = 1, 2, \ldots, n$*, is stable if*

$$1 \notin Co(\{g_i(j\omega) : \omega \in \mathbb{R}_+, i = 1, 2, \ldots, n\}) \,. \tag{D.3}$$

The proof of the above proposition can be found in [85].

Appendix E

Time-scale decomposition

In this appendix, we give the procedure of time-scale decomposition based on the singular perturbation analysis [89, 90], which is used in Section 7.2. The material in this appendix is largely borrowed from [4].

Consider a system

$$\frac{d\mathbf{x}}{dt} = \mathbf{f}(\mathbf{x}, \mathbf{y}) \ , \tag{E.1a}$$

$$\epsilon \frac{d\mathbf{y}}{dt} = \mathbf{g}(\mathbf{x}, \mathbf{y}) \ , \tag{E.1b}$$

where $\mathbf{x}$ and $\mathbf{y}$ are state variables. In (E.1b), the derivative of $\mathbf{y}$ is multiplied by a small parameter ϵ, which justifies a time-scale decomposition.

The time-scale decomposition consists in deriving two reduced-order subsystems such that one describes the slow dynamics and the other the fast dynamics of the system (E.1). We denote by $\mathbf{x}_s$, $\mathbf{y}_s$ the slow components and by $\mathbf{x}_f$, $\mathbf{y}_f$ the fast components of the state variable such that

$$\mathbf{x} = \mathbf{x}_s + \mathbf{x}_f \ , \tag{E.2a}$$

$$\mathbf{y} = \mathbf{y}_s + \mathbf{y}_f \ . \tag{E.2b}$$

A quasi-steady-state approximation of the slow subsystem can be obtained by setting $\epsilon = 0$ in (E.1) as

$$\frac{d\mathbf{x}_s}{dt} = \mathbf{f}(\mathbf{x}_s, \mathbf{y}_s) \ , \tag{E.3a}$$

$$0 = \mathbf{g}(\mathbf{x}_s, \mathbf{y}_s) \ . \tag{E.3b}$$

For a given $\mathbf{x}_s$, (E.3b) is the equilibrium condition for $\mathbf{y}$. However, since this is achieved by $\epsilon = 0$, we can still have $d\mathbf{y}_s/dt \neq 0$. Besides, $\mathbf{y}_s$ are allowed to change so that (E.3b) is satisfied as $\mathbf{x}_s$ varies during slow transients.

E.1 Slow dynamics

For the linear system (E.1), its slow manifold is such that the fast dynamics are not excited, so that $\mathbf{x} = \mathbf{x}_s$ and $\mathbf{y} = \mathbf{y}_s$. The slow manifold can be defined by

$$\mathbf{y}_s = \mathbf{h}(\mathbf{x}_s) \ . \tag{E.4}$$

For $\mathbf{y}_s$ to be solutions of the original system (E.1), $\mathbf{h}$ must satisfy the follow condition, which is obtained by substituting (E.4) in (E.1)

$$\epsilon \frac{\partial \mathbf{h}}{\partial \mathbf{x}} \mathbf{f}(\mathbf{x}_s, \mathbf{h}) = \mathbf{g}(\mathbf{x}_s, \mathbf{h}) \ . \tag{E.5}$$

The above partial differential equations are difficult, if not impossible, to be solved analytically. Thus, the slow manifold is approximated using a series expansion in ϵ. For $\epsilon = 0$, we obtain the first terms $\mathbf{h}_0$ of this expression, which amounts to

$$0 = \mathbf{g}(\mathbf{x}_s, \mathbf{h}_0) \ . \tag{E.6}$$

E.2 Fast dynamics

In order to approximate the fast dynamics, we assume that $\mathbf{w}$ is predominantly slow, i.e. $\mathbf{w} \approx \mathbf{w}_s$. Thus, the state variables of the fast subsystem are the fast components $\mathbf{x}_f$, $\mathbf{y}_f$ introduced in (E.2a), (E.2b)

$$\mathbf{y}_f = \mathbf{y} - \mathbf{y}_s = \mathbf{y} - \mathbf{h}(\mathbf{x}_s) \ . \tag{E.7}$$

Substituting (E.7) in (E.1b) yields

$$\epsilon \frac{d\mathbf{y}_f}{dt} = \epsilon \frac{d\mathbf{y}}{dt} - \epsilon \frac{d\mathbf{y}_s}{dt} \approx \mathbf{g}(\mathbf{x}_s, \mathbf{y}_f + \mathbf{h}) \ . \tag{E.8}$$

Note that (E.8) defines a off-manifold whose equilibrium point is at the slow manifold, i.e. $\mathbf{y}_f = 0$. In addition, the slow variables $\mathbf{x}_s$ are parameters for the fast subsystem.

Linearizing (E.8) around a point $(\mathbf{x}_s, \mathbf{h}(\mathbf{y}_s))$ on the slow manifold yields

$$\epsilon \frac{d\Delta\mathbf{y}_f}{dt} = \frac{\partial \mathbf{g}}{\partial \mathbf{y}} \Delta\mathbf{y}_f \ . \tag{E.9}$$

Thus, the stability of the fast subsystem is determined by the Jacobian matrix $\partial\mathbf{g}/\partial\mathbf{y}$.

Bibliography

[1] P. Kundur, J. Paserba, V. Ajjarapu, G. Andersson, A. Bose, C. Canizares, N. Hatziargyriou, D. Hill, A. Stankovic, C. Taylor, T. Van Cutsem, and V. Vittal, "Definition and classification of power system stability," *IEEE Transactions on Power Systems*, vol. 19, pp. 1387–1401, August 2004.

[2] P. Kundur, *Power System Stability and Control*. McGraw-Hill, 1994.

[3] UCTE, "UCTE operation handbook." Available : http://www.entsoe.eu/resources/publications/ce/oh/, July 2004.

[4] T. Van Cutsem and C. Vournas, *Voltage Stability of Electric Power Systems*. Kluwer Academic Publishers, 1998.

[5] E. Hirst and B. Kirby, "Ancillary services," in *American Power Conference*, vol. 1, (Chicago, Illinois), February 1996.

[6] Y. G. Rebours, D. S. Kirschen, M. Trotignon, and S. Rossignol, "A survey of frequency and voltage control ancillary services part I: Technical features," *IEEE Transactions on Power Systems*, vol. 22, pp. 350–357, February 2007.

[7] A. Oudalov, D. Chartouni, and C. Ohler, "Optimizing a battery energy storage system for primary frequency control," *IEEE Transactions on Power Systems*, vol. 22, pp. 1259–1266, August 2007.

[8] R. Billinton and A. V. Jain, "Interconnected system spinning reserve requirements," *IEEE Transactions on Power Apparatus and Systems*, vol. PAS-91, pp. 517–525, March 1972.

[9] R. Billinton and N. A. Chowdhury, "Operating reserve assessment in interconnected generating systems," *IEEE Transactions on Power Systems*, vol. 3, pp. 1479–1487, November 1988.

[10] N. S. Rau, C. Necsulescu, K. F. Schenk, and R. B. Misra, "A method to evaluate economic benefits in interconnected systems," *IEEE Transactions on Power Apparatus and Systems*, vol. PAS-102, pp. 472–482, February 1983.

[11] N. G. Hingorani and L. Gyugyi, *Understanding FACTS: Concepts and Technology of Flexible AC Transmission Systems*. IEEE press, 1999.

[12] M. P. Bahrman and B. K. Johnson, "The ABCs of HVDC transmission technologies," *IEEE Power and Energy Magazine*, vol. 5, pp. 32–44, March-April 2007.

[13] G. Asplund, K. Eriksson, and K. Svensson, "DC transmission based on voltage source converters," in *CIGRÉ*, (South Africa), 1997.

[14] V. Lescale, A. Kumar, L.-E. Juhlin, H. Bjorklund, and K. Nyberg, "Challenges with multi-terminal UHVDC transmissions," in *Joint International Conference on Power System Technology and IEEE Power India Conference, 2008. POWERCON 2008*, pp. 1–7, August 2008.

[15] C. E. Grund, M. P. Bahrman, N. Balu, L. Bergstrom, W. F. Long, R. J. Newell, D. Osborne, and R. V. Pohl, "Dynamic performance characteristics of north american HVDC systems for transient and dynamic stability evaluations," *IEEE Transactions on Power Apparatus and Systems*, vol. PAS-100, pp. 3356–3364, July 1981.

[16] C. W. Taylor and S. Lefebvre, "HVDC controls for system dynamic performance," *IEEE Transactions on Power Systems*, vol. 6, pp. 743–752, May 1991.

[17] A. E. Hammad, "Stability and control of HVDC and AC transmissions in parallel," *IEEE Transactions on Power Delivery*, vol. 14, pp. 1545–1554, October 1999.

[18] S. G. Johansson, G. Asplund, E. Jansson, and R. Rudervall, "Power system stability benefits with VSC DC-Transmission systems," in *CIGRÉ*, (Paris, France), 2004.

[19] Z. Hu, C. Mao, and J. Lu, "Improvement of transient stability in AC system by HVDC light," in *2005 IEEE/PES Transmission and Distribution Conference and Exhibition: Asia and Pacific*, pp. 1–5, 2005.

[20] L. Zhang, L. Harnefors, and P. Rey, "Power system reliability and transfer capability improvement by VSC-HVDC (HVDC light©)," in *CIGRÉ Regional Meeting*, (Tallinn, Estonia), June 2007.

[21] P. de Toledo, J. Pan, K. Srivastava, WeiGuo Wang, and Chao Hong, "Case study of a multi-infeed HVDC system," in *Joint International Conference on Power System Technology and IEEE Power India Conference, 2008. POWERCON 2008.*, pp. 1–7, October 2008.

[22] Z. Huang, B. Ooi, L.-A. Dessaint, and F. Galiana, "Exploiting voltage support of voltage-source HVDC," in *IEE Proceedings Generation, Transmission and Distribution*, vol. 15, pp. 252–256, March 2003.

[23] M. Baker, K. Abbott, and B. Gemmell, "Frequency and system damping assistance from HVDC and FACTS controllers," in *Proceedings of IEEE Power Engineering Society Summer Meeting*, vol. 2, (Chicago, IL, USA), pp. 770–773, July 2002.

[24] K. Papadogiannis and N. Hatziargyriou, "Optimal allocation of primary reserve services in energy markets," *IEEE Transactions on Power Systems*, vol. 19, pp. 652–659, February 2004.

[25] L. L. Grigsby, *Power System Stability And Control*. The Electrical Engineering Handbook Series, CRC Press Inc., 2007.

[26] M. L. Ourari, L.-A. Dessaint, and V. Q. Do, "Generating units aggregation for dynamic equivalent of large power systems," in *IEEE Power Engineering Society General Meeting*, vol. 2, pp. 1535–1541, June 2004.

[27] J. Dai, Y. Phulpin, A. Sarlette, and D. Ernst, "Coordinated primary frequency control among non-synchronous systems connected by a multi-terminal HVDC grid," Submitted.

[28] J. Dai, Y. Phulpin, A. Sarlette, and D. Ernst, "Impact of delays on a consensus-based primary frequency control scheme for AC systems connected by a multi-terminal HVDC grid," in *Proceedings of the IREP Symposium VIII*, (Buzios, Brazil), August 2010.

[29] R. Olfati-Saber, J. Fax, and R. Murray, "Consensus and cooperation in networked multi-agent systems," *Proceedings of the IEEE*, vol. 95, no. 1, pp. 215–233, 2007.

[30] J. A. Fax and R. M. Murray, "Information flow and cooperative control of vehicle formations," *IEEE Transactions on Automatic Control*, vol. 49, pp. 1465–1476, September 2004.

[31] B. Naduvathuparambil, M. Valenti, and A. Feliachi, "Communication delays in wide area measurement systems," in *Proceedings of the Thirty-Fourth Southeastern Symposium on System Theory*, (Huntsville, Alabama, USA), pp. 118–122, March 2002.

[32] A. Snyder, D. Ivanescu, N. HadjSaid, D. Georges, and T. Margotin, "Delayed-input wide-area stability control with synchronized phasor measurements and linear matrix inequalities," in *Proceedings of IEEE Power Engineering Society Summer Meeting*, (Seattle, WA, USA), pp. 1009–1014, July 2000.

[33] R. Olfati-Saber and R. M. Murray, "Consensus problems in networks of agents with switching topology and time-delays," *IEEE Transactions on Automatic Control*, vol. 49, no. 9, pp. 1520–1533, 2004.

[34] K. Meah and A. H. M. S. Ula, "A new simplified adaptive control scheme for multi-terminal HVDC transmission systems," *International Journal of Electrical Power & Energy Systems*, vol. 32, pp. 243–253, May 2010.

[35] K. R. Padiyar and N. Prabhu, "Modelling, control design and analysis of VSC based HVDC transmission systems," in *2004 International Conference on Power System Technology – PowerCon 2004*, vol. 1, (Singapore), pp. 774–779, November 2004.

[36] K. Ogata, *Modern Control Engineering*. Prentice Hall, 5 ed., September 2009.

[37] J. Dai, Y. Phulpin, A. Sarlette, and D. Ernst, "Voltage control in an HVDC system to share primary frequency reserves between non-synchronous areas," in *Proceedings of the 17th Power Systems Computation Conference (PSCC 2011)*, (Stockholm, Sweden), August 2011.

[38] J. Hazra, Y. Phulpin, and D. Ernst, "HVDC control strategies to improve transient stability in interconnected power systems," in *Proceedings of the 2009 IEEE Bucharest Power Tech Conference*, (Bucharest, Romania), pp. 1–6, 2009.

[39] H. F. Latorre, M. Ghandhari, and L. Söder, "Active and reactive power control of a VSC-HVdc," *Electric Power Systems Research*, vol. 78, pp. 1756–1763, October 2008.

[40] M. Ghandhari, G. Andersson, and I. A. Hiskens, "Control lyapunov functions for controllable series devices," *IEEE Transactions on Power Systems*, vol. 16, pp. 689–694, November 2001.

[41] Hongzhi Cai, Zhihua Qu, and Deqiang Gan, "A nonlinear robust HVDC control for a parallel AC/DC power system," *Computers and Electrical Engineering*, vol. 29, pp. 135–150, January 2003.

[42] A. Lotfjou, M. Shahidehpour, Yong Fu, and Zuyi Li, "Security-constrained unit commitment with AC/DC transmission systems," *IEEE Transactions on Power Systems*, vol. 25, pp. 531–542, February 2010.

[43] B. H. . Bakken and H. H. Faanes, "Technical and economic aspects of using a long submarine HVDC connection for frequency control," *IEEE Transactions on Power Systems*, vol. 12, pp. 1252–1258, August 1997.

[44] S. Bhamidipati and A. Kumar, "Load frequency control of an inter-connected system with DC tie-lines and AC-DC parallel tie-lines," in *Proceedings of the Twenty-Second Annual North American Power Symposium, 1990*, vol. 1, (Auburn, AL, USA), p. 390, October 1990.

[45] G. Fujita, G. Shirai, and R. Yokoyama, "Automatic generation control for DC-link power system," in *IEEE/PES Transmission and Distribution Conference and Exhibition 2002: Asia Pacific.*, vol. 3, pp. 1584–1588, October 2002.

[46] Yu Tao, Shen Shande, Zhu Shouzhen, Zhao Yuzhu, and Zhu Weijiang, "A novel auxiliary frequency controller for HVDC transmission links," in *Proceedings of International Conference on Power System Technology, PowerCon*, vol. 1, (Kunming, China), pp. 515–519, October 2002.

[47] S. Sterpu and M. N. Tuan, "Sharing frequency response between asynchronous electrical systems," in *IEEE Power & Energy Society General Meeting, PES*, (Calgary, AB), pp. 1–6, July 2009.

[48] Changsong Li, Y. Okada, M. Watanabe, and Y. Mitani, "Modeling Kita-Hon HVDC link for load frequency control of eastern japan 50-hz power system based on application of the CampusWAMS," in *Proceedings of 2010 IEEE International Symposium on Circuits and Systems (ISCAS)*, (Paris, France), pp. 2307–2310, Mai-June 2010.

[49] T. M. Haileselassie and K. Uhlen, "Primary frequency control of remote grids connected by multi-terminal HVDC," in *Proceedings of IEEE Power & Energy Society General Meeting, PES*, (Minneapolis, MN, USA), pp. 1–6, July 2010.

[50] I. Ngamroo, "A stabilization of frequency oscillations in a parallel AC-DC interconnected power system via an HVDC link," *Science Asia Journal of the Science Society of Thailand*, vol. 28, no. 2, pp. 173–180, 2002.

[51] R. Thottungal, P. Anbalagan, T. Mohanaprakash, A. Sureshkumar, and G. V. Prabhu, "Power system stabilization in multi area system by using HVDC link," *Academic Open Internet Journal, ISSN 1311-4360*, vol. 19, 2006.

[52] Y. Phulpin and D. Ernst, "Ancillary services and operation of multi-terminal HVDC grids," in *Proceedings of International Workshop on Transmission Networks for Offshore Wind Power Plants*, (Aarhus, Denmark), pp. 1–6, October 2011.

[53] M. Sanpei, A. Kakehi, and H. Takeda, "Application of multi-variable control for automatic frequency controller of HVDC transmission system," *IEEE Transactions on Power Delivery*, vol. 2, pp. 1063–1068, April 1994.

[54] T. M. Haileselassie, R. E. Torres-Olguin, T. K. Vrana, K. Uhlen, and T. Undeland, "Main grid frequency support strategy for VSC-HVDC connected wind farms with variable speed wind turbines," in *Proceedings of the 2011 PowerTech*, (Trondheim, Norway), June 2011.

[55] Y. Phulpin, "Communication-free inertia and frequency control for wind generators connected by an HVDC-link," pp. 1–2, 2011. Submitted.

[56] Y. Kia Yong Lim and Rujing Zhou, "Decentralised robust load-frequency control in coordination with frequency-controllable HVDC links," *International Journal of Electrical Power & Energy Systems*, vol. 19, pp. 423–431, October 1997.

[57] Y. Wang, R. Zhou, and C. Wen, "Robust load-frequency controller design for power systems," *IEE Proceedings-C Generation, Transmission and Distribution*, vol. 140, pp. 11–16, January 1993.

[58] CIGRE Task Force 38-02-14, "Large frequency disturbances: analysis and modeling needs," in *Proceedings of IEEE Power Engineering Society 1999 Winter Meeting*, (New York, NY , USA), pp. 554–558, January-February 1999.

[59] A. Molina-García, F. Bouffard, and D. S. Kirschen, "Decentralized demand-side contribution to primary frequency control," *IEEE Transactions on Power Systems*, May 2010.

[60] N. Jaleeli, L. S. VanSlyck, D. N. Ewart, L. H. Fink, and A. G. Hoffmann, "Understanding automatic generation control," *IEEE Transactions on Power Systems*, vol. 7, pp. 1106–1122, August 1992.

[61] D. L. E. E. Michael Milligan, Pearl Donohoo, B. Kirby, H. Holttinen, D. F. Eamonn Lannoye, M. O'Malley, N. Miller, P. B. Eriksen, A. Gøttig, B. Rawn, M. Gibescu, E. G. Lázaro, A. Robitaille, and I. Kamwa, "Delayed-input wide-area stability control with synchronized phasor measurements and linear matrix inequalities," in *Proceedings of 9th Annual International Workshop on Large-Scale Integration of Wind Power into Power Systems*, (Québec, Canada), pp. 1–16, October 2010.

[62] M. Ourari, L.-A. Dessaint, and V.-Q. Do, "Dynamic equivalent modeling of large power systems using structure preservation technique," *IEEE Transactions on Power Systems*, vol. 21, pp. 1284–1295, August 2006.

[63] J. Arrillaga, *High Voltage Direct Current Transmission*. No. 29 in Power and Energy Series, The Institution of Electrical Engineers, 1998.

[64] V. G. Agelidis, G. D. Demetriades, and N. Flourentzou, "Recent advances in high-voltage direct-current power transmission systems," in *IEEE International Conference on Industrial Technology, 2006. ICIT 2006.*, (Mumbai, India), pp. 206–213, December 2006.

[65] W. Long and S. Nilsson, "HVDC transmission: yesterday and today," *IEEE Power and Energy Magazine*, vol. 5, pp. 22–31, March-April 2007.

[66] W. D. Stevenson Jr, *Elements of Power System Analysis Third Edition*. Power Electronics and Power Systems, New York: McGraw-Hill, 1975.

[67] D. G. Fink and H. W. Beaty, *Standard Handbook for Electrical Engineers 11th Edition*. McGraw-Hill, 1978.

[68] N. G. Hingorani, "High-voltage DC transmission: a power electronics workhorse," *IEEE Power and Energy Magazine*, vol. 33, pp. 63–72, April 1996.

[69] ABB, "ABB HVDC website." www.abb.com/hvdc.

[70] Siemens AG, "Siemens HVDC website." www.energy.siemens.com/hq/en/power-transmission/hvdc/.

[71] N. M. Kirby, Lie Xu, M. Luckett, and W. Siepmann, "HVDC transmission for large offshore wind farms," *Power Engineering Journal*, vol. 16, pp. 135–141, June 2002.

[72] Lie Xu, B. Williams, and Liangzhong Yao, "Multi-terminal DC transmission systems for connecting large offshore wind farms," in *IEEE Power and Energy Society General Meeting - Conversion and Delivery of Electrical Energy in the 21st Century, 2008*, pp. 1–7, July 2008.

[73] S. Chaudhary, R. Teodorescu, and P. Rodriguez, "Wind farm grid integration using VSC based HVDC transmission - an overview," in *IEEE Energy 2030 Conference, 2008. ENERGY 2008.*, pp. 1–7, November 2008.

[74] J. Reeve, "Multiterminal HVDC power systems," *IEEE Transactions on Power Apparatus and Systems*, vol. PAS-99, pp. 729–737, March 1980.

[75] K. R. Padiyar, "Stability of converter control for multiterminal HVDC systems," *IEEE Transactions on Power Apparatus and Systems*, vol. PAS-104, pp. 690–696, March 1985.

[76] H. Jiang and A. Ekström, "Multiterminal HVDC system in urban areas of large cities," *IEEE Transactions on Power Delivery*, vol. 13, pp. 1278–1284, October 1998.

[77] J. L. Thomas, S. Poullain, and A. Benchaib, "Analysis of a robust DC-bus voltage control system for a VSC transmission scheme," in *Proc. of Seventh International Conference on AC-DC Power Transmission, 2001*, pp. 119–124, November 2001.

[78] Hairong Chen, Chao Wang, Fan Zhang, and Wulue Pan, "Control strategy research of VSC based multiterminal HVDC system," in *Power Systems Conference and Exposition, 2006. PSCE '06*, pp. 1986–1990, 2006.

[79] C. Schauder and H. Mehta, "Vector analysis and control of advanced static VAR compensators," *IEE Proceedings-C Generation, Transmission and Distribution*, vol. 140, pp. 299–306, July 1993.

[80] T. Nakajima and S. Irokawa, "A control system for HVDC transmission by voltage sourced converters," in *Proceedings of IEEE Power Engineering Society Summer Meeting, 1999*, vol. 2, (Edmonton, Alberta, Canada), pp. 1113–1119, July 1999.

[81] Lie Xu, B. R. Andersen, and P. Cartwright, "Control of VSC transmission systems under unbalanced network conditions," in *Transmission and Distribution Conference and Exposition, 2003 IEEE PES*, pp. 626–632, September 2003.

[82] J. M. Mauricio and A. G. Exposito, "Modeling and control of an HVDC-VSC transmission system," in *IEEE/PES Transmission & Distribution Conference and Exposition: Latin America, 2006. TDC '06.*, pp. 1–6, August 2006.

[83] R. E. Torres-Olguin and T. Undeland, "An adaptive direct power control for multi-terminal hvdc transmission system under unbalanced conditions," in *Proceedings of International Conference on Electric Power and Energy Conversion Systems, EPECS '09*, (American University of Sharjah, UAE), pp. 1–6, November 2009.

[84] R. D. Middlebrook and S. Ćuk, "A general unified approach to modelling switching-converter power stages," in *Power Electronics Specialists Conference Record*, (Cleveland, Ohio), pp. 18–34, June 1976.

[85] I. Lestas and G. Vinnicombe, "Scalable decentralized robust stability certificates for networks of interconnected heterogeneous dynamical systems," *IEEE Transactions on Automatic Control*, vol. 51, no. 10, pp. 1613–1625, 2006.

[86] F. R. K. Chung, *Spectral Graph Theory*. No. 92 in Regional Conference Series in Mathematics, AMS, 1997.

[87] L. Moreau, "Stability of multiagent systems with time-dependent communication links," *IEEE Transactions on Automatic Control*, vol. 50, pp. 169–182, February 2005.

[88] M. Green and D. J. N. Limebeer, *Linear Robust Control*. Information and System Sciences, Prentice Hall, 1994.

[89] R. E. O'Malley, *Introduction to singular perturbation*. North-Holland Series in Applied Mathematics & Mechanics, Academic Press, 1974.

[90] P. Kokotović, H. K. Khali, and J. O'Reilly, *Singular Perturbation Methods in Control: Analysis and Design (Classics in Applied Mathematics)*. Academic Press, 1986.

Index